SOME KINETIC AND THERMODYNAMIC ASPECTS OF

MOLECULAR BEAM EPITAXY

A Thesis
submitted to the Faculty of Engineering
of the University of Glasgow
for the degree of

Doctor of Philosophy

by

Robert Laurie Smith Devine, B.Sc.

March 1985

ProQuest LLC.
789 East Eisenhower Parkway
P.O. Box 1346
Ann Arbor, MI 48106 – 1346

This Thesis is Dedicated to My Family

CONTENTS

Acknowledgements

I wish to thank Professor J. Lamb for provision of the research and computing facilities in the Department of Electronics and Electrical Engineering.

I also thank my supervisor, Dr. C. R. Stanley, for his encouragement and advice throughout the duration of this work.

The Be diffusion work presented in this thesis was carried out at Philips Research Laboratories under the supervision of Dr. C.T. Foxon, to whom I owe my deepest thanks. I am also indebted to Dr. B.A. Joyce for his encouragement and advice on both the thermodynamic calculations and Be diffusion studies. Also at PRL, special thanks are due to Mr. J. Bellchambers for obtaining and discussing the Polaron Profiles. I also thank Dr. P. Blood for discussions on the Polaron, Mr. J.B. Clegg for the SIMS profiles, Dr. G. Duggan for the use of his envelope-function computer program and Dr. P.J. Dobson for discussion of the dimer work.

I also wish to sincerely thank Dr. B.C. Webster of the Department of Chemistry for his constant encouragement and advice, for explaining many aspects of theoretical chemistry and for provision of computing facilities.

Finally, I would like to thank my sister Nancy for typing this thesis and also my fellow research students and friends both in and outwith the department for making the past three years so enjoyable. In particular I would like to mention G. Muirhead, S. McLaughlin, T. Kerr, R. Hutchins, N. Orr, T. Martin, K. Simpson, D. Parry, the nutters from next door, A. Kamat and the "landlord", Stuart McGuinness.

Financial support from the Science and Engineering Research Council and from Philips Research Laboratories (through a CASE award) is gratefully acknowledged.

Abstract

The main aim of the work presented in this thesis is to investigate the role of kinetics and thermodynamics in some of the processes encountered during Molecular Beam Epitaxial growth of III-V semiconductors. Comparisons are made with conventional Liquid Phase and Vapour Phase Epitaxial growth which are governed mainly by thermodynamic and kinetic influences respectively.

A symmetry-induced kinetic barrier to the incorporation of group II dopants has been identified by application of gas-phase Molecular Orbital (MO) methods to reactions on solid surfaces. As a precursor to this, MO methods have also been used to explain the nature of the surface dimer structure on the (100) surfaces of semiconductors.

A thermodynamic model has been developed to describe the native defect concentrations in GaAs and AlGaAs in an ambient As-overpressure. The applicability of this model to MBE growth is discussed.

Conditions leading to the diffusion of Be in GaAs and AlGaAs during growth have been examined. This has led to an understanding of the practical growth limits within which Be-doping can be utilised. Thermodynamic and kinetic factors influencing the behaviour of the Be have been discussed.

The above-mentioned effect has been used to provide a controllable source of Be for diffusion studies in AlAs/GaAs superlattices. In particular, the role of the superlattice electronic structure in determining the diffusivity has been illuminated.

CHAPTER 1

INTRODUCTION

Modern electronic and optical devices usually require starting materials of high structural perfection and low impurity content in order to operate satisfactorily. Material grown by any of the bulk methods available is usually of relatively poor quality with respect to structural properties and non-radiative recombination centres. In order to overcome this the bulk material is often used as a substrate, upon which a thin epitaxial layer of higher quality material is grown. This approach also has the advantage that multilayer structures can be fabricated, involving several different materials.
Various techniques for accomplishing this are in existence, involving deposition either from the liquid phase or the vapour phase. This thesis is concerned with some of the fundamental processes involved in one of these methods, namely Molecular Beam Epitaxy (MBE).

MBE is a sophisticated evaporation technique for growing semiconductor crystals which is carried out under Ultra High Vacuum (UHV) conditions. The constituents of the material to be grown are evaporated from separate sources which are directed at the substrate onto which deposition is to take place. UHV conditions are required in order to minimise the incorporation of impurities into the growing layer which would degrade its transport and optical properties. As a result of steady improvements in the technology associated with MBE it is now possible to obtain layers which are comparable in quality to those obtained by more established techniques such as Vapour Phase Epitaxy (VPE) and Liquid Phase Epitaxy (LPE). This in turn means that it is now possible to fabricate high performance devices such as lasers, FETS and photodetectors using MBE material. As well as the more conventional devices there are also those designed to exploit the special characteristics of MBE such as the ability to produce very abrupt heterojunctions and very thin layers.

The abruptness obtainable is largely due to the lower growth temperatures used in MBE compared to VPE and LPE. MBE also differs from conventional VPE in that the overpressures encountered during growth are very much greater for the latter.

Another distinguishing feature of MBE growth is the ability to study the growth processes and surface structures in-situ using a wide range of experimental techniques, enabling problems encountered during the techniques development to be studied more directly, as well as direct monitoring of growth conditions.
A particular advantage of MBE is its ability to produce very smooth interfaces. With devices being made increasingly smaller, the effect of the interface on the device performance becomes ever more important. An example of this is the effect of interface roughness on the luminescence from thin quantum wells.

Up to the present time a wide range of semiconductors, both compound and elemental, have been grown using MBE, including III-V, II-VI, IV-VI and group IV crystals. Undoubtedly, most effort has been directed at the III-V materials due to their utility in device fabrication, and it is the III-V materials with which this thesis is mainly concerned.

The aim of this thesis is to illuminate the roles played by Kinetics and Thermodynamics in some of the processes encountered in MBE. Thermodynamics defines the behaviour of a system at equilibrium, while the kinetics control the way in which the system moves towards this equilibrium. In order to understand the kinetics it is necessary to have a knowledge of the growth processes at the atomic level. This is an extremely complex problem, an appreciation of which is gained when it is realised that many aspects of reactions involving even small molecules are still poorly understood. However, some progress can be made and as a means of achieving this the obvious first step is to apply the methods which have been developed for the reactions of small molecules.

Although the quantitative details of a gas-phase reaction may be unknown, much qualitative information can be obtained by applying powerful methods, such as Frontier Orbital Theory and Orbital Symmetry Rules, to the system under study (the main techniques available will be outlined in chapter 3). There is, however, no guarantee that these rules will be applicable to reactions on a solid surface. Chapters 5 and 6 are theoretical chapters which investigate this problem in relation to semiconductor surfaces and MBE growth.

Chapter 5 is a discussion of the properties of the semiconductor surfaces, an understanding of which is required before conclusions can be drawn regarding possible microscopic models for the chemical reactions. As well as this, however, chapter 5 stands alone as a study of the factors involved in determining the structure of semiconductor (100) surfaces.

Chapter 6 is concerned with the kinetic factors in the chemical reactions which take place during growth. The conclusions obtained are used to explain the behaviour of the group II dopants during growth of III-V layers, as well as shed some light on the growth processes themselves.

The work in chapter 7 consists of a set of thermodynamic calculations to determine the concentrations of native defects in GaAs and AlGaAs, together with a discussion of the thermodynamic factors which determine the formation of the defects.

Chapters 8 and 9 are concerned with diffusion, both being thermodynamic-based discussions. Chapter 8 is a study of Beryllium diffusion during the growth of GaAs and AlGaAs at elevated temperatures, while the work in chapter 9 examines such diffusion through a superlattice composed of alternate layers of GaAs and AlAs. As well being of direct practical interest, the experiments in chapters 8 and 9 provide some information on thermodynamic processes during growth.

There is a strong emphasis in the introductory chapters on the theoretical aspects of chemical reactions. This does not reflect the emphasis of the thesis itself but rather the relative difficulty and obscurity of many of the concepts involved.

CHAPTER 2

FUNDAMENTALS OF MOLECULAR BEAM EPITAXY

2.1 Introduction

MBE differs from the other popular growth methods in that the sources and substrate are all held at different temperatures. This introduces complications into any model of the growth process, particularly if thermodynamics are involved, where equilibrium implies that the system is in an isothermal state. The effect of the different temperatures can be ignored if the incident atoms and molecules aquire the temperature of the substrate before being incorporated into the growing film. There is, however, no conclusive experimental evidence to support this [2.1]. As a result, the relative extent to which kinetic and thermodynamic factors influence the growth of III - V materials is still unclear, although it has often been assumed that kinetic factors play a dominant role.

The present chapter will outline those areas of relevance to the present investigation, more complete reviews of MBE growth being given by Foxon and Joyce [2.2] and by Ploog [2.3].

2.2 Thermodynamic Properties

Before discussing the processes thought to be involved in MBE growth it is necessary to have a knowledge of the thermodynamic properties of the material being grown. This is best illustrated by GaAs, which is the most commonly grown material, as well as being well characterised thermodynamically [2.4].

Shown in Fig. (2.1) and Fig. (2.2) are the phase diagram [2.5] and vapour pressure curves [2.6] respectively for the Ga-As system, the existence region for GaAs being shown greatly exaggerated in Fig (2.1). Numerous calculations have been carried out on the range of stoichiometry in which GaAs is stable [2.7]. The exact range depends sensitively on the model used but is known to be very narrow, usually within the range $0.499 < X_{As}$

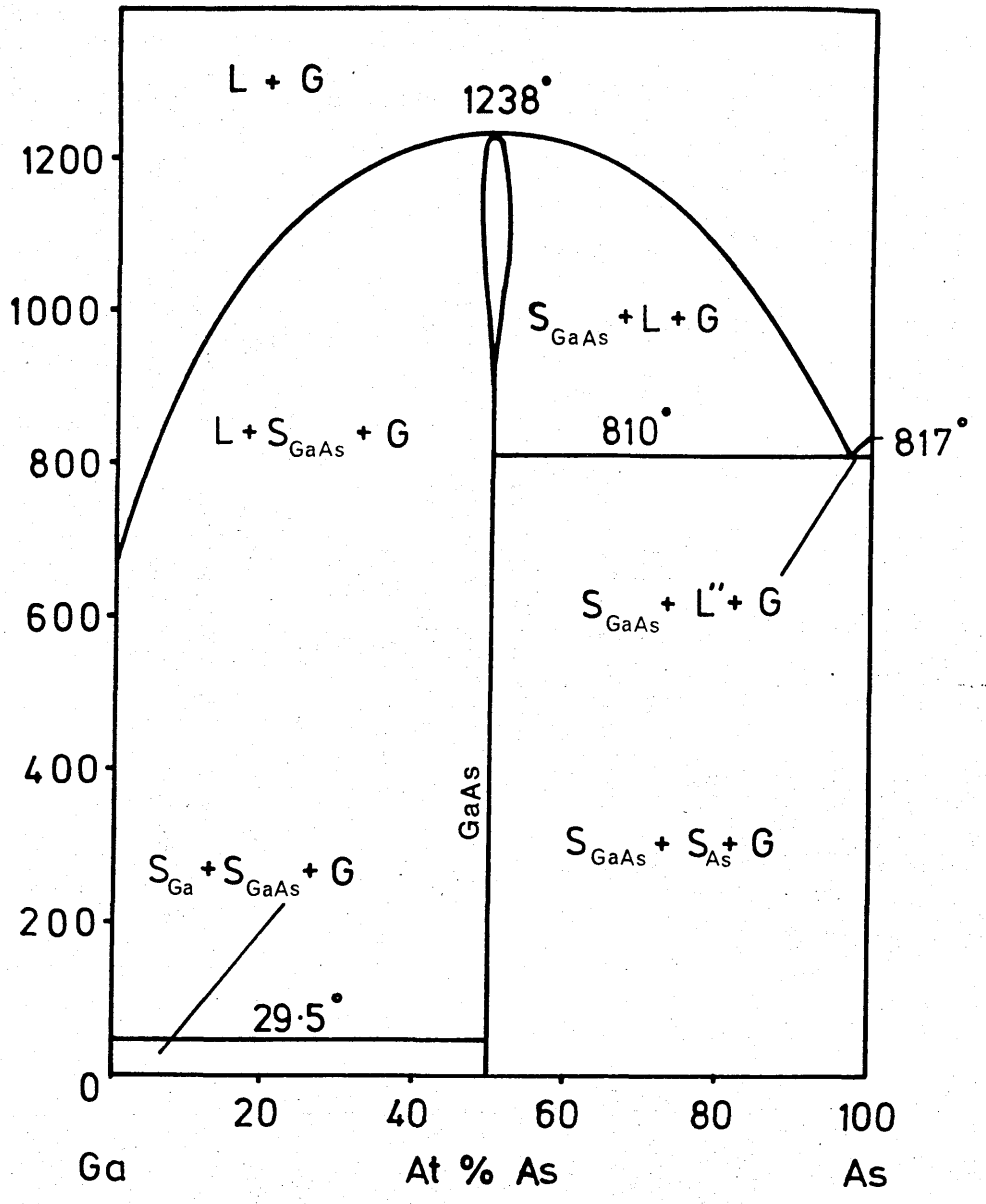

Figure 2.1 Phase Diagram (temperature versus composition) for the Ga-As system.

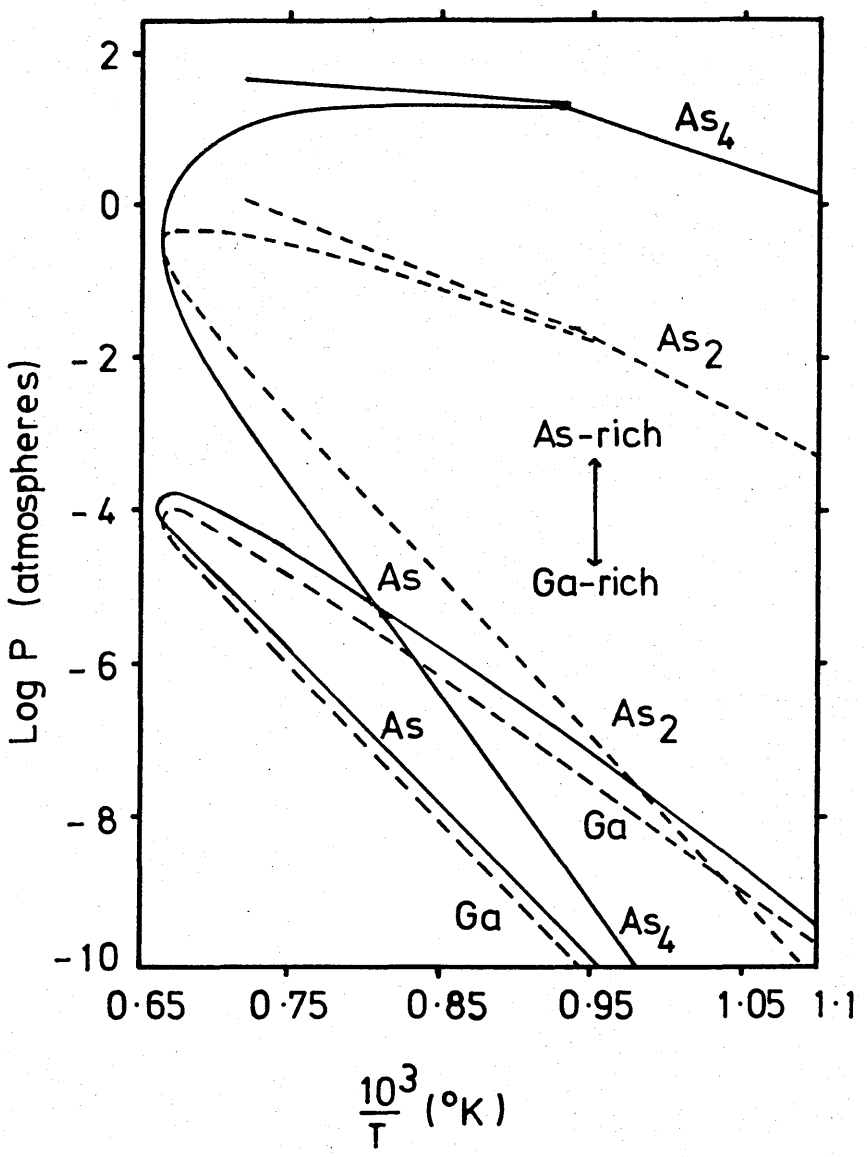

Figure 2.2 Equilibrium vapour pressures of As, As_2, As_4 and Ga along the binary liquidus. The straight lines are vapour pressures of As_2 and As_4 over pure liquid and solid As.

< 0.501.

An important property of a semiconductor is the temperature range over which congruent evaporation takes place, i.e. rates of evaporation of Ga and As are equal. The P-T data in Fig. (2.2) were obtained from a Knudsen cell and it is apparent that congruent evaporation occurs at one temperature only, (T_c = 898K as measured by Foxon et. al. [2.8]). Under Langmuir, i.e. free, evaporation conditions T_c is different from that for Knudsen conditions and is also an upper limit, congruent evaporation taking place at all temperatures lower than 930K [2.8]. Above this temperature the evaporation rate of As is greater than that of Ga.

In order for growth to take place an overpotential must exist, i.e. the rate of incorporation must be faster than the rate of evaporation. Hence, MBE growth at temperatures lower than T_c requires equal fluxes of Ga and As atoms, while growth at higher temperatures requires substantially more As than Ga. Failure to supply enough As leads to the formation of Ga droplets on the surface.

From the vapour pressure data in Fig. (2.2) it is evident that there is no overpotential for the deposition of elemental As under the conditions employed in MBE growth. In practical terms this makes the control of the fluxes straight-forward since the As-flux need only be set larger than the Ga-flux, any excess As simply re-evaporating.
Note that although this will lead to GaAs with a composition at some point in the existence region, the precise stoichiometry can still be influenced by variation of the substrate temperature and the Ga/As flux ratio. For example, at a growth temperature below T_c, Ga-rich material is obtained by keeping the Ga-flux slightly greater than the As-flux. A more detailed discussion of the stoichiometry of MBE grown layers will be given in chapter 7.

2.3 Interactions of Ga and As_2 with the GaAs surface

The behaviour discussed in the previous section can also be explained by consideration of the kinetics involved in the interactions between the incident atoms (or molecules) and the substrate. Central to this is the concept of a sticking coefficient of an atom or molecule. This is simply a measure of its ability to bond to the surface, and in MBE can be defined as being unity if the surface residence lifetime is long enough for incorporation into the growing lattice to take place. Before discussing the detailed behaviour of Ga atoms and As_2 molecules on a GaAs surface it is necessary to review the behaviour of the GaAs surface as a function of temperature. Note that only As_2 is considered here since this is the species employed in the growth experiments described in this thesis. A more detailed discussion of the kinetic effects is given in the review by Foxon and Joyce [2.2].

2.4 Behaviour of the Substrate

The surface normally used for MBE growth is the (100) orientation since this leads to better quality layers. It is also the surface on which most kinetic studies have been performed. The (100) surface is polar and may be terminated in either cations, anions or a combination of the two. On GaAs either a Ga-rich or As-rich surface can be prepared by appropriate choice of substrate temperature and flux ratio. At room temperature the surface is normally As-rich. It can be simply converted to Ga-rich by heating to a temperature above about 600K where, according to Arthur [2.9], about 0.5 monolayer of As_2 is lost. Above about 850K the evaporation of the GaAs as Ga and As_2 becomes measurable mass spectrometrically [2.8]. From this temperature up to T_c the evaporation rate of the GaAs increases from 0.01 to 1.0 monolayers s^{-1}.

The surface populations of the Ga and As atoms during growth will be dependent on the factors described above (as well as possible diffusion from the bulk) and will have an important effect on the

properties of the grown layers.

2.5 Sticking Coefficients

The sticking coefficient of Ga on (100) GaAs is always unity under the conditions most commonly employed for MBE growth [2.10] (i.e. growth temperatures up to T_c), and has been shown experimentally to be mobile on the surface above about 525K. If an adequate supply of As is not available for growth then any deposited Ga will simply form Ga-droplets, the desorbing flux being relatively small below T_c [2.8]. At higher temperatures (i.e. well above T_c) the re-evaporation of the Ga during growth becomes significant.

The interaction of As_2 with the surface is more complex, the sticking coefficient (S_{As2}) being dependent on the Ga surface population which is in turn dependent on such factors as the Ga flux, desorption rate, etc. Foxon and Joyce [2.11] have measured the sticking coefficient of As_2 as a function of the Ga adsorption rate and have found it to be linearly dependent on the latter, reaching unity when $J_{Ga} \approx 2J_{As2}$. If there is no surface Ga then S_{As2} is found to be zero, the surface lifetime being less than 10^{-6} s. Hence, as stated earlier, GaAs can be grown when $J_{Ga} < 2J_{As2}$, the excess As_2 being lost by desorption.

2.6 The Role of Kinetics

Fundamental to the MBE process is the occurence of chemical reactions at the surface, the progress of which will be determined by various kinetic and thermodynamic factors. The thermodynamics of the system determines the relative concentrations of the reactants and products at equilibrium while the kinetics determine the rate at which the system approaches equilibrium.

Shown in Fig. 2.3 is the potential energy curve for a simple reaction involving one degree of freedom. The activation barrier for the reaction is E_A and it is mainly this quantity which

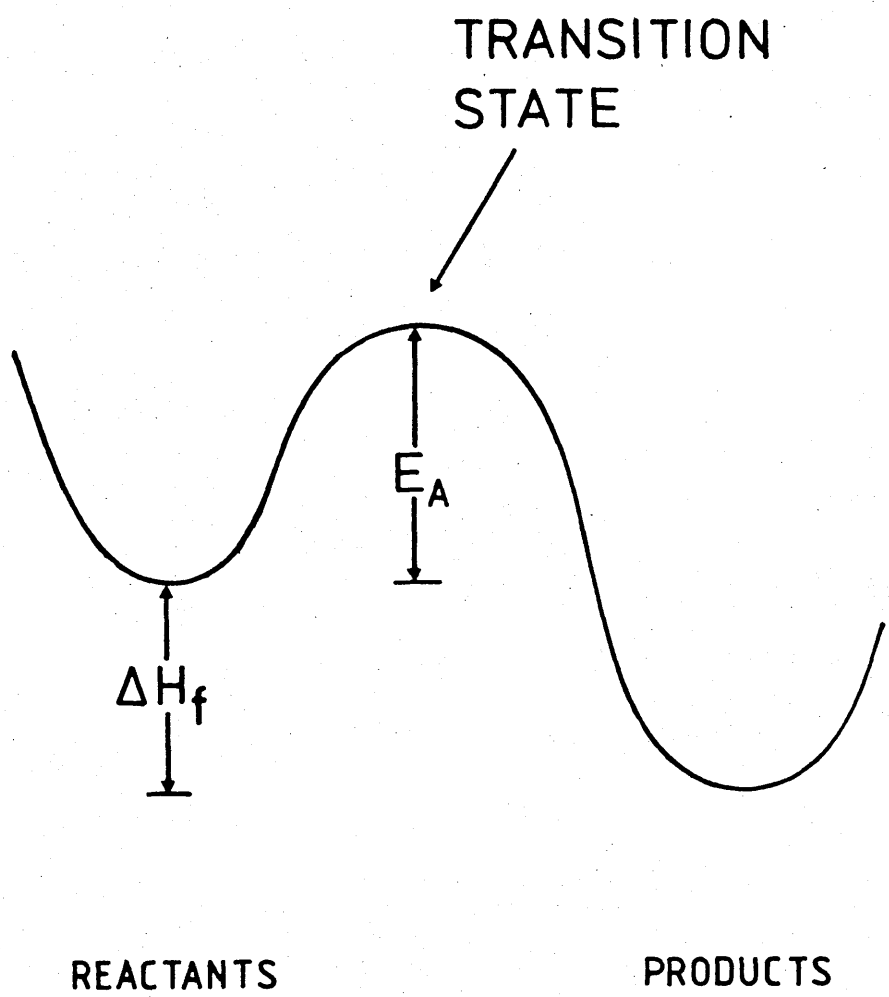

Figure 2.3 Potential energy surface for a system with one degree of freedom.

determines the rate at which the reaction progresses. The probability of surmounting this barrier is given by ;

$$p = p_o \exp(-E_A/kT) \qquad (2.1)$$

where p_o is a constant. The point on the energy surface at the peak of the activation barrier is known as the transition state. The interacting molecules are called an activated complex at this point.

The enthalpy change shown, ΔH_f, determines the relative concentrations of the reactants and products through the thermodynamic equations describing the reaction. Note, however, that thermodynamic equilibrium will not be easily attained if the kinetic factors are unfavourable.

Consider chemical reactions in the gas phase ; there are two distinct processes (i) diffusion of the reactants towards one another and (ii) actual occurrence of the chemical reaction. An analagous situation exists during MBE growth, the first stage corresponding to diffusion of the adatom across the surface and the second to incorporation into a lattice site. Both of these steps will be subject to kinetic influences. The surface mobility will be determined by the activation energy for surface diffusion, which is often relatively small. For example, Heckingbottom et. al. [2.12] have estimated that a Ga atom on GaAs at 600°C could make of the order of 10^6 site changes before incorporation. Certainly the effect of surface diffusion is unlikely to be significant at normal growth temperatures, i.e. > 550°C.

However, this will not necessarily be true for the chemical reactions leading to incorporation. For example, reactions involving As_2 and As_4 are generally regarded to be kinetically hindered and this is revealed by the different effect each species has on the deep trap concentration [2.13]. Kinetic factors have also been shown to be important in the growth of

III-V-V alloys [2.14].

Most reactions involving single atoms are unlikely to involve large activation energies. However, there are some cases where kinetic factors might be expected to intrude and this will be discussed more fully in chapter 6.

2.7 Doping of Layers

Doping of MBE layers can often be unpredictable due to low sticking coefficients, ambiguity as to the incorporation site and reactions of the dopants with impurities. This is an area where both kinetics and thermodynamics would appear to be important. For example, the group IV elements are all potentially amphoteric in theory but show a wide range of behaviours in practice. Ge in GaAs is strongly amphoteric, being pushed one way or the other by appropriate adjustment of the As/Ga flux ratio [2.15]. Si, on the other hand, is only ever observed as a donor in MBE material [2.16], while it is amphoteric in material grown by other methods. Again, the detailed properties of the various potential dopants will not be considered here since they are discussed in detail in the review articles mentioned earlier [2.2] [2.3].

2.8 Surface Structures and Stoichiometry

The surface stoichiometry of a III - V surface can be varied over a wide range, the most direct indicator being the surface structure. The different surface structures observed are due to rearrangements of the surface atoms, called reconstructions, which result in a reduction in the symmetry from that for the atoms at their bulk positions. The nature of the reconstructions on semiconductor surfaces will be discussed more fully in chapters 4 and 5. The As-stable surface on GaAs is observed to have a (2 x 4) reconstruction (that for atoms at bulk positions being (1 x 1)) while the Ga-stable surface at 600K and above has a (4 x 2) reconstruction. Other reconstructions exist for particular preparation conditions [2.17] but the two mentioned above, along with an intermediate (3 x 1) structure, are the most commonly encountered.

Note that although the surface reconstruction indicates the dominant atom type on the surface, a wide range in stoichiometry is still possible for a particular reconstruction. Different reconstructions have been observed on other III - V surfaces, for example the most stable structure on GaSb is the (2 x 3) reconstruction [2.18].

The surface structure present during growth has been shown to have a significant influence on the types of deep trap incorporated into the layer and can also influence the incorporation of dopants, particularly Ge. However, for most dopants the surface stoichiometry has little effect.

CHAPTER 3

METHODS OF THEORETICAL CHEMISTRY

3.1 Introduction

One of the principal aims of the work in this thesis is to attempt to understand some of the processes involved in MBE growth at a microscopic level. This inevitably requires the utilisation of some of the concepts and methods of theoretical chemistry which have been developed in recent years.
There are two basic approaches to the problem of understanding the reactions undergone by an ensemble of atoms or molecules. One of the ultimate aims of theoretical chemistry is to be able to calculate the complete energy surface for any chemical reaction to what is known as "chemical accuracy" i.e., of the order of 3 kcal mol^{-1} [3.1]. This goal is, however, a long way off because even to calculate the total energy for a single geometry of a molecule of, say, six atoms requires a massive amount of computing time. For reaction surfaces, only very simple systems, e.g. two hydrogen plus one oxygen atom, have been studied. Another significant disadvantage of this approach is that the results are rarely physically transparent and so a real "understanding" is not gained.
These calculations are called "ab-initio" [3.2] and involve expressing the molecular orbitals (MOs) as a linear combination of atomic orbitals which are themselves linear combinations of component functions.

From the studies which have been performed on various molecules it has been observed that, on changing the geometry, the dominant energy changes often involve a small number of orbitals, invariably the collection of highest energy occupied MOs. In the same way, the formation of new MOs during the interaction of two molecules normally involves mixing of the highest occupied and lowest unoccupied MOs (HOMOs and LUMOs) of the original molecules [3.1] [3.3].
Another important fact is that the directions of the energy

changes are usually well described by using simple one electron MO theory, i.e. ignoring the electron-electron repulsions which complicate the ab-initio calculations.
The normal method of analysing these interactions is through a perturbation theory (PT) approach [3.3] [3.4] and this will be discussed in section (3.5).

Another powerful method of studying chemical reactions is through the symmetry of the MOs [3.1] [3.5]. Certain symmetry relations must be satisfied between the reactants and products in order for the reaction to proceed with a low activation energy and these will be discussed in due course.
One approach to reducing the computation time in the quantum chemical calculations is to parameterise certain of the integrals involved (since it is computation of the integrals which requires so much time). These are referred to as semi-empirical calculations [3.6], and will be discussed later.
All of the above approaches are utilised in chapter 6 in an effort to understand the interactions of single atoms with a GaAs (100) surface. Semi-empirical calculations are also used in the study of reconstruction on (100) surfaces in chapter 5.
The aim of this chapter is to identify and briefly review the concepts and methods of theoretical chemistry which are used in this thesis. More detailed expositions are available in the literature and these are extensively referenced.

3.2 The One-Electron Approximation

This approximation is central to any tractable calculation of the properties of an atom or molecule [3.7]. The electrons in an atom or molecule do not move independently of one another, but rather in a correlated manner. The calculation of the properties of such a system is referred to as a many-body problem and is essentially impractical for any more than three electrons (being impossible for any system of practical interest). In the one-electron approximation an electron is assumed to move under the influence of an average potential due to the ion cores and all the other electrons. Hence the total Hamiltonian of the system

is expressed as a sum of one-electron Hamiltonians, and the many-electron wave function as a product of one-electron functions. The best possible one-electron-like solution to the Schrodinger equation is then obtained by carrying out a variational calculation using these approximations.

When this is carried through it leads to what is known as the Hartree-Fock (HF) solution to the Schrodinger equation. The details of the analysis are not relevant here and so only the final solution is given, the total energy being [3.8] ;

$$E = \sum_i 2\epsilon_i + (E_o - E_2) \qquad (3.1)$$

The ϵ_i are the eigenvalues of the Schrodinger equation and are identified with the energies of the molecular (or atomic) orbitals. The value of ϵ_i corresponds to the energy required to remove an electron from orbital ψ_i (an approximation known as Koopmans' theorem) [3.9].

The core-core repulsion energy, E_o, is expressed in terms of the nuclear charges $Z_{A,B}$ and their separation r_{AB} thus ;

$$E_o = \sum_{A>B} Z_A Z_B / r_{AB} \qquad (3.2)$$

E_2 is the sum of the electron -electron interaction terms;

$$E_2 = 2 \sum_{i,j=1}^{N/2} (2J_{ij} - K_{ij}) \qquad (3.3)$$

Both J_{ij} and K_{ij} are two-centre integrals and it is the computation of these terms which causes the problems in this method. J_{ij} is a simple coulomb repulsion integral and is a measure of the electrostatic repulsion between two electrons. K_{ij} is a term introduced by the antisymmetric nature of the wavefunction [3.7] [3.9] and is called an exchange integral. It is a more difficult quantity to define and does not, in fact, correspond to a physically measurable energy. These are the terms which are parameterised in the semi-empirical methods, and which can be ignored in the qualitative theories mentioned in the introduction.

Due to the approximations made in the above analysis, the calculated energy will be higher than the true total energy, i.e. the binding energy of a molecule will be underestimated. This is because, in reality, the motion of the electrons is not uncorrelated, as is assumed in the HF model. Put simply, they tend to avoid each other and this reduces the electrostatic repulsion and hence the total energy. Since the binding energy is always a small fraction of the total energy this can lead to significant errors and in some cases a molecule will be determined as being unbound. The result can be further improved by the use of a technique known as Configuration Interaction (CI) [3.2] [3.7]. This involves expressing the wavefunction of the system as a linear combination of the different possible electron configurations, i.e. the different ways of arranging the electrons in the atomic or molecular orbitals. The further lowering of the energy obtained from such a calculation is called the correlation energy. Again, this is not a physically measureable quantity, being wholly a result of the initial model used. The details of implementing CI will not be given here but an illustration of its role in chemical reactions will be given both in this chapter and in chapter 5.

Two important disadvantages of CI are that it further increases the computation time required and it makes the results even less physically transparent.

The practical aspects of performing Hartree-Fock calculations are described in the book by Richards and Cooper [3.2].

3.3 Molecular Orbitals and Localised Bonds

The Hartree-Fock method discussed above is an example of a Molecular Orbital method. The orbitals of the molecule are expressed as a linear combination of the atomic orbitals of all the constituent atoms (see Appendix A) and are hence delocalised over the whole molecule [3.9] [3.10]. An alternative approach is the localised Bond method, the qualitative aspects of which are

generally well known. These involve a picture of each orbital in the molecule as being a localised bond between each atom, occupied by two electrons. Any non-bonding electrons are taken to occupy dangling orbitals, known as lone-pairs. Fig (3.1) shows the localised bond picture of phosphine (PH_3) which has three bonds and one lone pair. Also shown is the energy sequence and symmetries of the occupied MOs.

The two approaches are in fact related since the localised bonds are obtainable from a linear transformation of the set of molecular orbitals [3.9].

The trouble with the localised bond approach is that there are many examples of molecules where there are more pairs of electrons than there are possible localised bonds between atoms (or lone pairs). The classic example is benzene (C_6H_6) where the localised bond approach gives three single and three double bonds. This, however, implies different bond lengths in the molecule, a situation which is not observed in practice. In this case the molecular orbital approach gives a more satisfactory description of the electronic structure.

In fact, this is true in general since it has been observed that MOs give a good description of the photoemission spectrum of molecules, i.e. the MO approach would appear to be more physically realistic. It must always be kept in mind, however, that experiment provides direct information on the many-electron ground and excited states, and not for one-electron molecular orbitals. Because of this, excited states are usually poorly described.

The first excited singlet-state of a molecule is obtained by removing one electron from the HOMO and placing it in the LUMO, keeping the spin unchanged. The energies of the occupied and unoccupied MOs are obtained from the HF method discussed earlier. It is important to note, however, that the energy required to produce the first excited singlet-state is not equal to the difference between the orbital energies for the HOMO and LUMO

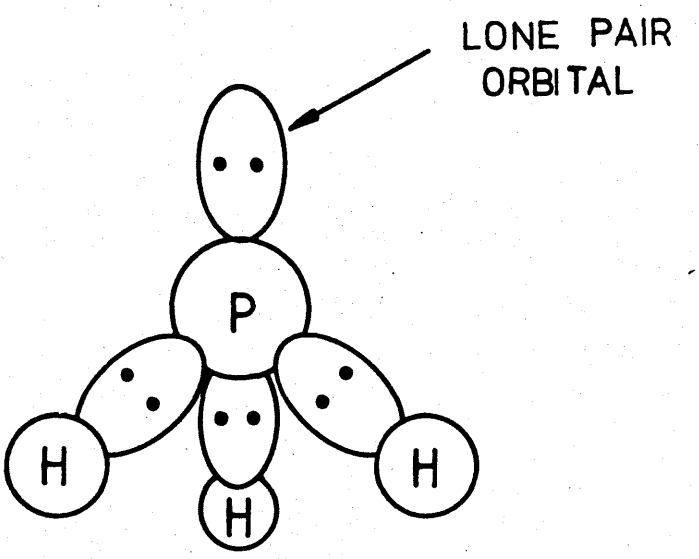

(a)

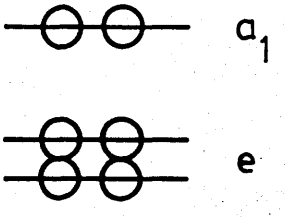

(b)

Figure 3.1 (a) Localised bond and (b) MO representations of phosphine. The e-symmetry MOs are doubly degenerate.

obtained from a HF calculation. This is because, not unexpectedly, the nature of the MOs changes drastically when the electronic structure is altered in the above way. Hence, in order to obtain an estimate of the excitation energy two total energy calculations have to be carried out, one each for the ground and excited states. The difference between these results will give an estimate of the excitation energy, subject to the limitations of the one-electron approximation and the calculational method used. The above effect must be kept in mind when discussing interactions between orbitals.

In this thesis the emphasis is on molecular orbital models although the localised bonding model will occasionally be used to illustrate some points. Localised bonds are conceptually simple and provide a simple picture of the bonding of an atom to a molecule or surface.

3.4 Semiempirical MO Calculations

Two particular methods based on this approach to the electronic structure problem are used extensively in this thesis, MINDO/3 [3.11] and MNDO [3.12]. These are based on the INDO (Intermediate Neglect of Differential Overlap) and NDDO (Neglect of Diatomic Differential Overlap) approximations which are discussed in detail in the classic text on semi-empirical techniques by Pople and Beveridge [3.6]. MINDO/3 and MNDO were both developed by Dewar and co-workers and have been widely used in studies of molecules and surfaces.
Semi-empirical techniques are often criticised by exponents of ab-initio methods, criticisms which have been rebuked by Dewar. There is no doubt, however, that MINDO/3 and MNDO give good results for the bond energies and electronic structure of a wide range of molecules. They are particularly useful in studies of surfaces since large clusters of atoms can be used (see chapter 5.

For both the first and second row atoms MNDO normally gives bond lengths accurate to about 0.05 Angstrom and bond angles to about

2^{o}. These figures are perfectly adequate for the applications discussed in this thesis. The actual accuracy obtained is dependent on the atoms involved and is often much better than the above values. Extreme caution must be exercised , however, when using MINDO/3 and MNDO to obtain bond energies since both methods often overestimate the strength of a bond. This is particularly true for MNDO calculations on unusual bonds involving Be (an area which is relevant to the work in chapter 6). In this thesis such cases have been studied using both MNDO and ab-initio calculations.

3.5 Interactions between Molecular Orbitals

3.5.1 Perturbation Theory

In principle an ab-initio calculation could be performed on every new molecule that is identified experimentally. However, it is more profitable to elucidate the primary factors affecting the orbital interaction energies and hence attempt a global view of the electronic structure problem. The use of perturbation theory (PT) is fundamentally important in this problem. If the solution of the Schrodinger equation is known for a particular system, then the new orbital energies and wavefunctions caused by a perturbation H' are readily obtained using PT. To second order, the energy of the i^{th} level ϵ_i' as a result of the perturbation is given by [3.13] ;

$$\epsilon_i' = \epsilon_i + \sum_{j,j\neq i} \left| \int \psi_i \, | H' | \, \psi_j \, d\tau \right|^2 / (\epsilon_i - \epsilon_j) \qquad (3.4)$$

Where the ϵ_k are the unperturbed energy levels and ψ_k their wavefunctions. Two basic rules governing the interactions are (i) only orbitals of the same symmetry may interact, otherwise the integral in the numerator of (3.4) will be zero, and (ii) when two levels interact, the lower one is stabilised (i.e. drops in energy) and the higher one is destabilised (i.e. rises in energy).

Perturbation theory may be applied to orbitals interacting on the one molecule or on different molecules. Only the latter will be

considered here since the former is discussed in detail in chapter 5.

3.5.2 Energy of the Interacting Molecules

Consider two interacting molecules, A and B. Using perturbation theory the total energy can be written as [3.4] ;

$$(3.5) \qquad E = E_A^{\,o} + E_B^{\,o} + \langle \psi_{AB}^{o} \mid H' \mid \psi_{AB}^{o} \rangle + \sum_k \langle \psi_{AB}^{o} \mid H' \mid \psi_{AB}^{k} \rangle / (E_A^{\,o} + E_B^{\,o} - E_{AB}^{\,k})$$

Where $E_A^{\,o}$ and $E_B^{\,o}$ are the energies of the isolated molecules. The third term is the first-order perturbation energy. This is a positive, i.e. repulsive, energy term due to the overlap between the occupied orbitals of the two molecules. ψ_{AB}^{o} is the ground state wavefunction for the combined system.
The final term is the second-order stabilisation energy due to the interaction between the occupied and empty MOs. By rule (ii) given in the previous section this will stabilise the occupied orbitals and hence will lower the energy. Note that equation (3.5) is valid only for small H' and closed -shell molecules. If the second-order energy is greater than the first-order then a bond will form, known as a Donor-Acceptor (DA) bond.

The two main criteria influencing the stabilisation energy, and hence the strength of a DA bond, are the energy separation and the overlap of the interacting orbitals [3.4]. Hence it is usually the highest occupied molecular orbital (HOMO) and the lowest unoccupied molecular orbital (LUMO) which dominate the reaction. In order for there to be a significant lowering of the energy the separation between the interacting MOs must be of the order of 6 eV or less, as measured by the difference in HF orbital energies.

Donor-Acceptor reactions are characterised by a formal transfer of electrons from one of the reactants to the other. They are usually relatively weak compared to the bonds within the

reactants. A good example of a simple DA bond is the H_3N-BH_3 system [3.14]. The localised bond description of NH_3 is the same as that for PH_3 (see Fig. (3.1)), while the isolated BH_3 molecule is planar due to the dangling bond being empty. A formal transfer of two electrons from the HOMO of NH_3 to the LUMO of BH_3 results in a Donor-Acceptor interaction. This is also easily understood in the localised bond formalism where the empty dangling orbital receives charge from the full dangling orbital.

3.5.3 The Frontier Orbital Method

This is a method proposed by Fukui [3.15] for predicting the most probable mode of interaction of two molecules from the relative density of the "frontier" electrons in the HOMO, and their overlap with the LUMO on the other molecule. This method, like PT, has mainly been applied to organic chemical reactions but is equally applicable to inorganic systems. A good example of the use of Frontier Orbital Theory is the addition of ethylene (C_2H_4) to butadiene (C_4H_6) [3.1]. The interacting MOs are shown pictorially in Fig. (3.2)a and Fig. (3.2)b. The MO diagrams deduced using PT are shown in Fig. (3.3). As stated in section (3.5.1), only MOs of the same symmetry can mix. This criterion can also be described in terms of overlap (as is observed in Fig. (3.2)), i.e. the symmetry considerations enter into the analysis in an indirect way.

Fig. (3.3)a shows the first-order orbital interactions which are repulsive in nature. It is these interactions which lead to the activation barrier for the reaction. Comparison with Fig. (3.3)b shows that the effect of this is to narrow the energy separation between the MOs which are involved in providing the stabilisation energy. Note that these are the second-order interactions which result from the overlaps shown in Fig. (3.2). For this reaction the second-order eventually becomes dominant and a bond is formed. However, if the energy separation is too large then the repulsion energy will dominate and no bond will form.

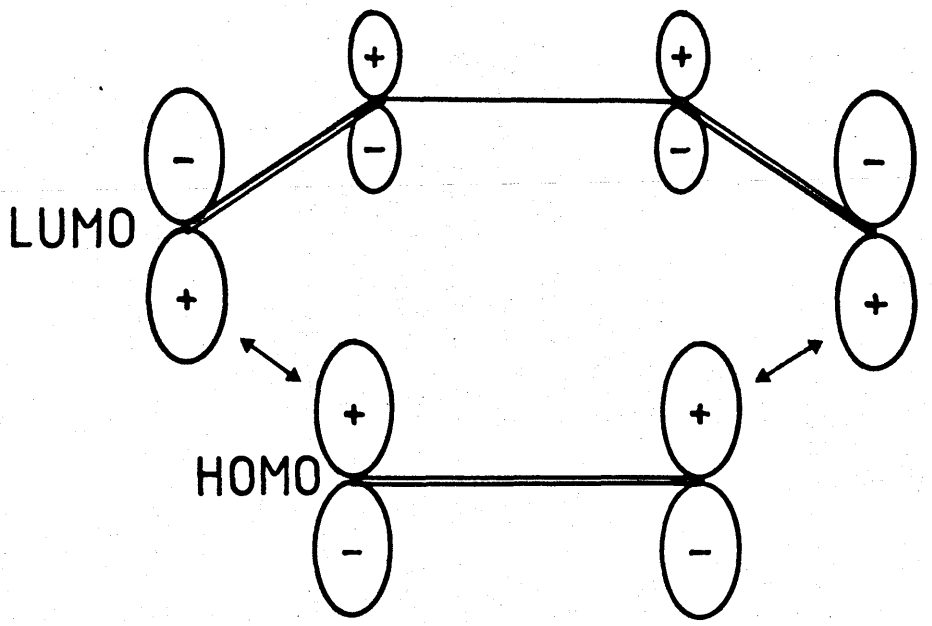

(a)

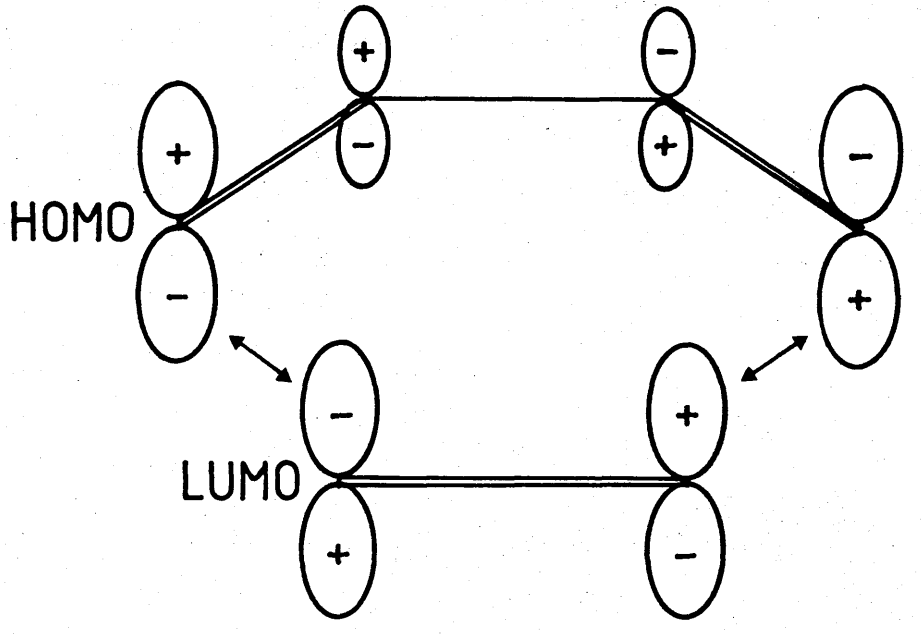

(b)

Figure 3.2 Topologies of the MOs involved in the addition of butadiene and ethylene.

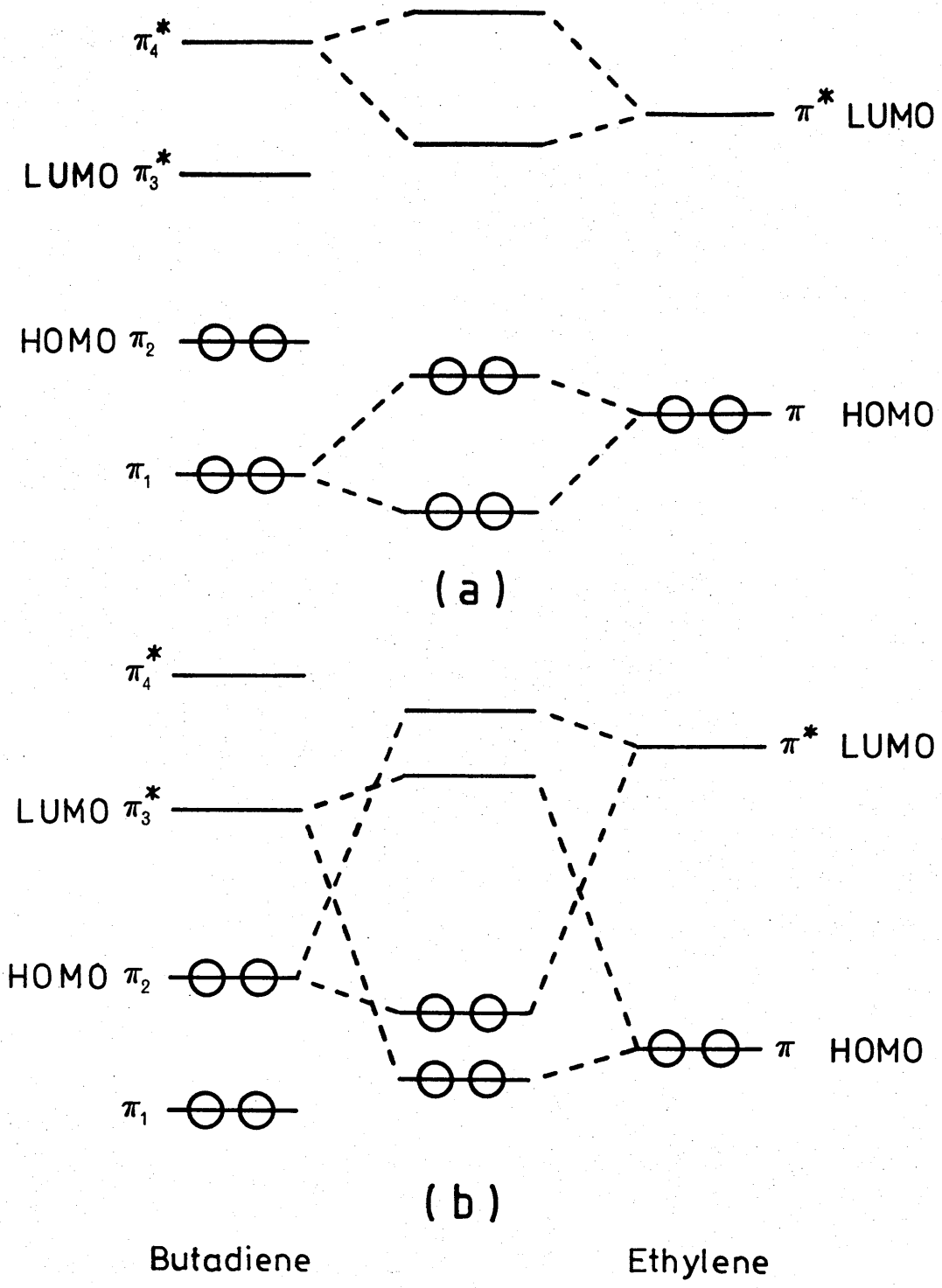

Figure 3.3 Orbital interaction schemes from perturbation theory for the addition of ethylene and butadiene, (a) first-order and (b) second-order.

The reaction considered above is one of the simpler examples of the use of Frontier Orbital Theory since no bonds are broken. The method is equally applicable, however, to more complex reactions since the same principles of overlap and energy separation will apply. A chemical bond can be broken in two ways (i) injection of charge density into an antibonding orbital or (ii) removal of charge density from a bonding orbital. There are numerous examples which illustrate this and one which is of particular relevance to this thesis is that involving a diatomic molecule.

This will be discussed more fully in chapter 6, details of other reactions being given in the book by Salem [3.1] and the article by Klopman [3.3].

Frontier orbital theory has also been applied to reactions involving free radicals, although with less success [3.1]. The difficulty lies in the fact that the singly-occupied molecular orbital (SOMO) on the radical can interact with both the LUMO and the HOMO on the closed-shell molecule. Which of these reactions predominates is often not clear since the energy separation can be similar. This type of interaction is of importance to the work in this thesis due to the presence of a free-radical-type site on the GaAs (100)-(2 X 4) surface [3.16].

3.6 Symmetry Effects in Chemical Reactions

As was briefly mentioned in section (3.5) symmetry considerations play an important role in determining the outcome of a particular reaction. The examples considered so far have only involved the topological properties of the interacting MOs. There are, however, some more specific factors which must be taken into account and these are best illustrated by considering the following reaction [3.4] ;

(3.6) $$H_2 + I_2 = 2HI$$

Initially it was assumed that this reaction took place via a

broadside collision with a four-centre transition state. However, it was shown experimentally that this is not the case but rather that the reaction takes place over a number of steps. The reason for this is now demonstrated : Fig.(3.4) shows a MO correlation diagram for the broadside approach of the two molecules. On the left side is the electronic structure of the separated reactants and on the right that for two separated HI molecules. H_2I_2 is the activated complex which is formed at the transition state. Note that the point group symmetry of the broadside attack is C_{2v} and that the MOs in Fig. (3.4) are labelled accordingly.

The fundamental rule which must be remembered when constructing correlation diagrams is that an MO on the reactants must correlate with an MO on the products which has the same symmetry. Note that care must be taken when correlating the MOs of the same irreducible representation since the topological evolution must also be taken into account.

From Fig. (3.4) it is observed that the σ_g orbital of the H_2 molecule, which is occupied, correlates with the σ^* orbital of 2HI, which is unoccupied. Hence the ground state of H_2+I_2 correlates with a doubly excited configuration of 2HI. Only the b_2 and a_1 MOs of the activated complex are shown in Fig. (3.4) since these are the only ones which cross.

This crossing of an occupied and an unoccupied MO leads to a large activation barrier as is illustrated by the large rise in energy of the σ_g orbital. The activation barrier could be reduced if there were empty orbitals of a_1 symmetry with which mixing could take place.

In practice the orbitals will not cross because configuration interaction will lead to a gradual mixing-in, and eventual dominance, of the doubly-excited configuration. The behaviour observed can also be understood in terms of overlap as is demonstrated in Fig. (3.5). This again illustrates the importance of the frontier orbital topologies.

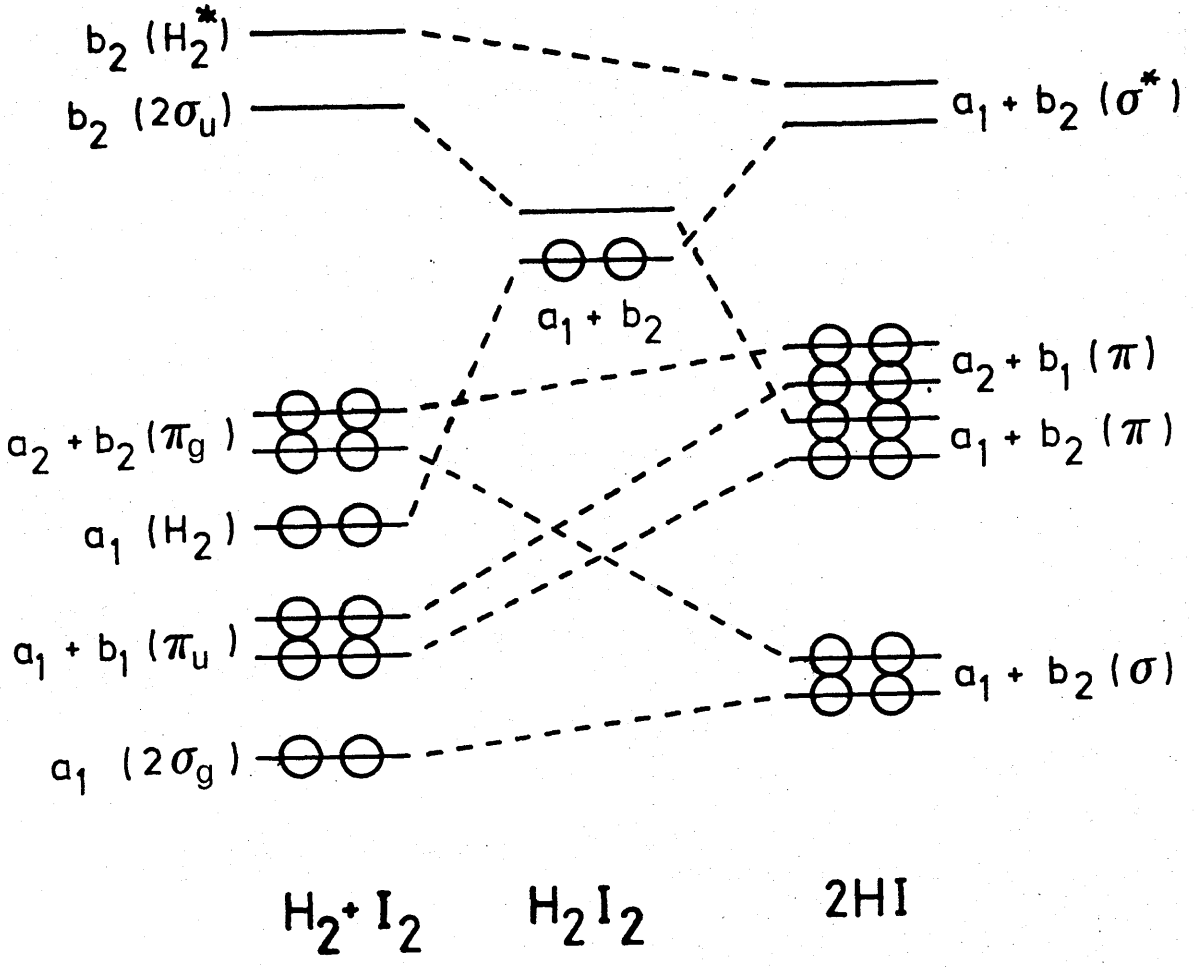

Figure 3.4 MO correlation diagram for a broadside approach of $H_2 + I_2$. C_{2v} symmetry is preserved throughout (σ_g and σ_u orbitals of I_2 not shown). Note that only the crossing MOs of the transition state are shown.

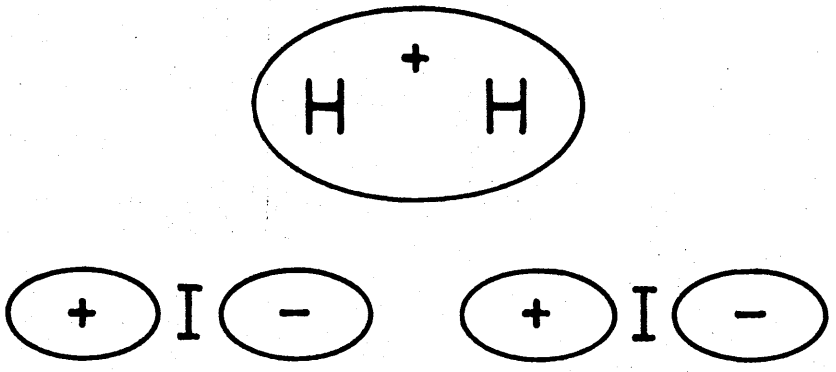

(a)

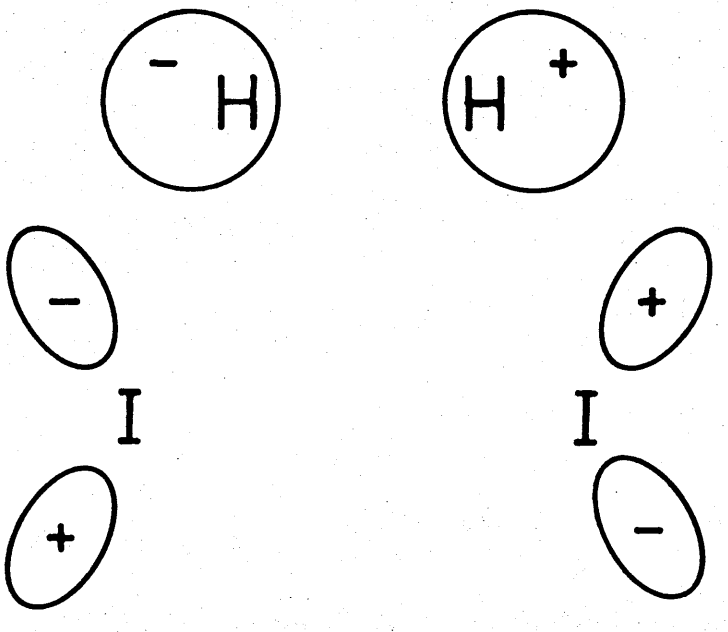

(b)

Figure 3.5 Topologies of the Frontier Orbitals of H_2 and I_2.

3.7 Application to Surfaces

The techniques mentioned so far have been developed for studying reactions between small molecules in the gas-phase. The application of these methods to reactions in solid surfaces has been rather limited, although in principle many of the concepts should be transferable. This will be discussed in more detail in the following chapter.

CHAPTER 4

PROPERTIES OF SOLID SURFACES

4.1 Introduction

The discussions in the two preceeding chapters have illustrated the complexity of the processes encountered in MBE growth and it is now appropriate to discuss some of the properties of solid surfaces, an understanding of which is necessary for modelling the growth processes.

The termination of a solid by a surface results in changes in the bonding and electronic structure, both being intermediate between that of the bulk crystal and the free atom. Since the surface atoms are unable to complete their full complement of possible bonds, being surrounded by fewer neighbours, the creation of a surface requires energy. Some of this energy can be regained, however, by displacements of the surface atoms away from their bulk positions. The types of change in physical structure observed will be discussed in more detail in section 4.2.

The electron wavefunctions at surfaces are drastically altered due to the need to match the Bloch functions in the bulk to the vacuum, giving additional solutions to the wave-equation [4.1]. These additional solutions are known as surface states surface states and are localised perpendicular to the surface. This localisation leads to them having a significant effect on the atomic structure.

4.2 Relaxation and Reconstruction

These are the two types of change observed in the surface atomic structure, the extent to which either occurs being dependent on the type of crystal. Relaxation involves a simple movement of the surface atoms, the surface space-symmetry being conserved. Reconstruction, on the other hand, implies a change in the surface space-symmetry and often involves drastic changes in the bonding (particularly on semiconductors). Simple metals do not

exhibit reconstruction due to the non-directionality and extreme delocalisation of the bonding. Relaxation is observed, however, and takes the form of a uniform movement of the surface plane of atoms towards the bulk [4.2]. The reason for this is best illustrated by considering the change in the electronic charge distribution at the surface. The decay of the charge density into the vacuum leads to an asymmetry in the charge surrounding a surface atom which in turn alters the electrostatic "centre-of gravity". Hence the surface atoms (or more correctly the surface ions) will now feel a nett field which will cause a movement to the new electrostatic centre-of-gravity.

This decaying of the charge density obviously also occurs on transition metal and semiconductor surfaces. On these surfaces, however, the situation is considerably more complex due to the directional character of the bonding, this directional character obviously being greatest on the semiconductor surfaces. The directional character of the bonding leads to changes in surface space-symmetry because the atoms are no longer restricted to move in a direction normal to the surface. This is usually the source of the reconstructions on transition-metal surfaces.

On semiconductor surfaces another possibility exists, namely the formation of new bonds between surface atoms [4.3]. This will be favoured particularly on those surfaces with a greater number of dangling bonds, such as the (100) orientation.
Yet another possibility is the formation of surface vacancies [4.4], a mechanism which can occur on both transition-metal and semiconductor surfaces. A combination of the above mechanisms, together with various types of surface buckling, introduces a high level of complexity into the surface-structure problem.

A comprehensive review of the reconstructions observed on semiconductor surfaces has been given by Khan [4.3], although it should be noted that the detailed surface structure is, in most cases, not known. The most important orientation, from the viewpoint of MBE, is the (100). Reconstruction on (100) surfaces is the subject of chapter 5 and so will not be discussed in

detail here.

Finally, it should be mentioned that the overall surface structure is due to an interplay between short- and long-range forces. This is nicely illustrated by the behaviour of the reconstruction on the W(100) surface [4.2]. The surface atoms on W(100) undergo lateral displacements which increases the interaction with substrate. Above a certain temperature entropy considerations lead to a randomising of the lateral displacements. However, below this temperature an interaction between occupied and unoccupied surface states close to the Fermi energy, leads to a lowering of the energy of the occupied states (see chapters 3 and 5 for discussions of this type interaction), and hence the total energy.
Note that this coupling of states is not the only long-range force affecting the overall surface structure. On semiconductor surfaces in particular, more readily visualised influences such as substrate strain and repulsive interactions between dangling orbitals play a major role.
The role of long-range forces on semiconductor (100) surfaces will be briefly discussed in chapter 5.

4.3 Surface Electronic Structure

The calculation of the electronic structure of a solid surface is also a very complex problem, although such calculations are generally more successful than those for the total energy. The two most important pieces of information obtainable from these calculations are, (i) the energies and dispersions of the surface states and, (ii) the surface density of states.
Comparison of experimental and theoretical results is often used as a means of determining the geometry of a particular surface. Although quantitative results cannot be obtained in this way there have been many successes in that certain structures can often be ruled out. The details of such calculations are not important here, examples being given in references [4.2] and [4.5].

4.3.1 Methods of Calculation

Both momentum-space i.e. using Bloch functions, and cluster methods can be used to calculate the total energy and electronic structure of a particular reconstruction. By cluster methods is meant that a collection of atoms is used to mimic a part of the surface, the properties of the cluster being calculated using a quantum-chemistry method (see previous chapter). Obviously, in this approach only the effects of the nearest-neighbouring atoms can be taken into account and so the overall surface structure cannot be obtained. However, many properties of the surface which are relatively localised in nature, such as the bonding of an adatom and the local density of states, can often be investigated using this method. This is particularly true of semiconductor surfaces, provided a large enough cluster is used. Many workers have discussed the merits and drawbacks of the cluster approach, the present state-of-the-art being discussed in the articles by Goddard and McGill [4.6], Post and Baerends [4.7] and Simonetta and Gavezzotti [4.8].

Although, for example, the dispersion of a surface state can be obtained using a cluster calculation (e.g. the study on the Si(111) surface by Redondo et.al. [4.9]), the most popular approach involves the use of the momentum-space (i.e. k-space) methodology. There are many different calculational schemes in use, most being based on either tight-binding [4.5] or pseudopotential [4.10] models.
The calculation of surface properties using k-space methods has the advantage that the overall surface structure can be studied, and they usually provide the most direct comparison with the results of, for example, photoemission experiments [4.5]. Total energy calculations can also be carried out within this framework [4.11] and they are widely used in studies on semiconductor surfaces [4.12].

Another advantage of k-space methods is that surface states are rigourously defined through the need to satisfy the boundary conditions for the wavefunctions at the surface. As mentioned in the introduction, the change from the periodic boundary conditions to surface boundary conditions can introduce a type of solution in which the electrons are bound to the surface and have a large density near the surface atoms. This density decays exponentially towards the bulk of the crystal.

In cluster calculations the correspondence between the cluster orbitals and the surface states is often unclear. In the studies described in this thesis (chapter 5) this difficulty is overcome by comparing the cluster orbital topologies with those (given in the literature) obtained using a k-space method.

Despite the above advantages there are significant drawbacks in using k-space methods in studies of surface reactions. At best the final geometries can be obtained, although even this is not always possible.
In this, a similar situation to that mentioned in chapter 3, regarding the geometries of small molecules, is encountered in that physical insight into the processes determining the properties of the surface is usually lacking.

The obvious step is to apply the qualitative models described in chapter 3 to surface studies. However, very little work has been carried out along these lines, particularly with regard to semiconductors. The natural approach to take in this case is the cluster calculation.

4.4 Applicability of MO Models to Surface Studies

The breaking of a bond can be achieved in either of two ways, (i) removal of electron density from a bonding orbital, or (ii) insertion of electron density into an anti-bonding orbital. Both can be achieved simultaneously in a molecule by exciting an electron from its bonding to its corresponding antibonding

orbital. This can lead to decomposition of the molecule (i.e. a unimolecular reaction).
The analogous excitation in a semiconductor is when an electron is excited from the valence band (bonding) into the conduction band (antibonding). However, in this case the destabilising effect is spread over all the bond because the conduction bands are delocalised throughout the solid. Hence, there is a negligible effect on the structure of the solid.

The surface states on a semiconductor are intermediate between these two extremes, and this is apparent from the effect of adsorbates on the surface structure. For example, the delocalised nature of the surface states is demonstrated by the altering of the reconstruction on the GaAs (100) surface by sub-monolayer deposition of Pb or Sn.
This delocalisation will reduce the effect of any insertion of charge into, say, the dimer σ-antibonding orbital (see chapter 5). However, the same principles for breaking bonds must apply, otherwise no chemical reactions would take place on the surface.

The fact that adsorption on surfaces is governed by the type of topological considerations discussed in chapter 3 is illustrated by the interaction of ethylene (C_2H_4) with an aluminium surface. Al is a simple sp-bonded metal and hence is reasonably well represented by a free-electron gas confined to a half-space by an infinite barrier. The orbital interaction diagram for the system is shown in Fig. 4.1 along with the HOMO and LUMO of ethylene. Note the large energy difference between the ethylene HOMO and LUMO as obtained from the HF model (see section 3.3, chapter 3). The inner potential, E_I, for Al is -0.5834 a.u. and the Fermi level E_F is -0.1544 a.u., as shown in the figure (1 a.u. = 27.21 eV).

A full analysis of this system has been given by Grimley [4.13] and only a summary of the important conclusions will be given here. The actual analysis given by Grimley utilises k-space methodology and involves expressing an approximate many-electron wave-function as a summation of the unperturbed wave-function

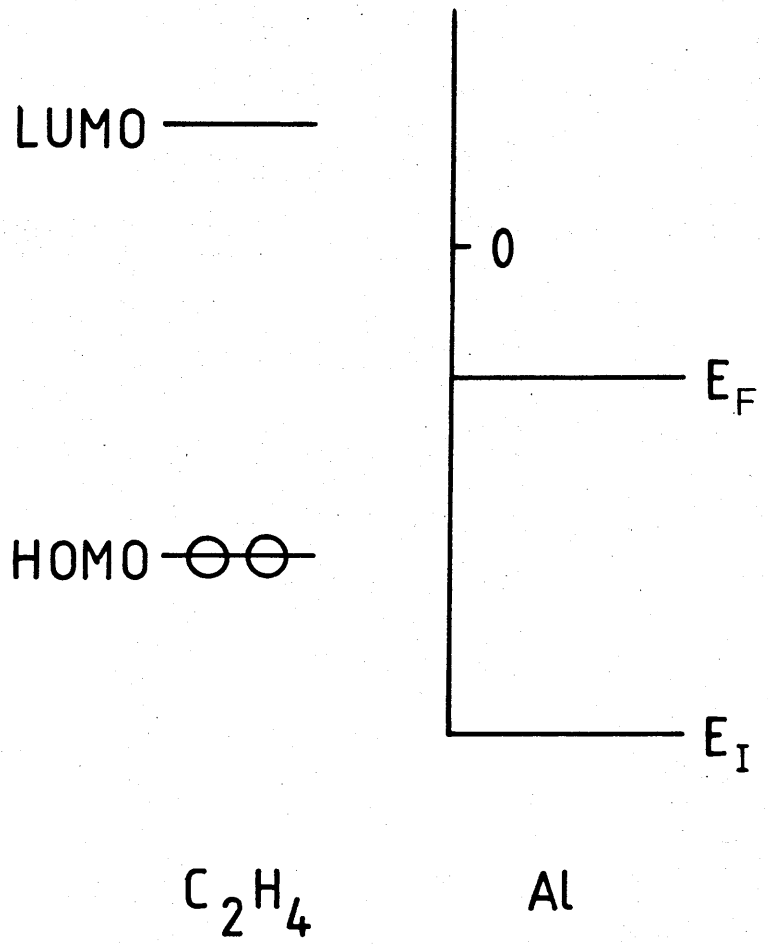

Figure 4.1 Orbital interaction diagram for C_2H_4 on an Al surface.

$\psi(C_2H_4,Al)$ for the no-bond state with the wave-functions for the two charge-transfer states, $\psi(C_2H_4^+,Al^-)$ and $\psi(C_2H_4^-,Al^+)$. Already the necessity for good overlap would be intuitively expected in order that the contribution from the charge-transfer states be significant. The equation for the total energy is ;

$$(4.1) \qquad E = E_o + \sum_{k<k_f} |U_{ok}|^2/\epsilon_k - \epsilon_{LUMO} + \sum_{k>k_f} |U_{ok}|^2/(\epsilon_{HOMO} - \epsilon_k)$$

where E_o is the energy of the separated system, $k<k_F$ and $k>k_F$ denote states below and above the Fermi level respectively and the ϵ denote the energies of the states or orbitals.

In the present analysis it is assumed that C_2H_4, $C_2H_4^+$ and $C_2H_4^-$ are all described by the same MOs (the rigid orbital approximation). Hence in equation (4.1), U_{ok} is an interaction between a metal orbital, k, and one of the frontier orbitals of ethylene. If $k>k_F$ then the interaction is with the HOMO, and with the LUMO if $k<k_F$. This is to be expected from the discussion in chapter 3 regarding HOMO-LUMO interactions for small molecules, equation (4.1) being basically similar to equation (3.5).

It is U_{ok} which is strongly dependent on the overlap of the interacting orbitals, and is in fact often taken to be directly proportional to it in qualitative discussions of chemical bonding. This is the case in the present analysis. Subsequent manipulation of the equations leads to the definition of the spectral densities of the HOMO and LUMO in the substrate eigenstates ;

$$(4.2) \qquad \rho_{LUMO}(\epsilon) = \sum_k |\langle LUMO|k\rangle|^2 \delta(\epsilon - \epsilon_k)$$

$$(4.3) \qquad \rho_{HOMO}(\epsilon) = \sum_k |\langle HOMO|k\rangle|^2 \delta(\epsilon - \epsilon_k)$$

where $\langle LUMO|k\rangle$ and $\langle HOMO|k\rangle$ denote the overlaps between the Al eigenstates, k, and the LUMO and HOMO respectively. If ρ_{LUMO} has little of its density in the occupied substrate states and ρ_{HOMO} has little of its density in the unoccupied substrate

states then the energy lowering due to the last two terms in (4.1) will be insignificant and no bond will form, i.e. the ethylene will not chemisorb.

Before calculating the spectral densities it is first necessary to define a chemisorption geometry. The most likely configuration is shown in Fig. (4.2)a. This is the one used by Grimley and the resultant spectral densities given by him are reproduced in Fig. (4.2)b. From this it is observed that there is indeed little of ρ_{LUMO} in the occupied states and little of ρ_{HOMO} between E_F and the vacuum level.

This weak interaction can be readily understood in terms of the overlap considerations discussed in chapter 3. For example, ρ_{LUMO} will be large where there are metal states with large amplitude but opposite sign at two points on the surface separated by 0.133 nm (i.e. the C=C bond length in ethylene). Likewise, ρ_{HOMO} will be large when there are metal states with the same sign at these points. Obviously these conditions cannot be met by the free-electron substrate utilised in the present analysis.

The situation is changed completely, however, if the chemical properties of the Al states are introduced. In this case the Al $3p_y$-orbitals (lying parallel to the surface plane) have the same symmetry as the ethylene LUMO while the Al 3s-orbitals and $3p_z$-orbitals (normal to the surface) have the same symmetry as the ethylene HOMO. Hence the topological requirements can be satisfied and a bond can form. Experimentally, ethylene does in fact bond to the {001} surface of Al.

Although the above discussion has been qualitative it clearly illustrates the, not unexpected, important role played by orbital topology in bonds to solid surfaces. A logical extension of this is to apply these concepts to bonding on semiconductor surfaces in an effort to illuminate certain aspects of MBE growth. It is this with which chapter 6 is concerned.

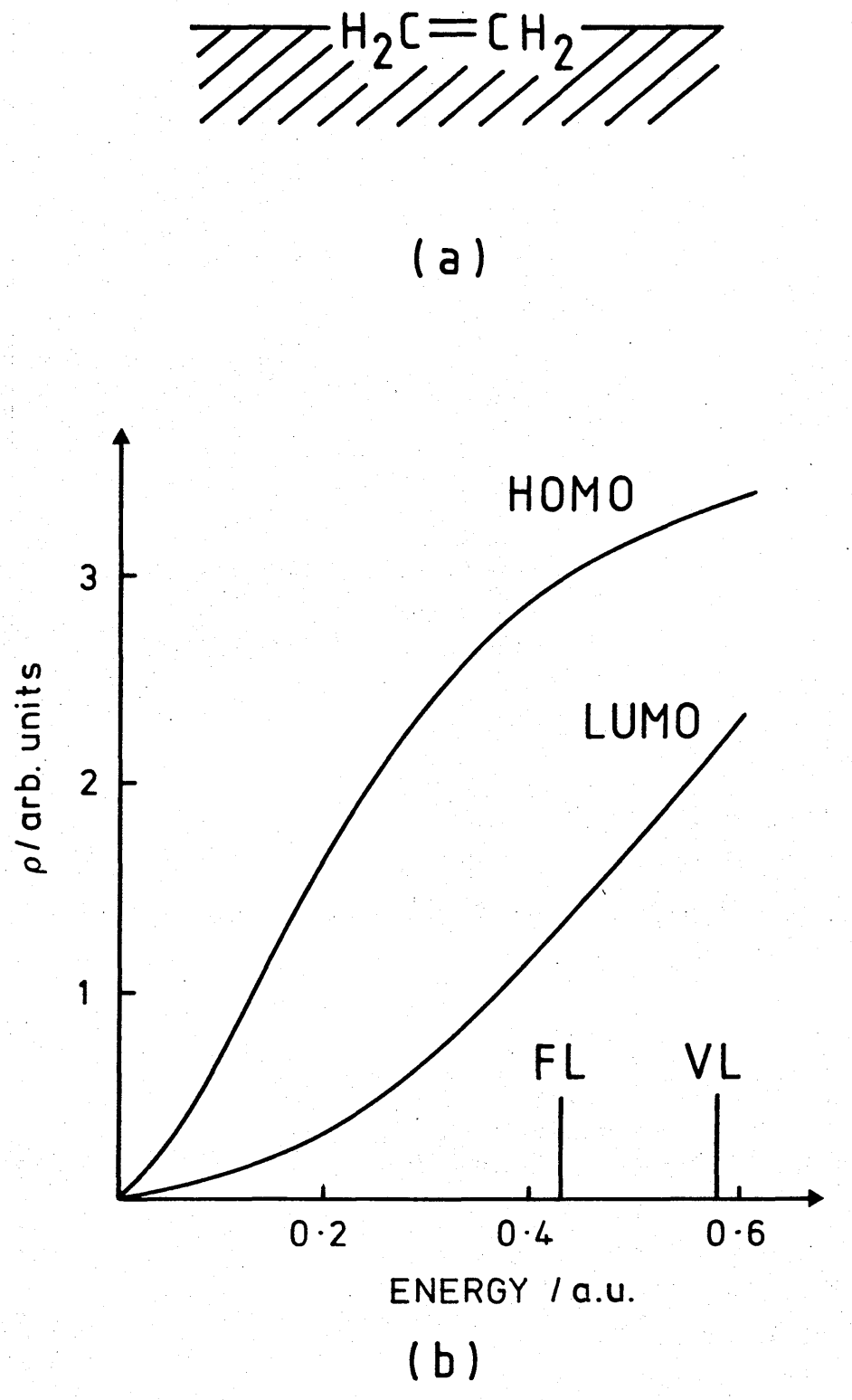

Figure 4.2 (a) Probable adsorption geometry for ethylene on Al and (b) Spectral densities of the ethylene Frontier Orbitals in the electronic states of the Al.

CHAPTER 5

THE NATURE OF THE DIMER ON (100) SURFACES

5.1 Introduction

A rich range of reconstructions is observed on the (111) and (100) surfaces of the A^NB^{8-N} semiconductors [5.1], the actual structure observed usually being strongly dependent on the method used for preparing the surface. For example, the reconstruction on the GaAs (100) surface is a complex function of temperature and As-overpressure [5.2], these being the factors determining the surface stoichiometry. For a particular stoichiometry the arrangement of the surface atoms is dependent on the interactions between them. Note, however, that a wide variation in the stoichiometry can be observed for a particular reconstruction.

In the case of the III-V semiconductors, most effort in the past has been directed at the (110) surface, being the easiest to understand since it undergoes only relaxation. This orientation is, however, of little technological importance. The (100) surface, as well as being the most technologically important, is also the most complex. Little is known about the detailed atomic arrangements for the various reconstructions observed, and this leads to extra difficulties when trying to understand the adsorption of atoms and molecules on this surface.

5.2 The Surface Dimer

Shown in Fig. (5.1) is a section of the unreconstructed (100) surface, i.e. the surface atoms are at their bulk positions. The surface symmetry in this case is (1 X 1). The best understood of the (100) reconstructions are the Si (100)-(2 x 1) and GaAs (100)-(2 x 4). In both cases the two-fold periodicity has been shown to be due to dimerisation of surface atoms [5.3] [5.4]. This is depicted in Fig. (5.1) where the two surface atoms move to form a new bond (lying in the surface plane). The surface dimer would appear to be the basic unit involved in many (100)

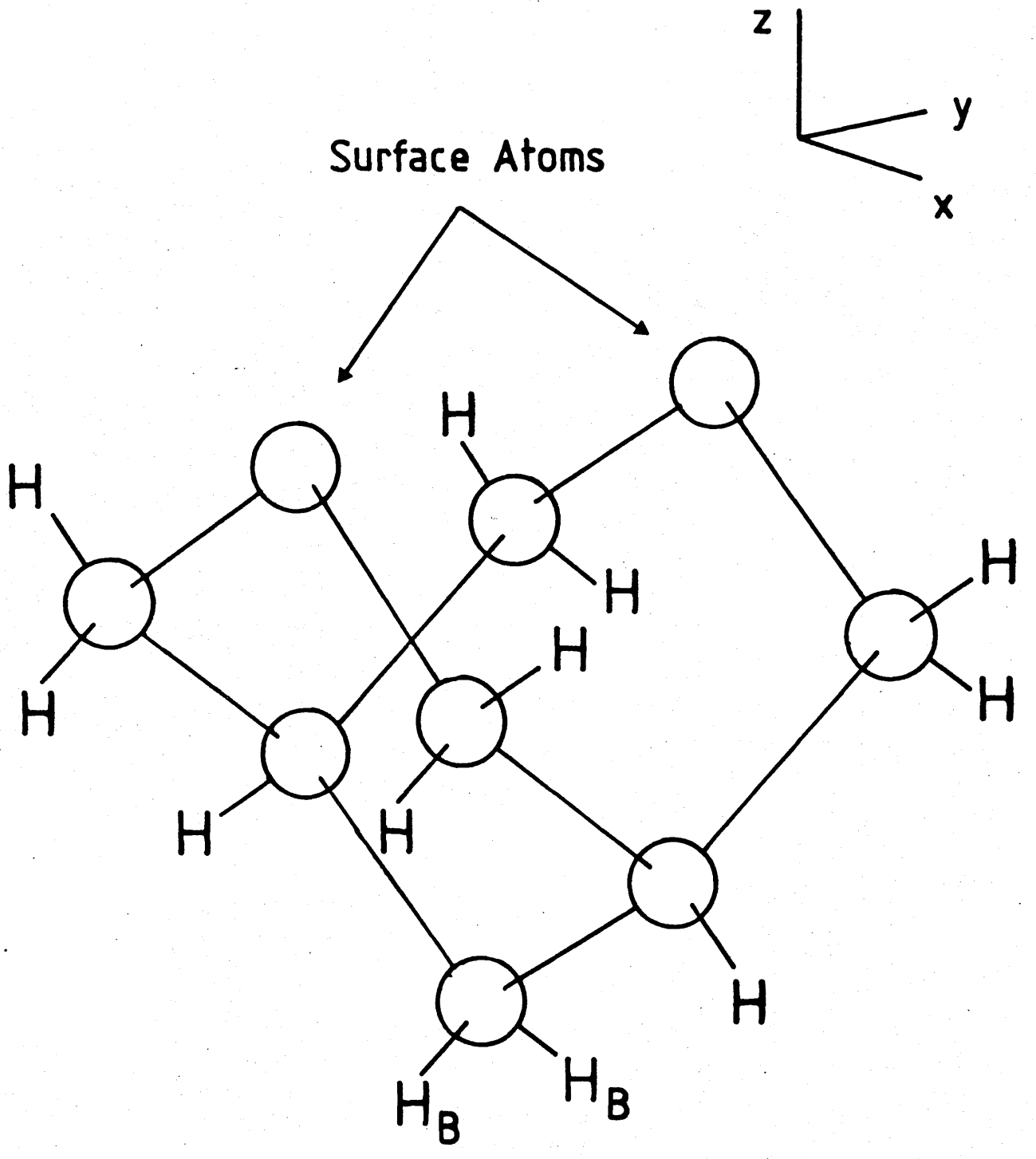

Figure 5.1 Section of the first four layers of a semiconductor (100) surface. This cluster of atoms is useful for studying the surface dimer. The Hydrogen atoms are used to tie-off any dangling bonds.

reconstructions, the different structures being due to the different possible arrangements of the dimers.

Although the existence of the surface dimer is now well established there is still controversy as to its precise geometry. The two basic structures possible are the symmetric and asymmetric dimers [5.5], shown in Fig. (5.2)a and (5.2)b respectively using the localised bond representation. An asymmetric dimer has been proposed for the Si(100)-(2x1) surface on the basis of LEED data [5.3], and is also required to satisfactorily explain the GaAs (100)-(2 x 4) reconstruction [5.4]. Many total energy calculations (both tight-binding and cluster) have been carried out and it is probably true to say that the weight of evidence is in favour of the asymmetric dimer.

Despite the extensive number of theoretical investigations in the literature, the physical driving force behind the distortion of the dimer has never been adequately studied. It is this problem with which this chapter is mainly concerned, and it will be shown that the tilting of the dimer can be understood using Molecular Orbital concepts. The role of long-range forces in determining the overall reconstruction will also be discussed.

The electronic structure of the surface is calculated using a cluster approach, as described in chapter 4.

Some of the reconstructions which can be obtained using the asymmetric dimer are shown in Fig. (5.3).

5.3 The Second-Order Jahn-Teller Effect

The mechanisms which have been quoted in the literature as being the cause of the tilted dimer are (i) the Jahn-Teller (J-T) distortion due to degenerate electron states [5.6] and (ii) the Peierls distortion [5.7] (i.e. band-structure analogue of the J-T effect). An important point which must first be clarified here is that there are no degenerate states either on the cluster used by Verwoerd [5.6] (which has a C_{2v} point group) or on the real

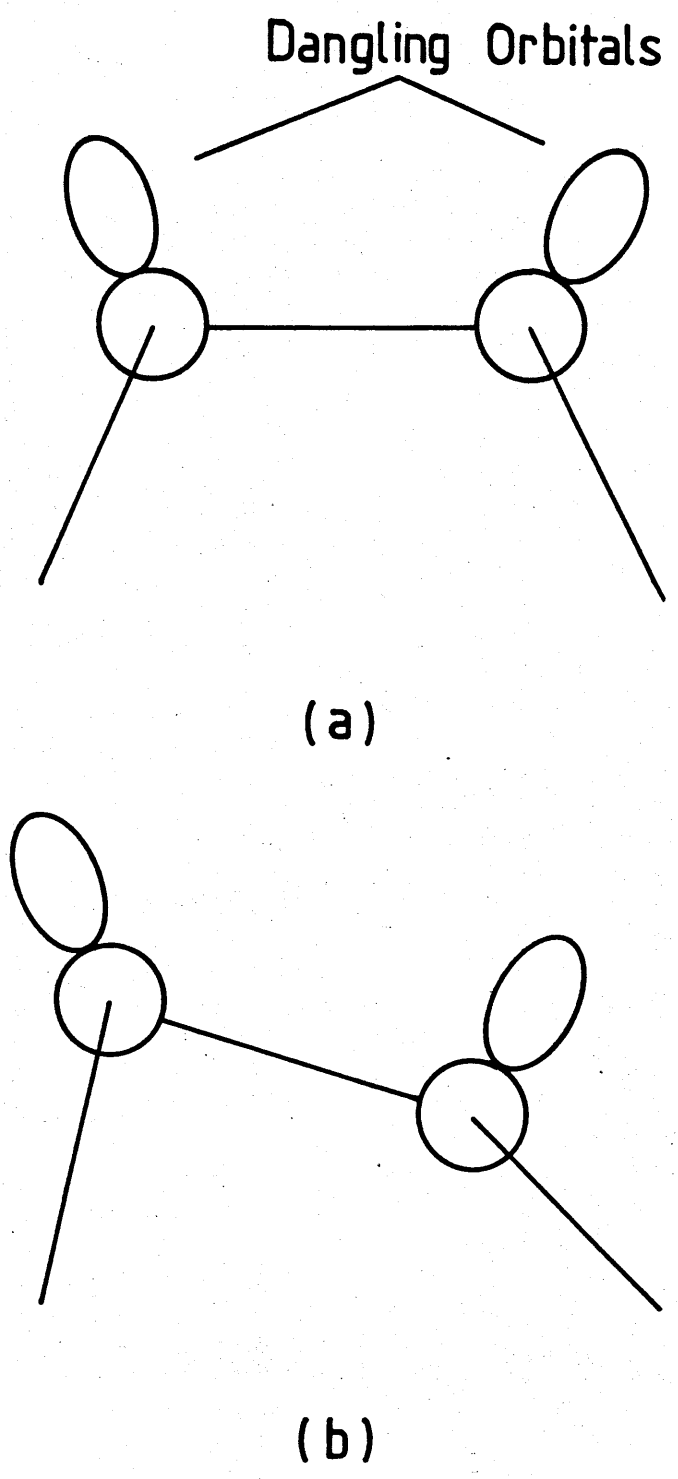

Figure 5.2 Side elevations of the (a) symmetric (b) asymmetric dimers.

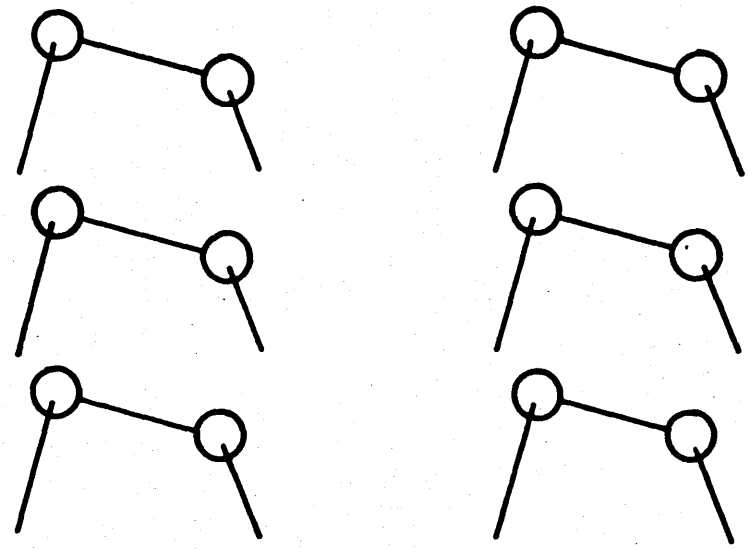

(a)

(2 × 1)

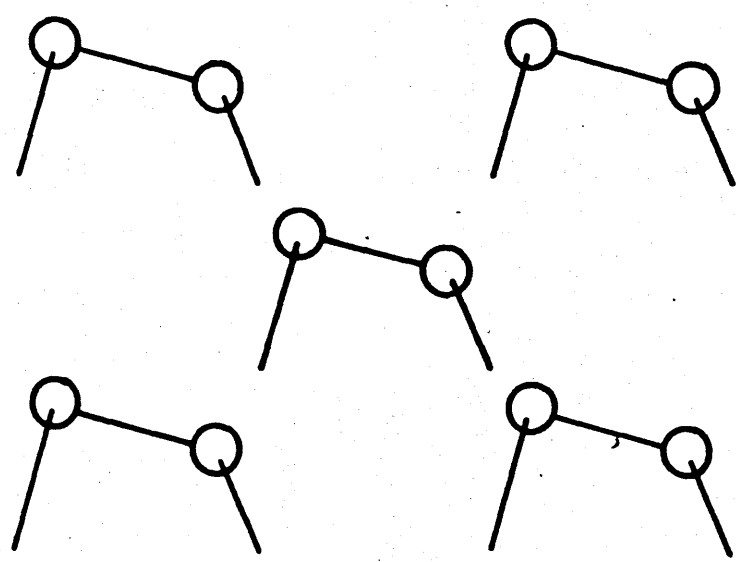

(b)

C(2 × 2)

Figure 5.3 Two possible reconstructions on a (100) surface derived from asymmetric dimers.

surface (the local symmetry of the surface dimer is also C_{2V}). In the light of this the explanation involving the Jahn-Teller effect is seen to be erroneous. The J-T effect is the most widely known mechanism which leads to distortions in molecules and solids, but it is not the only one. In order to gain insight into this problem consider the following analysis which is due to Pearson [5.8].

What is required is an expression relating the energy, E, of a system of atoms to its position, Q, on a potential energy surface. An initial point Q_o is chosen and the nuclei are moved a small distance Q along the reaction co-ordinate. Second order perturbation theory is then used to calculate the new ground-state energy. After the distortion the Hamiltonian is written as a Taylor-MacLaurin series ;

$$(5.1) \qquad H = H_o + (\partial U/\partial Q)Q + {}^1/_2(\partial^2 U/\partial Q^2)Q^2 + \ldots.$$

where H_o is the unperturbed Hamiltonian, U is the nuclear-nuclear and nuclear-electronic potential energy and Q is the small displacement along the reaction coordinate. The energy is given by ;

$$(5.2) \qquad E = E_o + \langle\psi_o|\partial U/\partial Q|\psi_o\rangle Q + \langle\psi_o|\partial^2 U/\partial Q^2|\psi_o\rangle Q^2/2 + \Sigma\,[\langle\psi_o|\partial U/\partial Q|\psi_k\rangle Q]^2/(E_o - E_k)$$

where E_o is the energy at the point Q_o, the second and third terms are the first-order perturbation energy and the final term is the second-order perturbation energy. Note that since this is a perturbative approach the distortions must be small. However it can be applied at each point along the reaction coordinate, hence overcoming this restriction. It is important to note that the different terms in (5.2) are symmetry dependent i.e. certain symmetry conditions must be satisfied for the integrals to be non-zero. This symmetry dependence is useful in that it provides information on the symmetry properties of the potential energy surface.

The terms in (5.2) which are responsible for the molecular distortions are the second and the last terms, (the third term is always positive and provides a restoring force which opposes the distortion). Consider the second term. The wavefunction ψ_o can be either degenerate or non-degenerate. From simple group theory, the direct product of a degenerate wavefunction with itself will always contain the totally symmetric representation plus at least one other symmetry species. Jahn and Teller [5.9] have shown that there will always be at least one non-symmetric vibrational mode of the molecule that has the same symmetry as ψ_o^2 . Distortion of the molecule along this mode always lower the total energy, leading to the destruction of the original symmetry and also the degeneracy of ψ_o. If there are no degenerate levels then the term linear in Q disappears. The above is known as the First-Order Jahn-Teller (FOJT) effect.

The final term in (5.2) always lowers the energy because E_o-E_k, where E_k is the energy of an excited state, is always negative. The value of the integral will be non-zero only if the integrand is non-zero and for this to be the case the following must apply;

$$\Gamma_{\psi_o} \times \Gamma_{\psi_k} \subset \Gamma_Q \tag{5.3}$$

i.e. the symmetry species obtained from the product of the wavefunctions must include that of the reaction coordinate. If this term is to lower the energy then it must be large enough to overcome the restoring force induced by the distortion (described by the third term in (5.2)). The two obvious factors which determine its magnitude are (i) the integral discussed above and (ii) the energy differences E_o-E_k. Hence, for the distortion to lower the total energy there must be low-lying excited states of the correct symmetry. This is known as the Second-Order Jahn-Teller effect [5.10].

Usually in small molecules only excitations from the LUMO (ψ_i) to the HOMO (ψ_f) are considered [5.11]. In practice for there to be a significant interaction, the energy difference must normally be less than 5 eV. The possible magnitudes of the

distortions induced differ considerably for the above two mechanisms. The FOJT effect destroys the symmetry which originally leads to the distortion and therefore is small in magnitude, certainly much smaller than the distortions observed on semiconductor surfaces. The SOJT effect is different in that the interacting MOs, ψ_i and ψ_f, are of the same symmetry in the new point group. This means that they can continue to interact, hence giving the possibility of large distortions.

It is proposed in this chapter that the SOJT effect is the driving mechanism leading to asymmetric dimers on group IV and III-V (100) surfaces. Results obtained from cluster calculations which support this model will be presented in due course.

Although the geometries of many small molecules have been determined to a high degree of accuracy using ab-initio quantum chemical methods (see chapter 3), such an approach provides little physical insight into the operating mechanisms. Many models exist which attempt to describe molecular geometries qualitatively, with varying success. Most of these models utilise localised bond concepts. The SOJT effect described above has been used to successfully explain the geometries of a wide range of molecules, hence demonstrating the utility of MO concepts in such studies.

For the case of a solid surface the interacting states are delocalised and this introduces additional complications. The topologies of the surface orbitals will, however, be conserved to a large degree and so an MO approach should still be applicable. Unlike small molecules, the geometries of solid surfaces are not easily obtained using accurate calculations. Hence an understanding of the basic mechanisms is even more important in this case. The aim of the present chapter is to establish some justification for the tilted dimer using an MO approach, i.e. the SOJT effect.

5.4 The Transition Density

When considering the SOJT effect applied to large clusters it is convenient to analyse the distortions using the concept of a transition density. The transition density is the change in the electron density distribution caused by the mixing of the occupied and unoccupied states [5.12]. In order to simplify the analysis, assume that the only significant mixing is that between the HOMO and the LUMO, i.e. the ground state ψ_o mixing with one excited state ψ_k. Let the coefficient of mixing be λ. Since we are using perturbation theory λ is assumed to be small. The new wavefunction is ;

$$\psi = \psi_o + \lambda \psi_k \tag{5.4}$$

giving (since λ is small) ;

$$\psi^2 \approx \psi_o^2 + 2\lambda \psi_o \psi_k \tag{5.5}$$

The square of the wavefunction is an electron density and hence (5.5) can be written as ;

$$\rho = \rho_{oo} + 2\lambda \rho_{ok} \tag{5.6}$$

where ρ_{ok} is the transition density. Hence if a positive part of ψ_o overlaps a negative part of ψ_k then ρ_{ok} will be negative in that region of space.

The transition density, ρ_{ok}, will be positive and negative in different parts of the molecule, a positive value corresponding to an increase in electron density. The positive nuclei will be attracted to regions of increased electron density and will move away from regions of decreased electron density, the symmetry of ρ_{ok} being simply that of the product wavefunction $\psi_o \psi_k$. An example of the use of the SOJT effect and the transition density is given in section 5.12.

5.5 Factors Affecting The Choice of Cluster

Obviously the first decision to be made must be the choice of clusters to be used to model the (100) surfaces. There are several important factors to be taken into account at this point, the most important being the effects of the other "surfaces" on the cluster. In order to minimise these effects there must be no empty or full dangling orbitals on the other surfaces, otherwise there will be unoccupied MOs lying low in energy and occupied (non-bonding) MOs lying high in energy (low lying unoccupied and high lying occupied non-bonding MOs). Due to the comparably small energy difference between them, these MOs and those of the surface being studied, will mix to form new MOs resulting in distortions of the cluster. This leads to erratic behaviour in, for example, the total dimer energy of the surface being studied.

Hence the irrelevant surfaces of the cluster must be "tied-up" by attaching boundary atoms to all dangling orbitals. These boundary atoms must not themselves leave more dangling orbitals. The simplest case is that of the group IV elements. Due to them being tetravalent, each sp^3 hybrid on a group IV atom contains one electron. Therefore, hydrogen atoms are commonly used for tying-off dangling orbitals on group IV clusters [5.13]. The smallest cluster used in this chapter to model the Si(100) surface is Si_9H_{12} , the basic structure being shown in Fig. (5.1). Variants of this cluster are used for the III-V surfaces.

For the III-V clusters the choice of boundary atom is not so straightforward due to there being a non-integral number of electrons in the dangling orbitals. In these cases it is better to work in terms of molecular orbitals rather than directed hybrid orbitals. The electronic structure of the cluster is described by a sequence of MOs with the highest occupied MO being determined by the valency of the surface being studied. This approach is used to describe the electronic structure of small molecules. For example, the change from BH_3 to CH_3 involves placing a single electron in the LUMO of BH_3 [5.8]. The absolute energies of the MOs change, but the ordering and symmetries

remain unchanged.

Consider an anion-terminated III-V surface, such as AlP, modelled using the cluster in Fig. (5.1). Replacing the Si atoms by Al and P atoms gives an $Al_5P_4H_{12}$ cluster. An electron count for all the described hybrids shows that the cluster is short of two electrons. Using the "electron-filling" approach described above the simplest way to compensate for this is to make the cluster negatively charged, i.e. $Al_5P_4H_{12}^{2-}$. There is, however, an alternative approach. Replacing the two bottom hydrogen atoms (labelled H_B in Fig. (5.1)) by two PH_3 groups gives a cluster with the correct number of electrons on the surface atoms, the notation used being $Al_5P_4H_{10}(PH_3)_2$. This cluster will have different eigenvalues from the negatively charged cluster but the qualitative properties of the surface state MOs will be the same, if the electron-filling model is correct.

5.6 Method of Calculation

The properties of the cluster were obtained using the MNDO and MINDO/3 semi-empirical quantum chemistry methods described in chapter 3. The first basic limitation of the MNDO method is that only elements of the first and second rows of the periodic table can be treated (excluding Li, Na and Mg). This in turn means that the only materials with a sphalerite structure which can be studied are: Silicon, Diamond, AlP, BP and BeS. (The MINDO/3 method is limited even further but in any case was used only for the Silicon calculations). This is, however, not a serious restriction since the object of the study is to obtain information on the SOJT effect rather than accurate geometrical data for the technologically important semiconductors. By the same token any recognised inaccuracies of the MNDO method, e.g. bond lengths, were regarded as being of secondary importance.

The clusters on which calculations were performed are given in Table (5.1). As well as those shown, calculations were also carried out on the $Al_5P_4H_{12}^{2-}$ cluster. As expected, only the eigenvalues were different from those on the $Al_5P_4H_{10}(PH_3)_2$

CLUSTER	BOND LENGTHS
Si_9H_{12}	d(Si-Si) = 2.35 A d(Si-H) = 1.44 A
C_9H_{12}	d(C-C) = 1.54 A d(C-H) = 1.09 A
$Al_5P_4H_{10}(PH_3)_2$	d(Al-P) = 2.24 A d(Al-H) = 1.43 A d(P-H) = 1.33 A
$Al_4P_5H_{10}(AlH_3)_2$	d(Al-P) = 2.35 A
$B_5P_4H_{10}(PH_3)_2$	d(B-P) = 1.97 A d(B-H) = 1.18 A d(P-H) = 1.33 A

Table 5.1 Details of the clusters used in the dimer bond strength calculations.

cluster, the eigenvectors and dimer bond energy being virtually unchanged and confirming the validity of the electron-filling model. Hence the $Al_5P_4H_{12}^{2-}$ cluster was not considered further.

The $Al_4P_5H_{10}(AlH_3)_2$ cluster was studied in order to obtain some information on the possibility of a cation-terminated (100) surface. Only an anion terminated BP cluster was studied. Virtually nothing is known about the nature of the reconstructions on II-VI surfaces. As has already been mentioned, the main aim of this chapter is to examine the SOJT effect on surfaces and so the BeS cluster will not be considered further here.

The bond lengths used in the different clusters are also given in Table 5.1. Note that the bond length used for AlP is that obtained from a full geometry optimisation of the $Al_6P_4H_{16}$ cluster (i.e. same geometry as the cluster in Fig. (5.1) with an AlH_2 between the surface atoms), rather than the experimental value. MNDO tends to underestimate the lengths of bonds involving P and use of the experimental bond length led to clusters with very high total energies and erratic behaviour in the P-dimer energies. The experimental value was used for the calculations on the Al-dimer.

5.7 Formation of the Symmetric Dimer

Intuitively the formation of a dimer on a (100) surface would appear to be the most obvious way of lowering the surface energy. Harrison [5.14], however, has argued that on a Si(100) surface the two dangling electrons will lie in low energy orbitals and that the energy gained from dimerisation will not compensate for the promotion energy required. Despite this the available experimental evidence is weighed heavily in favour of dimers on many III-V and on the Si (100) surfaces.

Using the clusters given in Table (5.1) the following were studied: (a) Total energy versus dimer bond length (for symmetric dimers), and, (b) symmetry and composition of surface

states and their change in character as the dimer bond forms.

5.7.1 Dimer Bond Energy

The total energy versus dimer bond length (obtained using MNDO) for the clusters given in Table (5.1) are shown in Figs. (5.4) and (5.5). Also shown is the energy curve for the Si_9H_{12} cluster obtained using MINDO/3. The MNDO curve obtained for C_9H_{12} is essentially the same as that obtained by Verwoerd [5.6] (using MINDO/3) while that for Si_9H_{12} is totally different. The Si_9H_{12} curve is similar in that there is a large discontinuity, however the final dimer has a higher energy than the separated atoms. This behaviour is due to a violation of orbital-symmetry-conservation [5.15] and will be discussed in more detail later. For the moment only the dimer bond energies will be discussed.

The first point to note from the results obtained is the large bond strength of the P-dimer in AlP and BP, compared with that for Si. This is certainly partly due to the reduced bending force constants for these two materials but may also be due to a contribution from double bonding. The most simple and direct way of determining the extent of any double bonding is to examine the dimer bond length. Notwithstanding the fact that MNDO usually the lengths of bonds involving P, the dimer bond length obtained is still significantly shorter than would be expected for a single bond, hence suggesting that a degree of double bonding does exist. Note that the P-dimer bond length is similar for both the AlP and BP clusters, although the bond energies differ considerably. This is due to the different strain energies, the elastic constants being greater in BP [5.14].

For the Si-dimer there does not appear to be any significant double bonding, it being more biradical-like in nature. A detailed discussion of the C and Si-dimer bond strengths has been given by Verwoerd [5.6].

The results for the $Al_4P_5H_{10}(AlH_3)_2$ cluster do not show any evidence of an Al-dimer bond. This is not unexpected considering

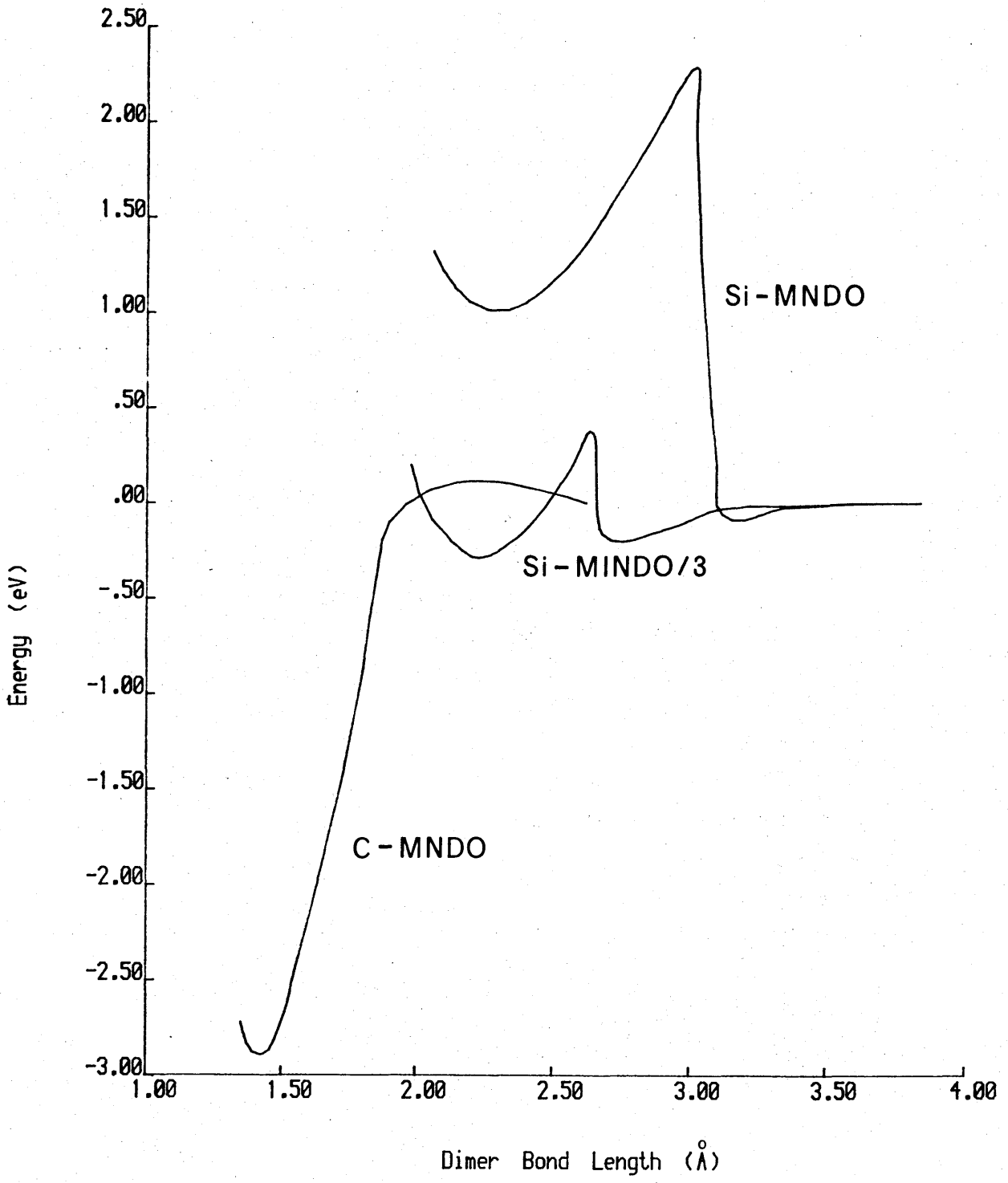

Figure 5.4 Dimer energy versus bond length for Si_9H_{12} and C_9H_{12} clusters. The curves obtained for both MNDO and MINDO/3 are shown for the Silicon cluster.

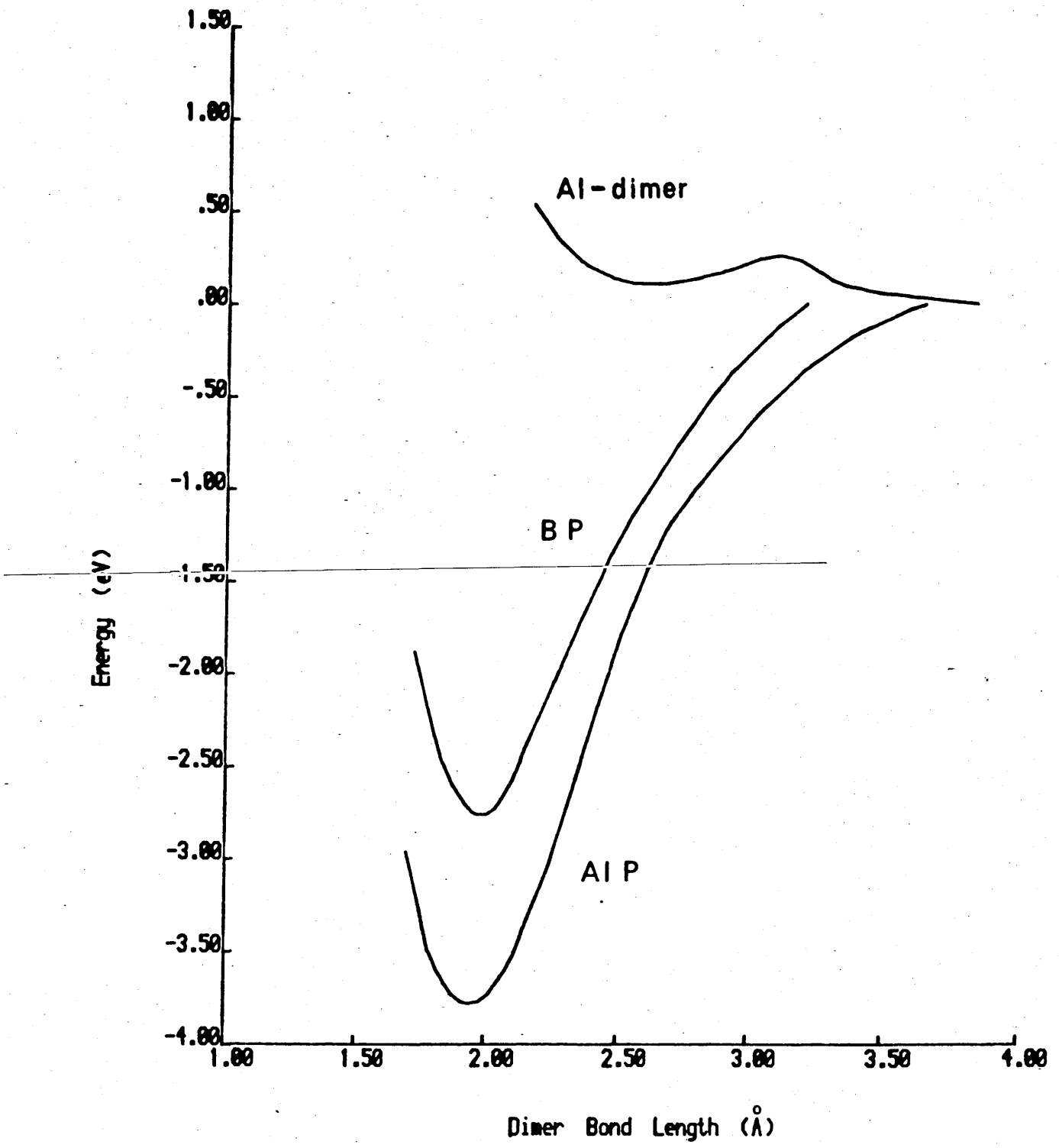

Figure 5.5 Dimer energy versus bond length for P-dimers on AlP and BP clusters and for Al-dimer on AlP cluster.

the relative weakness of Group III metal-metal bonds, and supports the assertion that the GaAs (100)-(4 x 2) reconstruction is not merely a rotated version of the (2 x 4) surface [5.16].

5.7.2 Topologies of Cluster Surface States

In this section the topologies of the occupied and unoccupied cluster molecular orbitals corresponding to surface states will be discussed. This immediately raises the question of how to decide which MOs do in fact correspond to surface states. Obviously the degree of localisation is the primary factor but quantifying this and defining a cut-off for a surface state is a rather arbitrary exercise. Fortunately the results obtained from the clusters studied make the assignment of surface states relatively easy. Comparison with k-space pseudopotential calculations also facilitates the comparison. The following discussion will involve only the Silicon and Diamond clusters since these cover the relevant details.

5.7.2.1 The Unreconstructed Surface

Shown in Figs. (5.6) and (5.7) are the dimer MOs for the Si_9H_{12} cluster with the atoms at the bulk positions. The MOs are depicted in terms of their component atomic orbitals, those on the dimer atoms being the only ones shown. Note that the wavefunctions shown are from one surface atom only. The total contribution from the dimer atoms is a sum or difference of that shown, depending on the symmetry. Note also that the back-bonding MOs are omitted for the present, these being discussed in more detail in section 5.8. The functional representations of the orbitals, as obtained from the eigenvectors, are also shown, as too are the orbital energies.

The orbital topologies obtained are basically as would be expected from simple MO and localised bond arguments. The two highest occupied MOs (Fig. (5.6)) are mainly sp_z in character and correspond to the lower gap surface state (LGSS) discussed by Appelbaum et. al. [5.17] for the Si (1 x 1) surface. These two

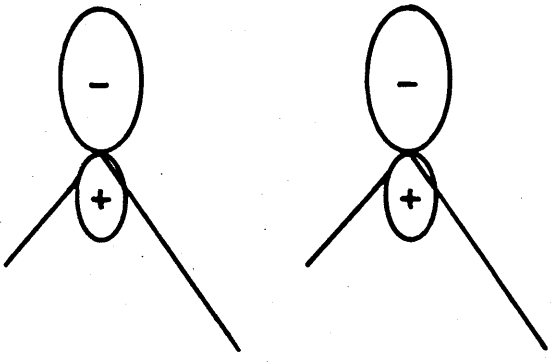

(a)

$E = -7{\cdot}80$ eV $\quad \Psi = 0{\cdot}20\,|s\rangle + 0{\cdot}47\,|p\rangle$

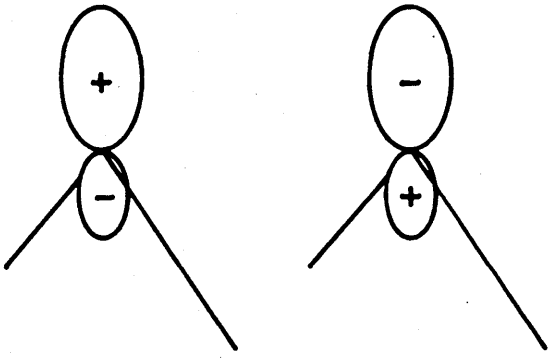

(b)

$E = -7{\cdot}72$ eV $\quad \Psi = 0{\cdot}22\,|s\rangle + 0{\cdot}47\,|p\rangle$

Figure 5.6 The two highest occupied MOs on the Si_9H_{12} cluster with the surface atoms at bulk positions.

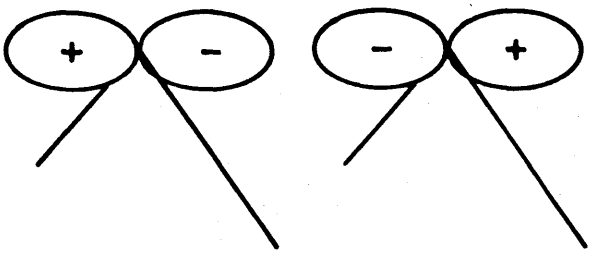

(a)

$E = -2 \cdot 28$ eV $\quad \psi = 0 \cdot 64 \, |p\rangle$

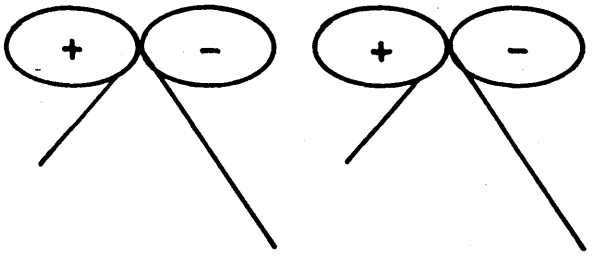

(b)

$E = -1 \cdot 17$ eV $\quad \psi = 0 \cdot 66 \, |p\rangle$

Figure 5.7 The two lowest unoccupied MOs on the Si_9H_{12} cluster with the surface atoms at bulk positions.

MOs are a symmetric and antisymmetric pair formed from the interaction of the sp_z orbital on each surface atom. It is important to recognise at this point that these two MOs do not correspond to separate surface states, as observed on an extended surface. Rather it is these orbitals interacting with others of the same type on the extended surface which form the surface energy band (LGSS), the dispersion of which is dependent on the strength of interaction of the orbitals.

The two lowest unoccupied orbitals on this cluster (Fig. (5.7)) correspond to the upper gap surface state (UGSS) of Appelbaum et. al. [5.17]. On a III-V anion-terminated surface this state is half-full and hence gives a metallic surface. Hence the states obtained from this cluster agree, qualitatively at least, with those obtained by k-space methods.

5.7.3 The Dimer Orbitals

The next stage involves studying the evolution of these states as the Si-dimer bond forms. The results of Appelbaum et. al. [5.18] show that the reduction in the surface space symmetry leads to a doubling of the number of surface states, the topologies of which can be obtained from the cluster. The dimer MOs obtained for the cluster with the surface atoms at the dimer energy minimum are shown in Figs. (5.8) and (5.9).

There are four surface MOs, again ignoring the backbonding orbitals, each one corresponding to a surface state on an extended surface. The orbital lying lowest in energy is the σ-type bonding orbital. The surface state obtained from this orbital has been found by Appelbaum et. al. [5.18] to be similar in character to the bulk bonds. Hence it does not have an independent identity, there being σ-bonding surface states and resonances throughout the valence band energy range.

The next highest orbital (which is the HOMO) is of π-bonding type, this being the orbital which leads to double bonding in the C (100) dimer. The LUMO is the antibonding correspondent of the

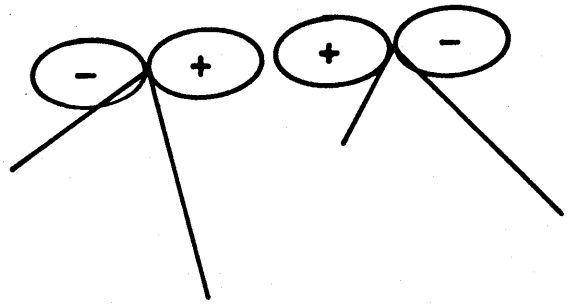

(a)

$E = -9{\cdot}49$ eV $\quad \psi = 0{\cdot}51\,|p\rangle$

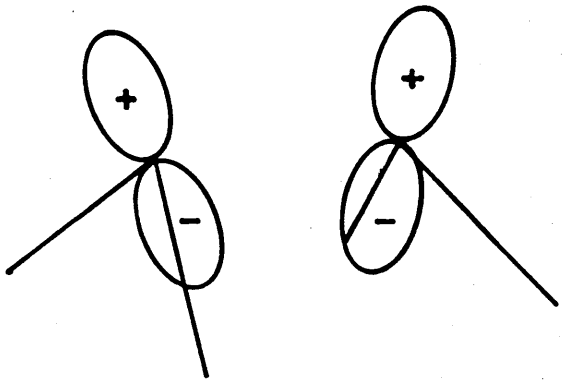

(b)

$E = -7{\cdot}16$ eV $\quad \psi = 0{\cdot}61\,|p\rangle$

Figure 5.8 The two occupied dimer MOs for the fully formed dimer on the Si_9H_{12} cluster, (a) σ_g-type and (b) π_u-type.

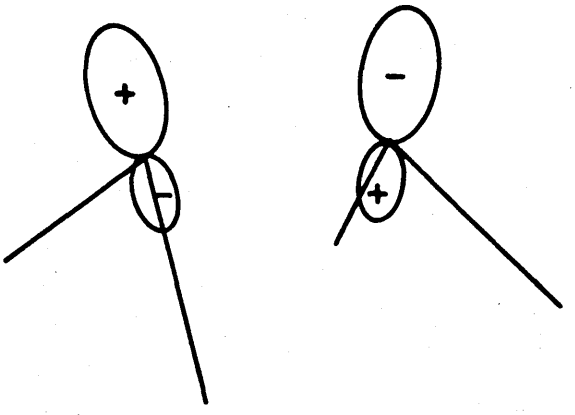

(a)

$E = -2{\cdot}20$ eV $\quad \psi = 0{\cdot}34\,|s\rangle + 0{\cdot}41\,|p\rangle$

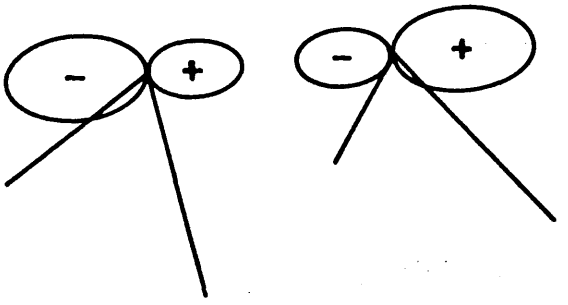

(b)

$E = +1{\cdot}39$ eV $\quad \psi = 0{\cdot}12\,|s\rangle + 0{\cdot}59\,|p\rangle$

Figure 5.9 The two unoccupied dimer MOs for the fully formed dimer on the Si_9H_{12} cluster, (a) π_g-type and (b) σ_u-type.

HOMO and above this lies the σ-antibonding orbital. The charge density distributions are in good agreement with those obtained by Appelbaum et. al. [5.18] for the symmetric dimer. This is illustrated by comparison of the cross-section of the HOMO in Fig.(5.8)b with Fig. (11) of their paper.

The orbitals of the $Al_5P_4H_{10}(PH_3)_2$ cluster are qualitatively the same as those on the Si_9H_{12} cluster, the π-antibonding orbital being singly occupied in this case. This confirms the validity of the electron-filling model and explains why varying the boundary conditions on the lower atoms of the cluster has little effect on the properties of the dimer.

An important point to note is the significant s-character of the π - and σ-antibonding orbitals as opposed to the bonding orbitals which are almost pure p-type. This will be shown to be of importance in the discussion on the SOJT effect.

5.7.4 Symmetry Effects

Ignoring the back-bonding states for the moment, it is apparent from a comparison of Figs. (5.6) and (5.9) that a substantial rearrangement in the ordering of the states has occurred. This can be represented by the simple MO diagram shown in Fig. (5.10). Note that the orbital labels used are those for a diatomic molecule. Throughout this chapter this notation will often be used for the dimer orbitals. The above diagram demonstrates that the orbital symmetries of the reactants (i.e. separated atoms) correspond to a highly excited state of the product (i.e. fully formed dimer). This is an example of a reaction which is forbidden due to orbital symmetry restrictions [5.15]. and it is the cause of the discontinuity in the Si-dimer energy curve (calculated using both MNDO and MINDO/3). Note that there is also a discontinuity in the energy curve for the C_9H_{12} cluster (although less severe and of a different type).

In order to properly describe the formation of the dimer a calculation involving configuration interaction (CI) is required.

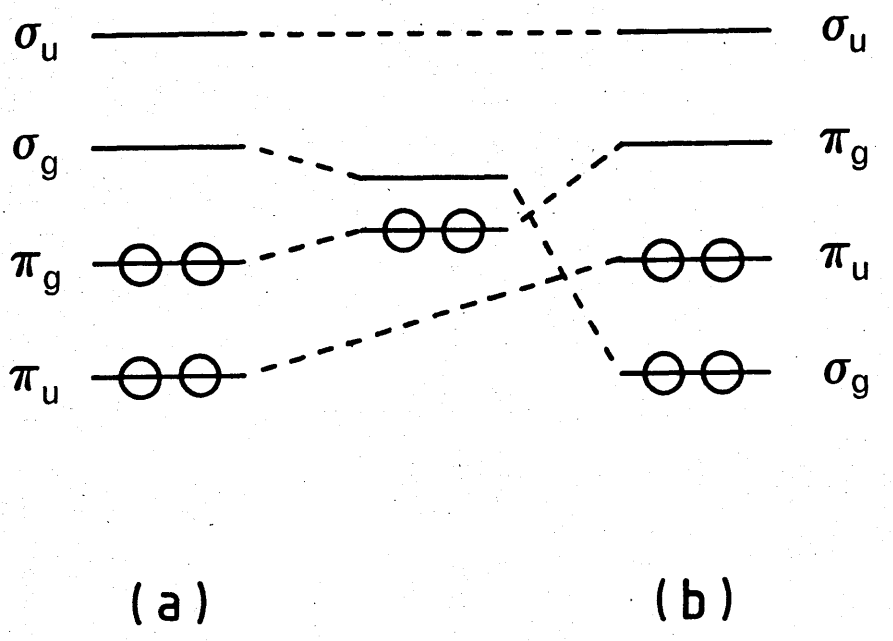

Figure 5.10 MO correlation diagram for the formation of the symmetric dimer on a group IV surface, (a) atoms at bulk positions and (b) fully formed dimer. Only the σ_g and π_g MOs are shown at the transition state.

Even very limited CI reduces the discontinuity (Verwoerd used a (2 x 2) CI calculation, i.e. one other configuration besides the ground state). As has often been pointed out the use of CI with MNDO and MINDO/3 is inconsistent since electron correlation effects are already taken into account by the parameterised repulsion integrals. However, it is apparent that MNDO does not always choose the lowest energy configuration. This is most clearly demonstrated by comparing the MNDO and MINDO/3 results for the Si_9H_{12} cluster in Fig. (5.4) where MINDO/3 does manage to choose the lowest energy configuration. This type of behaviour has also been observed in MNDO and MINDO/3 calculations on simple dissociation reactions in small molecules, where both methods lead to an overestimation of the bond-breaking energy. In the case of the AlP (100) cluster the MNDO calculation is well-behaved, probably due to the fact that the fully-formed dimer only corresponds to a singly excited state.

The effect of these symmetry restrictions on real surfaces is unclear. In practice dimers do form and this would be expected since the atoms will not be constrained to move together in the simple, symmetrical approach considered above. Atoms can migrate on the surface or be supplied from an external source such as a molecular beam, and so there are many possible reaction paths. Due to the principle of microscopic reversibility the inverse reaction, i.e. breaking of the dimer bond, is also symmetry forbidden. Hence it may be more fruitful to look at situations involving dimer dissociation for experimental effects.

Note, however, that the kinetic barrier to dimer formation may be the cause of the (1 x 1) reconstruction observed during room temperature deposition of Ge on GaAs (100). Only after heating to 600K is the C (2 x 2) reconstruction fully developed. It may also be the cause of the disappearance of the reconstruction as the substrate temperature is lowered during GaAs growth.

5.8 The Backbonding Orbitals

The calculations of Appelbaum et. al. [5.18] have shown that the dimer backbonds are sufficiently different from the bulk bonds to introduce surface states. The backbonding charge density is spread over a large number of states both in the pseudopotential calculations and in the cluster calculations reported here. Fig. (5.11) shows the two highest energy backbonding MOs obtained from the Si cluster. Examination of the energies of these two occupied orbitals, before and after dimer formation, shows an upward trend (albeit small in magnitude) in energy as the dimer forms (in agreement with AH). Note that these orbitals are of π-bonding type. Of the occupied backbonds, these are the most highly localised, the σ-type states being spread throughout the "valence-band".

The antibonding partners of the π-type orbitals are similar in localisation. This is not true, however of the σ-type antibonding states, there being two highly localised orbitals lying between the LUMO and the dimer-antibonding orbital. (Shown in Fig. (5.12)). Given the large magnitude of the eigenvectors and the relatively low energies of these orbitals their participation in SOJT distortions might be expected. This will be shown to be the case in section 5.13. Again, as in the case of the unoccupied π and σ dimer orbitals, the anti-backbonding orbitals have significant s-character while the occupied orbitals are almost purely p-type.

5.9 Formation of the Asymmetric Dimer

We come now to the study of the mechanism which leads to the asymmetric dimer. As already stated, there are no degenerate orbitals on the clusters used and hence the FOJT effect is not responsible for distorting the dimer. It was postulated in section 5.3 that the distortion is in fact due to the SOJT effect and this will now be investigated further.

The ability of the SOJT effect to produce a distortion in a

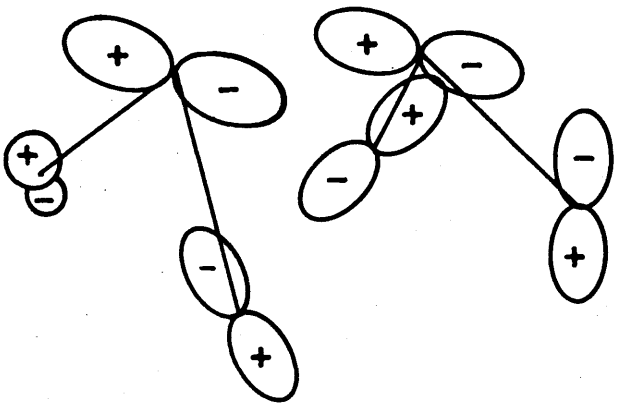

(a)

$$E = -8.96 \text{ eV} \qquad \psi = 0.34\,|p\rangle_1 + 0.31\,|p\rangle_2$$

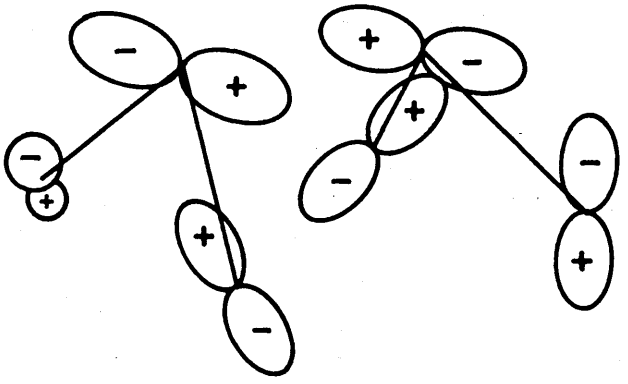

(b)

$$E = -8.33 \text{ eV} \qquad \psi = 0.32\,|p\rangle_1 + 0.38\,|p\rangle_2$$

Figure 5.11 The two highest energy occupied π-type backbonding orbitals for the Si_9H_{12} cluster. The wavefunction shown includes contributions from one first and one second-layer atom.

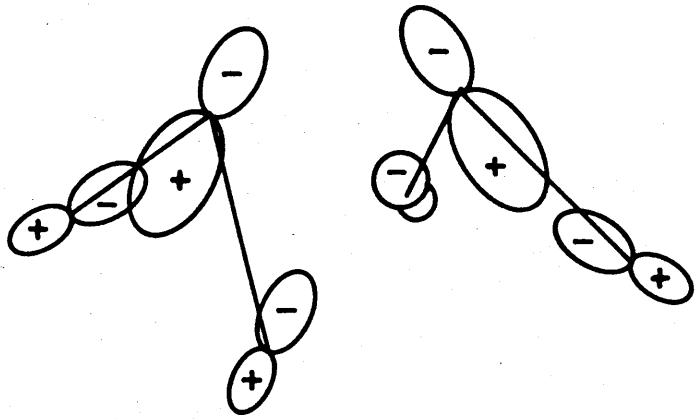

(a)

$$E = +0{\cdot}09 \text{ eV}$$

$$\Psi = 0{\cdot}26\,|s\rangle_1 + 0{\cdot}35\,|p\rangle_1 + 0{\cdot}16\,|s\rangle_2 + 0{\cdot}25\,|p\rangle_2$$

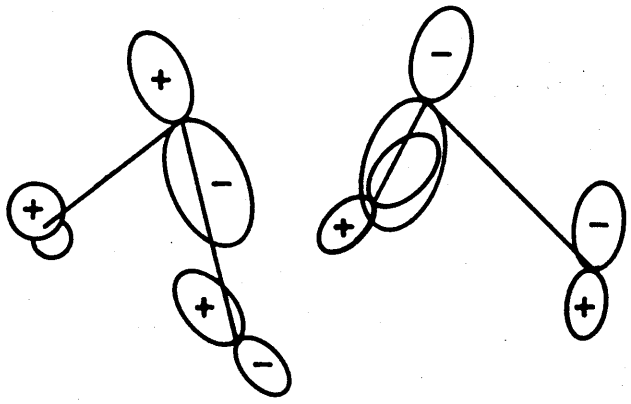

(b)

$$E = -0{\cdot}05 \text{ eV}$$

$$\Psi = 0{\cdot}27\,|s\rangle_1 + 0{\cdot}52\,|p\rangle_1 + 0{\cdot}15\,|p\rangle_2 + 0{\cdot}15\,|p\rangle_2$$

Figure 5.12 The two unoccupied σ-type anti-backbonding orbitals for the Si_9H_{12} cluster.

molecule is dependent on three important factors; (a) The energy spacing of the interacting excited states. This comes into play via the denominator of the relaxability term, i.e. the last term in (5.2), (b) the magnitude of the matrix element $\langle \psi_o | \partial U / \partial Q | \psi_k \rangle$. This is proportional to the overlap of the interacting orbitals, which is in turn dependent on the eigenvector amplitudes obtained using MNDO. It is also dependent on the occupancy of the orbital, i.e. a transition density involving a doubly occupied MO will obviously be greater than that for a singly occupied MO. (c) The restoring force due to the classical force constant, i.e. there is a positive energy term due to the bending and stretching of the bonds. Since bending force constants are always less than stretching force constants, the former type of distortion will be favoured.

At this juncture it is appropriate to give an example of the SOJT effect applied to small molecules. This simpler system will serve to illustrate the principles involved. Consider the phosphine molecule, PH_3. Experimentally this is found to have a pyramidal geometry, which is obtainable by distortion of the planar form. The HOMO and LUMO of the planar form of PH_3 are shown in Fig. (5.13), the eigenvectors being obtained from MNDO calculations. From the figure it is observed that the HOMO is derived entirely from a phosphorous p-orbital while the LUMO is derived from out-of-phase s-orbitals. MNDO also gives values for the transition energies to the first excited singlet states, and these were found to be 2 eV and 5 eV for the planar and pyramidal geometries respectively. Note, however, that MNDO tends to underestimate the energies of excited states, the experimental value for PH_3 lying between 5.5 and 7.0 eV. This should be borne in mind when obtaining excitation energies for the clusters.

From Fig. (5.13) it is apparent that the mixing of the p-orbital (HOMO) with the s-orbital (LUMO) on the phosphorous atom leads to a positive transition density above, and a negative transition density below the molecule. Hence there is a conversion from planar to pyramidal geometry.

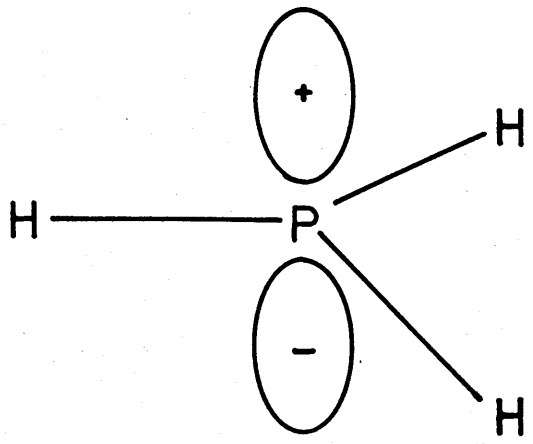

(a)

$E = -9 \cdot 27\ eV \quad \psi = 1 \cdot 0\,|p\rangle_P$

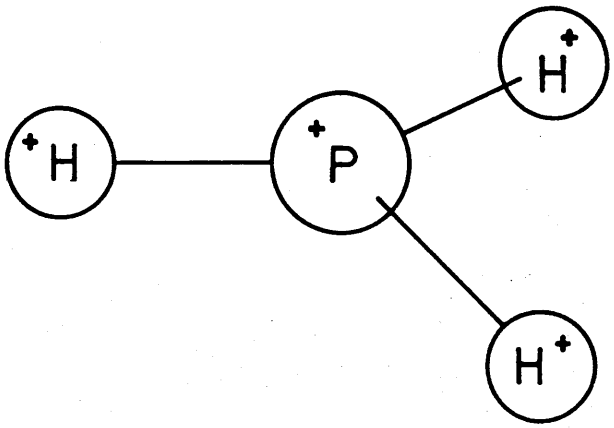

(b)

$E = +0 \cdot 21\ eV \quad \psi = 0 \cdot 51\,|s\rangle_P + 0 \cdot 5\,|s\rangle_{H_{1,2,3}}$

Figure 5.13 (a) HOMO and (b) LUMO for the phosphine molecule (PH_3).

Consider the Si cluster again. The initial task is to identify the orbital interactions which will lead to the correct transition density, i.e. above and below the dimer. It turns out that there are more than one, two of which are fairly obvious. These are interactions involving the dimer σ-bonding and antibonding orbitals with the π-type orbitals and using the notation for a diatomic molecule they are described by ;

$$\sigma_g \times \pi_u \Rightarrow \pi_g$$

$$\sigma_u \times \pi_u \Rightarrow \pi_g$$

In a diatomic molecule the π_g movement is a rotation [5.8]. Although these interactions have the required symmetry they are unlikely to have a significant effect due to the relatively large energy differences involved and the poor overlap. A third possibility is the HOMO-LUMO interaction, although the transition density is a little less obvious. A related example in small molecules is the HOMO-LUMO interaction in ethylene, (C_2H_4). This is a useful example because it illustrates one of the conditions which must be satisfied for a SOJT distortion to occur, namely that the transition density must lie in the region of the bonds to be stretched or bent. The two MOs of interest have been shown already in Figs. (5.8)b and (5.9)a.

In ethylene the HOMO-LUMO mixing is described by $b_{1u}xb_{2g}$. From the topologies of the b_{1u} and b_{2g} orbitals it is observed that the transition density lies above and below the plane. However, the B_{3u} vibration of ethylene corresponds to a C-H stretch, i.e., the transition density, although of the correct symmetry, is not in the right place to cause a distortion. In the case of the dimer on a surface there is a fundamental difference, i.e. the s-character of the π- antibonding orbital. Upon mixing, this will lead to a larger transition density above the dimer atoms than below (note that this will be partially compensated by the overlap with the second-layer atoms). Examination of the phases of the MOs in Fig. (5.8)b and Fig. (5.9)a shows that one of the dimer atoms will be lowered and the other raised, i.e. the dimer

will tilt.

Although appropriate interactions for a tilted dimer have been found to exist on the clusters, the three factors mentioned earlier must be favourable before a distortion can take place. Estimating the magnitudes and overall effect of the different factors is rather difficult, a total energy calculation being the only reliable method of obtaining the geometry. However, a useful guide as to whether a SOJT effect will take place can be obtained from the energy gap between the ground state and the first excited state. According to Pearson [5.8] if this transition energy is greater than about 5 eV then a distortion will not occur. Note, however, that a transition energy lower than this does not necessarily imply a SOJT distortion since the matrix elements and force constants may be unfavourable.

5.10 Geometry Optimisation for Tilted Dimer

The optimum dimer geometries on the different clusters were obtained by using the geometry optimisation option on the MNDO and MINDO/3 programmes. Only the dimer atoms were allowed full optimisation, all others being held rigid. Verwoerd [5.6] has already shown that an asymmetric dimer does not form on the C_9H_{12} cluster and this can be easily explained using the principles discussed earlier. From MNDO the first excited state of the C_9H_{12} cluster lies 3eV above the ground state. This is larger than for, say, planar PH_3 but is still well within the range given by Pearson.

The C_9H_{12} cluster has, however, the significant disadvantage of a large classical force constant, i.e. the restoring force in (5.2). By contrast, although the eigenvectors of the Si_9H_{12}cluster are of similar magnitude, the first excited state lies at a lower energy (2 eV from MINDO/3) and the restoring force is significantly smaller. Hence, an asymmetric dimer is obtained for the Si_9H_{12} cluster, the details of which are given by Verwoerd [5.6].

5.11 Eigenvectors on the Asymmetric Dimer

The localised bond picture of the tilted dimer on the Si(100) surface has the dangling bond on the raised atom fully occupied while that on the down-atom is empty, (obviously for an As-dimer on a GaAs(100) surface the dangling bond on the down-atom will be singly occupied).

This behaviour is also apparent from the eigenvectors obtained for the cluster MOs. For a symmetric dimer the π-type orbitals are weighted equally on both atoms. As the dimer tilts the π_u-type eigenvectors for the raised atom increase in magnitude while those on the down-atom decrease, i.e. the π_u-type orbital becomes more localised on the raised atom. The converse is true of the π_g -type orbital, which becomes more localised on the down-atom. This behaviour is more commonly encountered on heteropolar diatomic molecules, being due, in this case, to the difference in electronegativity of the two atoms. Here, the π_u (i.e. bonding) orbitals are localised on the more electronegative atom and the π_g (i.e. antibonding) orbitals on the more electropositive atom.

This asymmetry has important implications for the reactivity of the dimer, as will be discussed in the following chapter.

5.12 The Asymmetric Dimer on III-V Surfaces

The obvious difference between a group IV surface dimer and the anion dimer on a III - V surface is that the π_g - type orbital is now singly occupied. However, an interaction between the two π -type orbitals will still, potentially, lower the energy since that gained by two electrons will obviously still dominate the rise in energy of one electron. This is analagous to the HOMO - SOMO interaction discussed in chapter 3.

Because one electron is being raised in energy the factors

leading to a SOJT distortion will have to be even more favourable. Full geometry optimisation calculations were carried out on the aluminium phosphide and boron phosphide clusters and a symmetric dimer was found to be most stable in both cases. Hence the formation of an asymmetric anion dimer could not be studied since these are the only materials to which the MNDO method can be applied.

5.13 Twisting of the Dimer

Recent experimental observations have suggested that, in addition to being tilted, the dimers on some surfaces are also twisted about an axis normal to the surface. This geometry was first suggested by Yang et. al. [5.3] for the Si 100 (2 x 1) surface from an analysis of LEED I-V data. They found that a simple asymmetric dimer gave poor agreement with experiment. In a reappraisal of their initial structure for the GaAs 100 (2 x 4) surface, Dobson et. al. [5.19] have also concluded that a twisting of the As-dimer is required to explain the observed reconstruction. Since the SOJT effect has been successful in explaining the formation of the asymmetric dimer, it seems reasonable to try and extend these concepts to the twisted geometry.

5.13.1 Geometry Optimisation of the Twisted Dimer

A full geometry optimisation of the two dimer atoms (with the bulk atoms held rigid) has been shown to lead to a dimer which lies in the yz-plane (see Fig. (5.1) for axis convention used), i.e., there is no twist normal to the surface. This is not unexpected when it is realised that a twisting in this case requires stretching and compression of the back-bonds. For there to be a SOJT distortion the interacting states would have to be very close in energy. This is illustrated by the work of Nakajima et. al. [5.20] which shows that an E_0-E_1 of the order of 1.5 eV is required for rearrangements involving bond stretching. For distortions involving mainly changes in bond angle the

minimum separation can be much larger (of the order of 5 eV).

This result does not rule out the possibility of a twisted dimer since there is another way in which it can be achieved. From Fig. (5.1) it is observed that displacing alternate rows of second-layer atoms in the plus and minus x-direction leads to twisted dimers. This distortion need only involve changes in bond angle and hence will be significantly more favourable than the distortion mentioned above.

In order to investigate this another geometry optimisation was carried out for the Si_9H_{12} cluster using MINDO/3, allowing all second-layer atoms to optimise freely (as well as the dimer atoms). This did in fact lead to the type of distortion described above, with little effect on bond lengths. The details of the calculated geometry are not given here since no quantitative information can be obtained from such a small cluster.

At this point it is necessary to examine in more detail the cluster back-bonding orbitals in order to identify the interaction leading to the distortion. The orbitals which interact to give the correct transition density are those shown in Figs. (5.11)b and (5.12)a. The energy separation cannot be obtained using MINDO/3 although an estimate can be obtained from the eigenvalues (8.42 eV). From this it is apparent that the separation will most likely be small enough, remembering that the true energy difference will be much less.

In order to ensure that no phase changes occur on a real surface leading to a cancellation of the effect, the eigenvectors of a larger cluster ($Si_{15}H_{16}$) were examined. The orbital phases were found to be the same on both dimers.

5.14 Discussion and Conclusions

The calculations confirm that the tilted dimer is a possible building block for reconstructions on semiconductor (100) surfaces. They demonstrate that the distortion (i.e. tilting and twisting) of the dimer can be understood using MO concepts. It is worth noting that early attempts to find SOJT distortions in small molecules were not very successful. This would appear to be due to the fact that the observed structures are not slightly distorted but are often so different that the relationship to the original structure is obscure. The present study provides a good example of a SOJT distortion, the obvious original structure being the symmetric dimer.

The application of these concepts to other surface structures which cannot be so easily described using a cluster model presents some difficulties. This type of interaction (i.e. repulsion of empty and full delocalised states) does occur as is illustrated by the discussion on W(100) in chapter 4. In the language of solid state physics, such a distortion would be due to a coupling of the interaction with the lattice phonons.

Even for (100) semiconductor surfaces long-range forces introduce additional complexities, particularly on the III-V surfaces where there is a half-occupied dangling orbital on the dimer. Normally this would be expected to lead to a metallic surface, a situation which is not observed in practice. The structure proposed by Dobson et. al. [5.4] overcomes this by giving a fold-back of the bands. In chemical terms, their structure allows a better interaction between two singly-occupied dangling orbitals, possibly leading to a biradical-like entity. Interactions between singly-occupied dangling orbitals on semiconductor surfaces have also been discussed by Tosatti and Anderson [5.21].

Finally, it is necessary to consider the relationship of the results to reconstructions on real III-V surfaces (the Group IV surfaces have been discussed in detail elsewhere [5.6]). Unfortunately, any discussion is limited to only one surface,

i.e. AlP, since this is the only one which could be prepared relatively easily using MBE. Despite this, however, no reports could be found in the literature regarding the reconstruction on the AlP surface. The (2 x 4) has been observed on InP, InAs, GaAs, GaP and InSb surfaces. Notable exceptions are the GaSb and AlAs surfaces, the former of which has a (2 x 3) reconstruction and the latter a (3 x 2). A possible structure for the GaSb surface may involve dimers in a vacancy structure, the dimer again being responsible for the 2x reconstruction. The apparent absence of a dimer on the AlAs surface might be due to a requirement for a semiconducting surface (which would require a tilted dimer), i.e. the AlAs and AlP surfaces may have similar properties. This is, however, highly speculative. Unfortunately, the predictive powers of the present model are rather limited. Further progress must await the availability of Quantum Chemistry methods which are able to handle larger atoms, e.g. a $Ga_5As_4H_{10}(AsH_3)_2$ cluster.

Given the success of an MO model in explaining the formation of the tilted dimer it now seems appropriate to extend some of these concepts to reactions on the semiconductor surface during MBE growth. This is the subject of the following chapter, in which the topologies of the dimer orbitals obtained in the present chapter will be utilised.

CHAPTER 6

INTERACTIONS OF ATOMS WITH THE SURFACE DIMER

6.1 Introduction

Since the most direct way to dope a III-V semiconductor p-type during MBE growth is to incorporate group II atoms into the cation sublattice, this has led to wide spread use of elements such as Zn and Cd in LPE and VPE growth of GaAs. The use of either of these elements in MBE is, however, not possible due to their low sticking coefficient [6.1]. In order to explain this behaviour Heckingbottom et. al. [6.2] proposed a model in which it was assumed that MBE can be regarded as being dominated by thermodynamic factors, any kinetic effects being small. Hence the sticking coefficient is taken to be related to the equilibrium vapour pressure of Zn over GaAs. Since the vapour pressure of Zn over Zn is high then the activity of Zn in GaAs must be much less than unity in order for incorporation to take place.

The work described in this chapter was originally motivated by a desire to understand the behaviour of the group II atoms during MBE growth. However, the interactions of other atoms with the surface will also be discussed since this provides extra insight into the growth processes, due to the fundamental differences between the group II and open-shell atoms. The work will show that the group II atoms are restricted in the way in which they can interact with the dimer.

These restrictions will be shown to lead to kinetic barriers which hinder the incorporation of group II atoms into the growing lattice. Some possible adsorption sites of group II atoms will also be discussed. More generally, the factors which lead to a strong interaction with, and hence disruption of, the dimer bond will be considered.

Throughout this chapter extensive use is made of MO concepts when discussing the interaction between adatom and surface. This extension of concepts normally used when discussing small molecules to reactions on surfaces is not without precedent. In particular, Grimley [6.3], Johnson [6.4], Shustarovich et. al. [6.5] and Upton [6.6] have all used this approach to surface reactions. In addition, the chapter on the asymmetric dimer has demonstrated the utility of these concepts when discussing the properties of the surfaces.

From the application of MO methods to gas-phase reactions involving group II atoms the presence of kinetic barriers can be inferred from any violation of orbital symmetry rules. The extent to which these rules apply on a surface is unclear, and this will be investigated in the present chapter.
Trends in the strengths of some adatom/surface bonds will be studied using a cluster approach and the methods of calculation described in chapters 3 and 4. These calculations do not form an exhaustive study of adatom/semiconductor surface bonds, rather it is an attempt to elucidate some general principles governing these interactions and the implications for MBE growth.

6.2 The Molecular Orbital Approach

At this point it is appropriate to stress the aims of this chapter and to justify more fully the use of a MO approach. As has been shown in chapter 3, one of the fundamental factors influencing the course of a chemical reaction is the presence of nodes in the wavefunctions [6.7]. On a surface the orbitals on the atoms will interact to give delocalised surface states. Despite this delocalisation, however, in many cases the interacting orbitals will still retain their basic identity. For example, the π-type orbital on a surface dimer will interact with others to form a surface state but it will still be recognisable. Hence, the nodes in the orbitals will still exist and will still affect the reactivity. The delocalisation will alter the properties of the state but the fundamental topological rules governing the chemical reactions must still be obeyed.

The relationship between the k-space approach and the MO approach is well illustrated by the example (due to Grimley) [6.3] given in chapter 4. It is also worth mentioning that the recent study of Ni clusters by Upton [6.6] has also demonstrated the utility of the MO approach in illuminating aspects of reactivity on surfaces. He found that on transition metal surfaces the presence of low-lying unoccupied surface states often provides a means of overcoming symmetry - imposed activation barriers. This is in fact the basis of catalysis.

6.3 Experimental Observations

6.3.1 Zn on GaAs

Firstly, a review of experimental evidence available for the interaction of Zn with a GaAs (100) - (2 x 4) surface is in order. Laurence et. al. [6.8] have observed that the sticking coefficient of Zn on a clean surface at room temperature is unity. However, if an oxygen coverage of a few percent of a monolayer is present then the sticking coefficient drops to zero. At the time these results were published the (2x4) As-stabilised surface was regarded as having a 50% coverage of As [6.9], and so the behaviour of the Zn was not easily explainable. Since that time there have been more quantitative studies of the (2x4) surface using photoemission spectroscopy [6.10]. These results suggest an As-coverage close to 100%, although for any particular reconstruction there is a wide possible variation in stoichiometry [6.11]. If it is assumed that the perfect surface has 100% As-coverage then there are likely to be a few percent of As-vacancies as well as steps. At these vacancies and steps Ga atoms will be exposed and it would appear that both Zn and O_2 bond to either or both of these sites.

The surface lifetime measured by Laurence et. al. for a contaminated surface was less than 10^{-5} sec. Assuming the Frenkel relationship ;

$$\tau = \tau_0 \exp(E_D/kT) \qquad (6.1)$$

and a τ_o equal to 10^{-13}, then E_D is of the order of 0.5eV, i.e. 0.25eV per electron. This is a very weak bond and corresponds to an activity (of Zn over GaAs) of greater than unity. LPE and VPE data, however, show an activity much less than unity [6.2].

The above experimental evidence indicates that the interaction between a Zn atom and the As-dimer is very weak. This in turn suggests that the low sticking coefficient may be due to a kinetic barrier which prevents a strong chemisorption bond from being formed. Any decrease in activity must be due to bonding to other surface sites such as the vacancies or steps.

6.3.2 Other Group II Atoms

The behaviour of the group IIA and IIB atoms on a GaAs (2 x 4) surface at low coverages can be separated into three distinct types ; (i) Zn and Cd, negligible interaction with the dimer, hence zero sticking coefficient, (ii) Mg and Ca, unity sticking coefficient coupled with a change in the surface reconstruction to (2 x 2), (iii) Be, unity sticking coefficient but no reconstruction change.

The behaviour of Mg is at variance with the thermodynamic model of Heckingbottom et. al. [6.2] since MBMS desorption studies of Mg/GaAs have shown unequivocally that the sticking coefficient of Mg is unity for typical MBE growth conditions [6.12] (A more recent study uses Auger [6.13], this is, however, less direct and hence unreliable). In a more recent study of the role of kinetics and thermodynamics in MBE, Heckingbottom et. al. [6.14] have explained this behaviour as being due to a kinetic barrier to desorption. However, the situation becomes further confused when it is realised that there is a strong interaction between Zn (and Cd) and II-VI surfaces, e.g. MBE growth of CdTe at temperatures up to 200°C [6.15].

6.3.3 Bond Strengths

An idea of the expected bond strength for Zn and Mg on GaAs can be obtained in the following way. Shown in Table 6.1 are some bond strengths for typical examples of II-VI semiconductors and small molecules involving Be, Mg and Zn along with some Ga-containing molecules.

The cohesive energies of the group II metals are anomalously low when compared to neighbouring metals on the periodic table such as Al, Ga and In. This is due to their closed-shell electronic configuration. This behaviour is not observed in covalent bonds involving these atoms, however, and suggests that the use of vapour pressure data for these elements will not provide a reliable guide to sticking coefficients.

From the above data it would appear that the high activation energy for desorption of Mg is not unreasonable. Note also that, on average, bonds involving Zn are only of the order of 25% weaker than Mg bonds. This suggests that a reasonably strong chemisorption bond should exist for Zn on GaAs. Certainly the bond energy obtained from the lifetime measurements is much lower than expected. This further supports the idea that there is a fundamental restriction preventing the formation of a normal bond in the case of Zn and Cd.

6.4 Orbital Topology as a Guide to Reactivity

6.4.1 Reactions of Atoms with Diatomic Molecules

The group II elements are fundamentally different from the other elements encountered in MBE in that they have no unpaired electrons available for forming chemical bonds. It is important, to note, however, that this is not the same situation as is encountered in the noble gases since it is only the sub-shell (i.e. the s-orbital) which is filled in group II atoms. Bonding electrons can be made available through mixing with the p-orbitals which lie a few eV higher in energy. This lack of

MgTe	1.43 eV	Mg-Br	3.52 eV
ZnTe	1.14 eV	Mg-I	2.74 eV
ZnSe	1.29 eV	Zn-Br	2.79 eV
GaAs	1.63 eV	Zn-I	2.16 eV
Be-Br	3.87 eV	Ga-Br	3.13 eV
Be-I	3.00 eV	Ga-I	2.47 eV

Table 6.1 Energies of bonds involving Be, Mg, Zn and Ga. The values for MgTe, ZnTe, ZnSe and GaAs are cohesive energies for the solids.

available valence electrons has important implications for their chemical reactivity, often being the cause of a symmetry-induced kinetic barrier. The way in which this occurs is best illustrated by considering a broadside attack on a diatomic molecule by a single atom, an example which has relevance to reactions with a surface dimer.

Fig. (6.1) shows the MO correlation diagram (and reaction geometry) for reactants and products involved in the insertion of an atom X (which may be any atom other than hydrogen) into a hydrogen molecule. From the overlap principles discussed in chapter 3 it is observed that two electrons are required in the p_y-orbital which, on overlapping with the σ_u-orbital, will lead to a weakening of the σ_g-bond. A group II atom will obviously have no electrons in the p_y-orbital and hence a broadside attack will be forbidden, there being zero overlap for the s-orbital.

As well as a full occupancy of the p_y-orbital, however, there must also be no electrons in the p_z-orbital otherwise the product will be in an excited state. From this it can be deduced that there will be a large activation energy to insertion for ground state open-shell atoms, e.g. Cl. In this case the preferred attack geometry is end-on, hence leading to H-atom abstraction, i.e. ;

(6.2) $$Cl + H_2 = HCl + H$$

In this case the overlap is again with the σ_u-orbital, leading to dissociation of the molecule.

The obvious extension of this is that spin-paired excited atoms should be able to insert directly into the bond. This is in fact observed for the reaction of oxygen with H_2, where the spin-paired atoms react directly to give H_2O while the ground-state atoms react by H-atom abstraction.

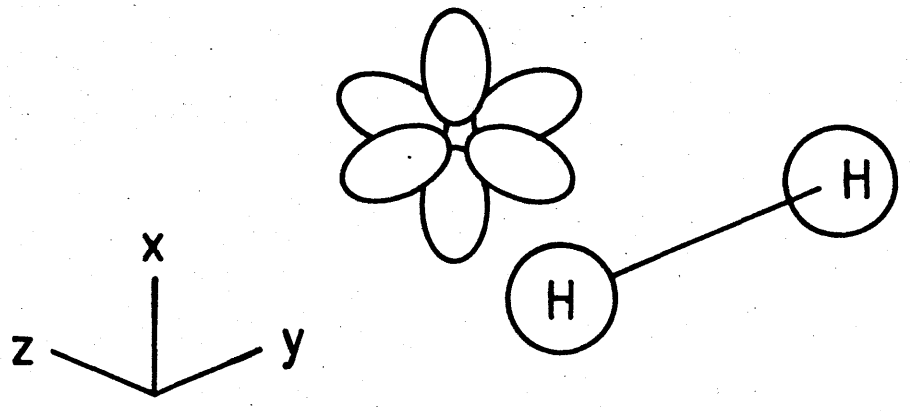

(a)

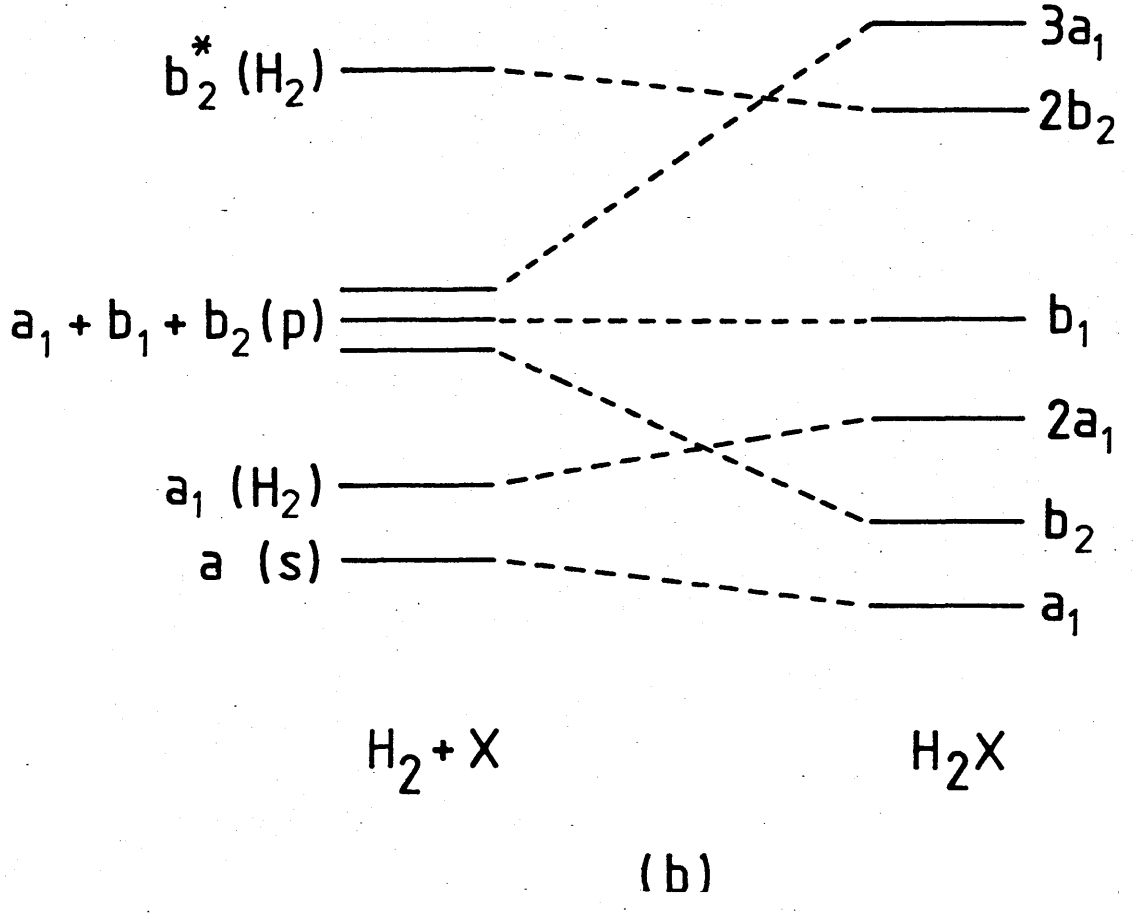

(b)

Figure 6.1 (a) reaction geometry and (b) MO correlation diagram for insertion of an atom into an H_2 molecule.

6.4.2 Reactions with π-Orbitals

The surface dimer differs from the example given above in that at least one of the π-type orbitals will be occupied. For the dimer on a group IV surface an obvious small-molecule analogy is ethylene (C_2H_4). This is a better example for discussion than, say, Si_2H_4 since there are more experimental results available. An end-on attack on ethylene is sterically difficult due to the two H-atoms and hence any interactions must take place with the π-lobes. Note that this restriction is relaxed slightly in the case of the surface dimer since the geometry is not planar.

Consider first the reaction of an occupied donor orbital with an empty π_g-orbital (Nucleophilic attack) (Fig (6.2)a). Interaction of the donor orbital with the appropriate lobe of the π_g-orbital cannot take place without there being an, unfavourable, interaction with the lobe of the opposite sign [6.16]. Hence, an interaction with a symmetric π_g-orbital will not take place. If the π_g-orbital is polarised, however, then the reaction can proceed, since the unfavourable interaction can be minimised. This example is an appropriate prototype for the reaction of a group II atom with a surface dimer and the conclusions will be developed further in a later section.

The second type of interaction to be considered is that between the occupied π_u-orbital and an unoccupied acceptor orbital (electrophilic attack). Again this is relevant to the group II/dimer interaction, the group II p-orbital being the acceptor. The orbital interactions involved are shown in Fig. (6.2)b from which it is observed that the overlap is favourable, thus leading to a stabilisation of the complex.

The above discussion shows that for the interaction of a group II atom with an ethylene double bond only one of the OMO-UMO interactions (the electrophilic attack) leads to a lowering of the energy. In general, both interactions are required in order for the stabilisation to become significant. This requirement becomes even more important if there is a large energy separation

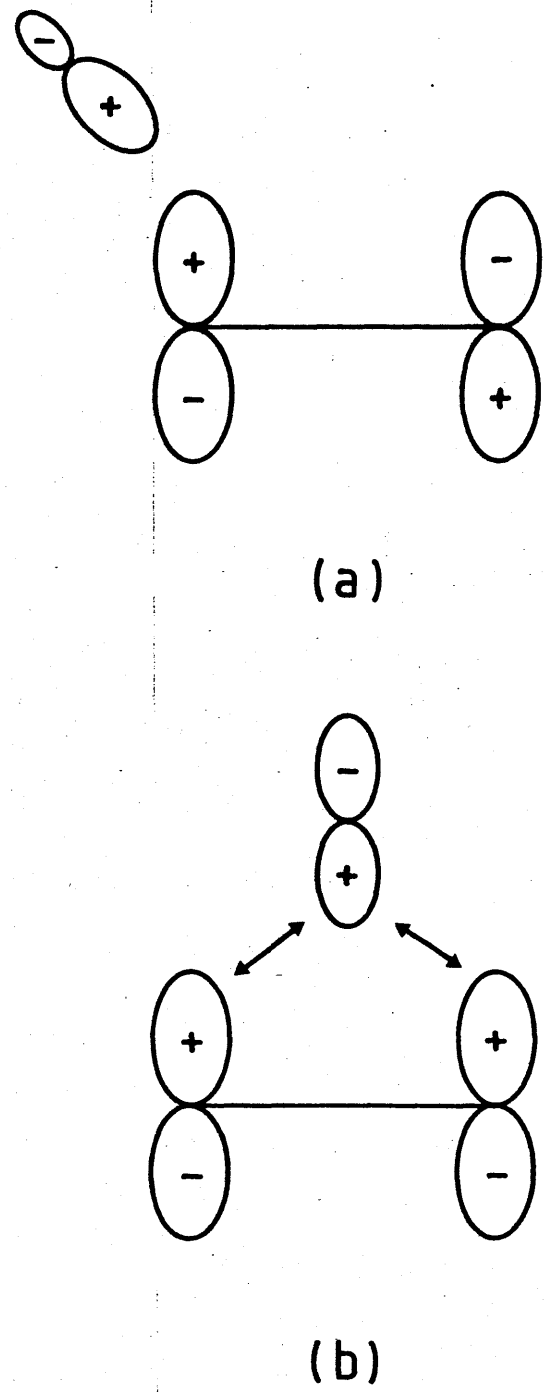

Figure 6.2 (a) nucleophilic attack on an unoccupied π_g-orbital by an occupied donor orbital and (b) electrophilic attack on an occupied π_u-orbital by an unoccupied acceptor orbital.

between the interacting orbitals (See chapter 3). A calculation exists in the literature for the Be + C_2H_4 system [6.17] and the results obtained are in agreement with the criteria given above. A broadside attack by a ground state Be-atom upon the ethylene double-bond leads to a purely repulsive energy curve. The interaction between an excited-state atom (i.e. $1s^2 2s^1 2p^1$) and the double-bond leads to a lowering of the energy, but only if the excited electron occupies the p-orbital lying parallel to the C-C bond-axis, leading to overlap with the π_g-orbital. Note that the expression obtained from PT (chapter 3) does not strictly apply here since it is an open-shell system. However, the same overlap considerations must still be satisfied and hence will be applicable.

6.4.3 Interactions Involving Open-Shell Atoms

The probable outcome of a reaction involving such a large molecule as ethylene is, not surprisingly, very difficult to predict. For example, the reaction between a ground-state oxygen atom and ethylene leads to the formation of CH_3 and HCO [6.7] which does not correspond to simple atom-abstraction. This is not unexpected when it is remembered that nucleophilic attack on a symmetric double bond is highly unfavourable. All that can be obtained with any confidence using this approach is a knowledge of which reactions are unlikely to occur.

Reactions involving spin-paired excited-state atoms are a little easier to understand. For example, an excited-state oxygen atom adds directly to the double bond in ethylene to form the oxide. An excited-state carbon atom initially forms a three-membered ring as in the case of oxygen but then goes on to insert between the two ethylene carbon atoms.

Another important factor influencing the reactions is the number of valence electrons on the attacking atom. This is particularly true for ground state atoms as is illustrated for the ground-state oxygen where there is a singly occupied p-orbital pointing towards the ethylene double-bond, this being an interaction which

will raise the total energy of the system.

6.5 Initial bond to the Surface Dimer

Having identified some of the symmetry restrictions controlling the attacks of atoms on bonds it is now appropriate to try and apply these rules to reactions with the surface dimer. The possible complexities involved are well illustrated by the reaction of a ground-state oxygen atom with ethylene mentioned in section 6.4. Hence, the aim here is to determine which interactions will be forbidden and which initial interactions will be most favourable. In this section the factors affecting the strength of a simple bond to the surface dimer on a III-V (100) surface will be discussed. This is obviously an important case since this bond will be the precursor to further reaction, ultimately leading to incorporation into the growing layer.

The most obvious way to obtain information on the initial bond to the dimer is through the use of small cluster calculations. Such calculations are frequently reported in the literature, sometimes utilising only one atom to represent the surface. The use of such small clusters is often an unsatisfactory way to obtain bond strengths, particularly for metals, as discussed by Post and Baerends [6.18]. However, in the present study the aim is to obtain trends in bond strength from the viewpoint of the adatom. In particular, the variation in bond strength for Be, Mg and Zn is of interest.

6.5.1 Topological Analysis

The topological analysis which was carried out for the ethylene molecule can be easily extended to the surface dimer. Consider first the symmetric dimer, since the effect of the tilting can easily be taken into account later. Fig. (6.3) shows the topologies of the interacting MOs (those for the dimer being obtained from chapter 5). Assume also for the moment that the π_g-type orbital is unoccupied, i.e. a dimer on a group IV surface.

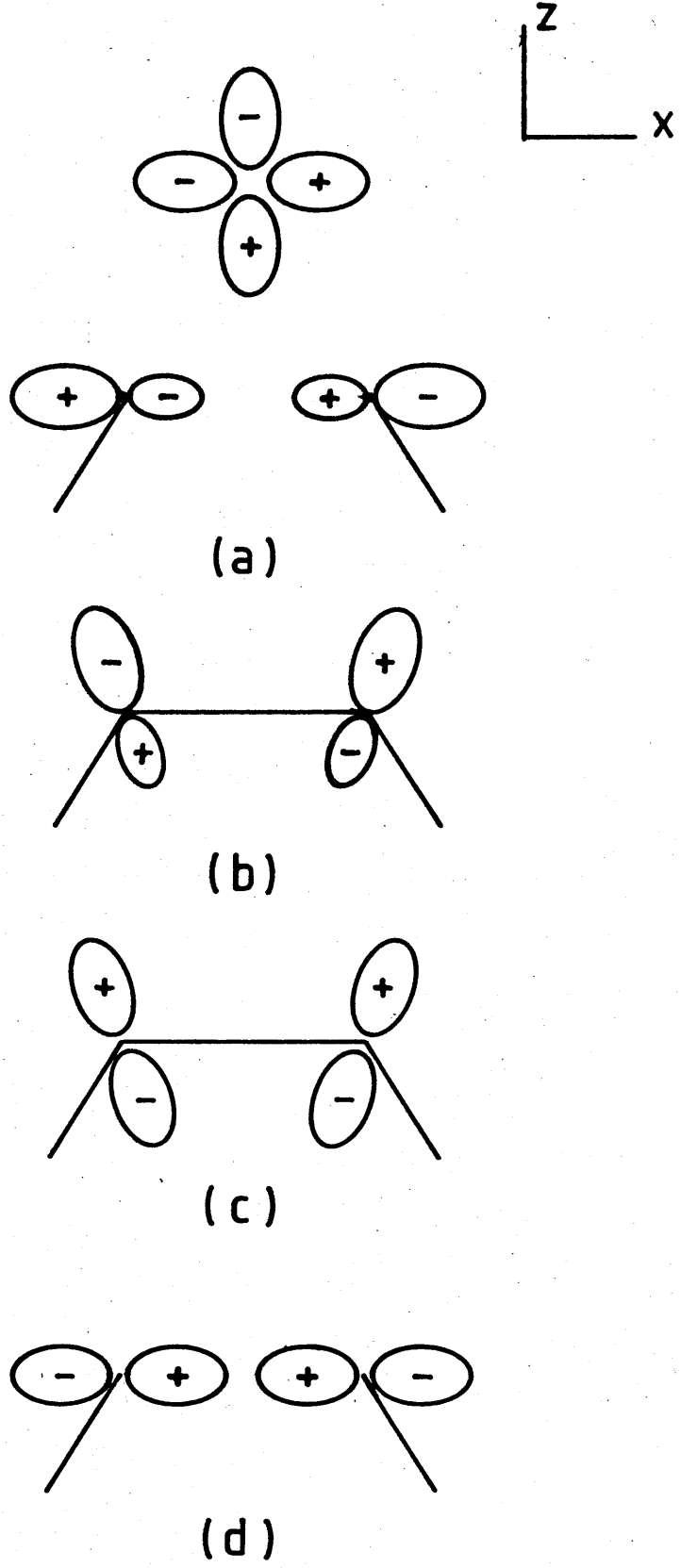

Figure 6.3 Topologies of symmetric dimer and adatom orbitals.

The s-orbital on the adatom is full and hence will not lower the energy by interacting with any of the dimer orbitals (only the σ_g- and π_u-type MOs are of the correct symmetry and they too are occupied). The interactions between the adatom p_z-orbital and the dimer σ_g and π_u orbitals will lead to a lowering of the energy if the p_z-orbital is empty. The only other useful interactions are those between the adatom p_x-orbital and the dimer σ_u and π_g orbitals. The former of these will weaken the dimer bond while the latter will lead to the formation of an intermediate bond, leaving the dimer intact.

What happens next will depend on the valence and electronic configuration of the adatom. In analogy with the discussion on the diatomic molecule, a spin-paired excited-state adatom will insert directly into the dimer with a low activation energy. A ground state open-shell atom (e.g. Ga) will form an initial bond to the dimer, i.e. giving a three-centre ring with the dimer bond left intact. From there it will either desorb or surmount an activation barrier for incorporation into the dimer. Note that in a gas-phase reaction such an initial bond often leads to a complex reaction, usually involving a rearrangment and dissociation of the molecule (c.f. the reaction of O with C_2H_4 discussed earlier). On a surface, however, the possibilities are more limited since more bonds would have to be broken for the dimer atoms to desorb. Hence, incorporation is the most likely outcome. This is the probable reaction mode for the group III atoms during MBE growth of III-V compounds.

The case of most interest in the present study is that of a group II atom on an anion dimer. Here, all the adatom p-orbitals will be unoccupied and there will be one electron in the dimer π_g-orbital. A group II atom interacting with a group IV dimer has only one stabilising interaction and hence will not form a significant bond (c.f. the Be(^{1}S) + C_2H_4 system discussed earlier). The extra electron on the anion dimer provides an extra interaction which may lead to a reasonably strong initial bond. In order to gain insight into this, it is necessary to

have some knowledge of interactions between the closed-shell group II atoms and SOMOs and hence cluster calculations are required.

The tilting of the dimer causes a polarisation of the π-type orbitals and hence will lead to an attack on the down-atom being most favourable. This will probably lead to a suppression of the SOJT effect since the total overlap will be greater for a symmetric dimer.

6.5.2 Cluster Calculations

From the localised bond description of the asymmetric anion dimer it is apparent that there are two types of bonding site (i) a singly occupied dangling orbital on the down atom (radical site) and, (ii) a doubly occupied dangling orbital on the raised atom. Each of these sites could possibly be modelled individually by molecules such as CH_3 and NH_3 for (i) and (ii) respectively, although neither of them can take into account the interaction with the other lobe of the π-type orbitals. The previous sections discussion has shown that it is the SOMO-p_x interaction which is of primary importance, and hence only cluster calculations involving such an interaction will be considered here.

Before discussing the results obtained from the cluster calculations it is appropriate to briefly consider the bond strengths of diatomic molecules involving group II atoms. Some information exists (both experimental and theoretical) for diatomic molecules involving the more electronegative first row atoms (e.g. BeO and BeF). These are, however, highly polarised molecules and this tends to obscure the trends in covalent bonding. One set of calculations which do not involve ionic bonds are those carried out by Jones [6.19] on LiBe, LiMg and LiCa for which he obtains bond energies of 0.46 eV, 0.17 eV and 0.27 eV respectively. The method used by Jones included some correlation energy and hence the bond energies are better than would be obtained by using Hartree-Fock only. Despite this, the

bond energies still tend to be slightly underestimated, e.g. the calculated E_B for Li_2 is 0.83 eV while the experimental value is 1.026 eV. Even allowing for this, the bonds are seen to be relatively weak. This, however, will be partly due to the Li, which normally forms weak covalent bonds.

6.5.2.1 Ab-initio Calculations

As was mentioned in chapter 3 (and is discussed more fully in Appendix A) the first step in an ab-initio calculation involves expressing the atomic orbitals as a sum of component functions, usually gaussians. The set of coefficients for such a set of gaussians is referred to as a basis set. The choice of the basis sets is the primary factor which must be considered before performing an ab-initio calculation. Details of the basis sets used in the following calculations are given in Appendix A.

The first cluster calculation to be considered was Be + SiH_3. The Si-based molecule was chosen rather than CH_3 due to it being more similar to the surfaces of interest. A series of ab-initio calculations on this system showed no evidence of any binding and this can be attributed to the large energy gap between the e-orbital and SOMO of SiH_3 and the LUMO (2p-orbital) of Be. The topologies and energies of the interacting orbitals are shown in Fig. (6.4) from which it is observed that the energy difference is greater than the value of 6 eV mentioned in chapter 3.

Hence, it would appear to be necessary to use a basic cluster with higher-lying Frontier MOs. One possibility, also based on Si, is $SiLi_3$. A HF calculation on this molecule gives a SOMO lying at -5.58 eV, i.e. close to the energy of the Be 2p-orbital. The details of the various HF calculations (bond energies and geometries) which were carried out using the $SiLi_3$ molecule are given in Table 6.2. There are several points worth noting, the most obvious being the relatively large bond energies obtained, particularly for Be. These initially suggest that the bond to the surface dimer might be quite strong, particularly when correlation energy is taken into account. Extreme caution must

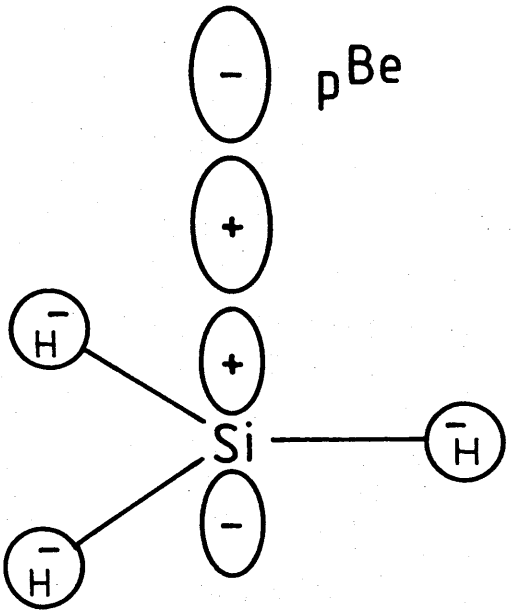

(a)

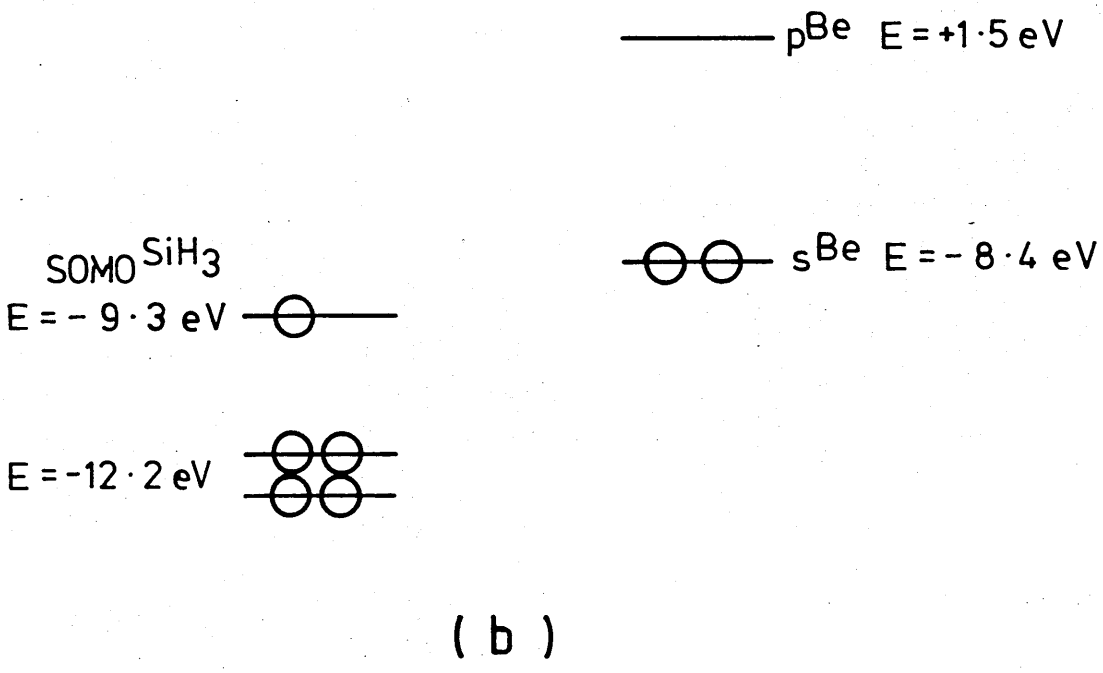

(b)

Figure 6.4 (a) schematic of interaction between Be p-orbital and SOMO of SiH_3 and (b) MO interaction diagram showing other MOs.

$SiLi_3$	d(Si-Li) = 2.7 A
Be + $SiLi_3$	d(Si-Be) = 2.3 A
	E_B(Si-Be)
MIDI-3/MIDI-3/MINI-3	0.15 eV
DH/MIDI-3/MINI-3	1.85 eV
DH/MIDI-3/DH	1.20 eV
Mg + $SiLi_3$	d(Si-Mg) = 2.5 A
	E_B(Si-Mg)
MIDI-3/MIDI-3/MINI-3	0.43 eV
MIDI-3*/MIDI-3/MINI-3	0.82 eV
Zn + $SiLi_3$	d(Si-Zn) = 2.6 A
MIDI-3/MIDI-3/MINI-3	E_B(Si-Zn) = 1.1 eV

Table 6.2 Results of ab-initio calculations using $SiLi_3$. The MIDI and MINI basis sets are those due to Huzinaga and co-workers while DH denotes that due to Dunning and Hay (see Appendix A).

be exercised, however, since the actual bond strength obtained is highly dependent on the basis set used. The effect of the basis set used for Li is particularly significant. The results in Table 6.2 show that improvement of the Li basis set leads to a reduction in the Be-Si bond strength. Hence, the real bond strengths are likely to be closer to those obtained for the Li-based molecules, although slightly greater.

In order to obtain more accurate estimates of the binding energies it is necessary to use larger basis sets and also include some CI. This was beyond the capabilities of the computer programs which were available. Such calculations are, however, unnecessary given the limitations of these small cluster models. The results obtained from the present calculations indicate, as expected, that the initial bond of a group II atom to a surface anion dimer will be relatively weak. It is important to note that the overlap of MOs on the dimer will also be less favourable. For example, the Be-dimer bond energy will certainly be less than 1.5 eV, and will be correspondingly weaker for the other group II atoms. Another point to note from the calculations is the similar strengths of the bonds involving Mg and Zn. Examination of Table 6.1 shows this to be not unexpected.

Initially, the weak bonds obtained from the above calculations appear puzzling given that the group II atoms do in fact form strong bonds in molecules. However, the difference is probably due to the greater flexibility of atomic orbitals as regards mixing to form new MOs. For example, the MOs on the $SiLi_3$ molecule are limited in their flexibility since any drastic change would weaken the $SiLi_3$ bonds. Hence, in this type of interaction the energy difference between the interacting MOs becomes extremely important.

One possible method of carrying out a more realistic calculation might be to use a $SiPLi_4$ cluster. This is similar to the dimer in that the π_u-type orbital will be localised on one of the atoms (P) and the π_g-type orbital on the other (Si). In this

case the asymmetry is due to the difference in electronegativity, that of P being greater than Si. Calculations were, in fact, carried out on the Be + $SiPLi_4$ system. However, the basis set effects discussed earlier were found to be even worse, a Be-Si bond energy of 3.21 eV being obtained. This can be traced to the P-Li bond since a calculation on the Be + PLi_3 system gave a bond energy of 4.0 eV. The strengths of such DA bonds are normally a few tenths of an eV, at most [6.20]. As a consequence of this, no useful results could be obtained from this cluster.

6.5.2.2 MNDO Calculations

As has been demonstrated in the previous chapter, MNDO (and MINDO/3) are very powerful techniques which can provide a great deal of information on chemical bonds and reactions on solid surfaces. Hence, at first sight the use of MNDO would appear to be the most obvious approach to the group II/surface problem. However, apart from the obvious fact that only Be could be studied, there is another problem in that MNDO often overestimates the strengths of bonds involving Be. An example of this is the anomalously large binding energy obtained for small Be clusters [6.21]. A repeat of the Be + SiH_3 calculation gave a bond energy of 2.1 eV, i.e. a gross overestimate.

The MNDO parameters are obtained from bonds where both of the Be 2s-electrons are involved, i.e. there is effectively a promotion of one of the electrons to the 2p-orbital. In cases where the energy separation of the interacting MOs would normally be too great for a strong bond to form, MNDO appears to overestimate the interaction integrals. Note, however, that that this does not preclude the the use of MNDO for calculating the bond strength of a Be atom inserted into the dimer although it is difficult to say how reliable the results would be.

6.6 Relevance to MBE

It is now necessary to reconcile the topological discussion and the bond energy calculations with the observed behaviour of the group II dopants in MBE. One of the primary aims of the present study is to explain the zero sticking coefficient of Zn and this becomes even more puzzling given the similar initial interaction energies obtained for Mg and Zn from the cluster calculations.

The most important conclusion of the topological discussion is that a significant activation barrier should be present during incorporation of the group II atoms. In simple chemical terms, the incorporation will require the promotion of an s-electron into the empty p_x-orbital (see Fig. (6.3). Hence, the activation barrier will be related to the energy required for such an excitation and herein lies the reason for the difference between Mg and Zn. These excitation energies are obtainable experimentally, being 2.5 eV and 5.8 eV for Mg and Zn respectively. If the activation barrier for incorporation is greater than that for desorption then the latter will obviously occur (assuming similar pre-exponentials, see equation (6.1)). This would appear to be the case for the interaction of Zn with the As-dimer on the GaAs surface, i.e. the incorporation of the Zn is kinetically hindered.

6.7 Conclusions

In the solid state physics approach to adsorption the interaction of the atom or molecule with the surface is modelled using an interaction potential. Unfortunately the microscopic factors leading to this interaction potential are often unclear, and little physical insight is gained. Although the same effective potential approach is used to describe small molecules (particularly diatomics), MO methods are much more common, giving greater physical insight.

Although the interaction with a surface is obviously more

complex, the above study has shown that a combination of cluster calculations and topological analysis can provide useful information on the processes involved in MBE growth. The discussion has shown that the surface lifetime of Zn on GaAs is incompatible with the expected bond strength, and that this is due to a symmetry-induced activation barrier. Note, however, that this does not necessarily imply that Zn would be a useful dopant for GaAs if the activation barrier could be overcome. This is illustrated by the fact that Zn desorbs rapidly from ZnSe above about 300°C. Despite this Zn could still be a useful dopant for materials grown at lower temperatures (e.g. InSb) if it could be incorporated (although the sticking coefficient would still be less than unity). A possible way of achieving this may be through the use of excited-state Zn atoms (as has been done for the O_2 molecule). Certainly such experiments would provide useful information on any activation barrier.

CHAPTER 7

NATIVE DEFECT CONCENTRATIONS IN GaAs AND AlGaAs

7.1 Introduction

Any semiconductor crystal at a temperature above absolute zero will have a finite concentration of native defects. These defects, and the resulting defect-complexes, have a significant effect on the transport and optical properties of the semiconductor and so have been intensively studied in different materials systems. The types and relative concentrations of the defects present are strongly dependent on the growth technique used and on the particular growth conditions (such as temperature and flux ratios). This is mainly due to the different thermodynamic and kinetic factors involved in the different growth methods. The effect of these factors is best illustrated by considering the differences among the three main methods of growing GaAs and AlGaAs, LPE, MBE, and VPE. The relative influence of kinetics and thermodynamics in a particular growth technique is also important, although to what extent either of them dominates is still not certain.

In LPE, growth takes place from a melt consisting of unassociated atoms. Hence kinetic factors would be expected to have little effect. Calculations of defect concentrations for a liquid phase system show that the total defect concentration increases with increasing growth temperature [7.1]. There is in fact some evidence for this in LPE laser structures [7.2] and in LPE epitaxial layers [7.3]. The situation for VPE layers is more complex. There is experimental evidence for the above behaviour at high growth temperatures [7.4] but no calculations exist for comparison. The defect concentration in VPE is a complex function of growth rate, flux ratios and growth temperature. This is also true of MBE where, in addition to the above, the group V species used (i.e. tetramer or dimer) also has a significant effect. An important observation in MBE is that, in general, the total defect concentration is lower at higher growth

temperatures [7.5]. This is normally viewed as an indicator of the significant role played by kinetics in MBE growth, a point which will be discussed in more detail later. The defect types considered in the present calculations are; (i) Group III antisite, Ga_{As} or Al_{As}, (ii) As-antisite, As_{Ga} or As_{Al}, (iii) Group III vacancies, V_{Ga} or V_{Al}, (iv) As-vacancies, V_{As}.

The only study in the literature which has considered all of these defects is the liquid-phase calculation of Blom [7.1]. Other studies are by Hurle [7.6] (liquid-phase, interstitials only), Munoz-Yague et.al. [7.7] (vapour-phase, vacancies only) and Logan and Hurle [7.8] (vapour-phase, vacancies only).

The aims of the work presented in this chapter are threefold ; (a) to obtain knowledge on the general thermodynamic trends during growth, (b) a knowledge of trends in defect concentrations is useful for the diffusion studies in chapters 8 and 9, and (c) to obtain information on the variation of the defect concentration with increasing Al-content. The latter of these is relevant to an understanding of recombination at AlGaAs/GaAs heterojunctions.

7.2 Thermodynamic Model

7.2.1 Defect Formation Reactions

The basic defect-formation reactions, for GaAs, considered in the model are as follows ;

(7.1) $$^1/_2As_2 = As_{As} + V_{Ga}^{x}$$

(7.2) $$0 = V_{As}^{x} + V_{Ga}^{x}$$

(7.3) $$V_{As}^{x} + Ga_{Ga} = Ga_{As}^{2-} + V_{Ga}^{x} + 2e^{+}$$

(7.4) $$V_{Ga}^{x} + As_{As} = As_{Ga}^{2+} + V_{As}^{x} + 2e^{-}$$

(7.5) $$V_{Ga}^{x} = V_{Ga}^{-} + e^{+}$$

(7.6) $$V_{As}^{x} = V_{As}^{+} + e^{-}$$

where the superscript x denotes a neutral vacancy. Using the Law of Mass-Action this gives the following equilibrium constants ;

(7.7) $$K_1 = [V_{Ga}^{x}]/p_{As2}^{1/2}$$

(7.8) $$K_2 = [V_{Ga}^{x}][V_{As}^{x}]$$

(7.9) $$K_3 = [e^{+}]^2[Ga_{As}^{2-}][V_{Ga}^{x}]/[V_{As}^{x}]$$

(7.10) $$K_4 = [e^{-}]^2[As_{Ga}^{2+}][V_{As}^{x}]/[V_{Ga}^{x}]$$

(7.11) $$K_5 = [e^{+}][V_{Ga}^{-}]/[V_{Ga}^{x}]$$

(7.12) $$K_6 = [e^{-}][V_{As}^{+}]/[V_{As}^{x}]$$

where $[V_{Ga}^{x}]$ denotes the concentration of neutral Ga vacancies and p_{As2} is the As-overpressure in atmospheres. An Analogous set of equations is used for AlAs, i.e. equations (7.1)b to (7.12)b.

7.2.2 Equilibrium Constants

The equilibrium constant of a reaction is given in terms of the entropy and enthalpy by,

(7.13) $$K_i = \exp(\Delta S_i/k)\exp(-\Delta H_i/kT)$$

where k is Boltzmann's constant. Hence in order to calculate the K_i for the above reactions the ΔS_i and ΔH_i require to be known.

Reaction (7.1) is used by Logan & Hurle (LH) [7.8] in their study of vacancy concentrations in GaAs. They obtained their values of entropy and enthalpy by an experimental fit to annealing data,

assuming the only defects present to be Ga and As-vacancies. As will be seen later, this is questionable and so a recalculation of the data which did not depend on such an assumption was carried out (see later). Since the type of data used by LH for GaAs does not exist for AlAs, a recalculation would have to be done in any case. Reaction (7.2) is also used by LH. They used estimates for S and H obtained from experimental data. Subsequently however, Van Vechten (VV) [7.9] has calculated theoretical values for the virtual enthalpies of vacancy formation in compounds. Since the theoretical values are required for AlAs, it was decided to be consistent and use them also for GaAs.

7.2.3 Calculation of Enthalpies and Entropies

The virtual enthalpies for neutral vacancy formation in GaAs are ;

$$\Delta H(V_{As}^{x}) = \Delta H(V_{Ga}^{x}) = 2.31 \text{ eV}$$

This results in $\Delta H = 4.62$ eV, which is reasonably close to the value used by LH (4 eV).
According to LH, typical values for the pre-exponential factors for Schottky defects lie in the range $1 - 10^{8}$. The value obtained by them is 1.15×10^{4} . For the entropy of formation of both an As and a Ga-vacancy VV gives ;

$$\Delta S(V^{x}) = k \ln(3) = 1.1k$$

For the pre-exponential this gives $K_2^{o} = 9.03$. This is vastly different from the LH value but is still within the range given by them. It is the value used in the present calculations. Note that the above entropy is also used by Blom in his calculations.

Reaction (7.3) is not used in any of the previous studies, but the enthalpy and entropy are easily obtained. The virtual enthalpies required are $\Delta H(Ga_{As})$, $\Delta H(V_{Ga})$ and $\Delta H(V_{As})$, all of which can be obtained from Van Vechten [7.9]. This gives ;

$$\Delta H_3 = 0.35 \text{ eV} + 2\ \Delta H_{cv}$$

where ΔH_{cv} and ΔS_{cv} are the band-gap enthalpy and entropy respectively. The entropy of the above reaction is just that of the fully ionised antisite defect since $\Delta S(V_{As}) = \Delta S(V_{Ga})$. Again from Van Vechten ;

$$\Delta S(B_A^{+\Delta Z}) = \Delta S(A_B^{-\Delta Z}) = \Delta Z \Delta S_{cv}(AB)$$

The enthalpy and entropy of the forbidden bandgap for both GaAs and AlAs are given in Bloms' paper. Note that Blom uses the ΔH_{cv} and ΔS_{cv} for GaAs (AlAs) when calculating the equilibrium constants for the GaAs (AlAs) reactions, rather than using an average value (i.e. for AlGaAs). The same approach is used here.

Reaction (7.4) is treated in the same manner as (7.3), the virtual enthalpies being $\Delta H(As_{Ga})$, $\Delta H(V_{Ga})$ and $\Delta H(V_{As})$. The enthalpies and entropies for reactions (7.5) and (7.6) are also given by Van Vechten, again used by Blom.

The enthalpies and entropies for reactions (7.1)b to (7.6)b are easily obtained in the same manner as for GaAs, and are denoted as $\Delta H_1' - \Delta H_6'$ and $\Delta S_1' - \Delta S_6'$. This now brings us to the question of ΔH and ΔS for reactions (7.1) and (7.1)b. Consider reaction (7.1), the enthalpy change of which can be split into a sum of two virtual enthalpies ;

(7.14) $$\Delta H_1 = \Delta H(1/2As_2) + \Delta H(V_{Ga}^{x})$$

LH obtain $\Delta H_1 = 0.57$ eV by using experimental data and assuming the dominance of vacancies in the material studied. Although this experimental data does not exist for AlAs, it is possible to obtain reasonable estimates of the enthalpy by other means.

An idea of the probable trends can be obtained from PbS which is a more fully characterised material. Consider first the reactions for vacancy formation in PbS from a monatomic vapour-

phase ;

(7.15) $S(g) = S_S + V_{Pb}^x$

(7.16) $Pb(g) = Pb_{Pb} + V_S^x$

Kroger [7.10] has obtained the enthalpy changes for these reactions from experimental data and found them to be within 3 kcal mol^{-1} of one another.

One would expect the following for the virtual enthalpies ;

(7.17) $\Delta H(V_{Pb}^x) > \Delta H(V_S^x)$

(7.18) $\Delta H(Pb,PbS) < \Delta H(S,PbS)$

Therefore it would appear that the inequalities cancel out. This is physically reasonable since $\Delta H(V)$ and the bond strength of an atom in a lattice are proportional to r_c^2, r_c being the covalent radius.

The corresponding reactions for GaAs are ;

(7.19) $Ga(g) = Ga_{Ga} + V_{As}^x$

(7.20) $As(g) = As_{As} + V_{Ga}^x$

and a reasonable first approximation is to take the enthalpies as being equal. Note that even a small difference in the enthalpies leads to a considerable distortion of the stoichiometry curve. However, the present study is concerned mainly with qualitative trends in defect concentrations and these are not expected to be significantly affected. The effect of variation in the enthalpies and entropies is, however, checked in the final calculations.

As already mentioned, Van Vechtens' results give the virtual enthalpies for vacancy formation in GaAs as being equal. This in

turn means that the virtual enthalpies for incorporation of an As and a Ga atom into the lattice from the vapour are also equal (from equations (7.19) and (7.20)),

i.e., $\Delta H(As,GaAs) = \Delta H(Ga,GaAs)$ these being the virtual enthalpies for the reaction [7.11] ;

(7.21) $\quad Ga(g) + As(g) = GaAs(s) \qquad \Delta H = 155 \text{ kcal mol}^{-1}$

Hurle gives $\Delta H = 44.4$ kcal mol^{-1} for the reaction,

(7.22) $\quad {}^{1}/_{2}As_2(g) = As(g)$

Hence giving ;

$$\Delta H(1/2As_2,GaAs) = 33.1 \text{ kcal mol}^{-1} = 1.44\text{eV}$$

Combining this with $\Delta H(V_{Ga})$ gives ;

$$\Delta H_1' = 0.87 \text{ eV}$$

This value is 50% greater than that given by LH.

The enthalpy change for reaction (7.1)b can be obtained in the same manner. The relevant reaction for AlAs is [7.12] ;

(7.23) $\quad Al(g) + As(g) = AlAs(s) \qquad \Delta H = 182 \text{ kcal mol}^{-1}$

Again, the similar atomic size means that the enthalpies of vacancy formation are equal and that equal apportionment should be a good approximation. Hence, $\Delta H(1/2As_2,AlAs) = 46.6$ kcal $mol^{-1} = 2.03$ eV

The virtual enthalpy of formation of an Al-vacancy is 2.42 eV. Therefore ;

$$\Delta H_1' = 0.39 \text{ eV}$$

Another calculation of these quantities has been carried out by

Chiang and Pearson [7.13] in their study of annealled GaAs. For the vacuum annealling results they considered the following reactions,

(7.24) $$As_{As} = {}^{1}/_{2}As_2(g) + V_{As}^{x}$$

(7.1) $${}^{1}/_{2}As_2(g) = As_{As} + V_{Ga}^{x}$$

i.e. they also assumed that vacancies were the only native defects formed. The enthalpies obtained were 2.9eV and -1.4eV respectively, the corresponding entropies being 9.8k and -23.2k. Hence the values obtained for reaction (7.1) are vastly different from these given by LH, even the sign of the enthalpy change is different. CP ascribe the difference in enthalpies of reactions (7.1) and (7.24) to the fact that the reactions are taking place at the surface. However, the concentrations are measured in the bulk (albeit close to the surface) and hence this explanation seems unlikely. Since these annealings were carried out in vacuum the GaAs sample would be expected to become Ga-rich. Therefore a significant concentration of Ga-antisites may be present. These also behave as acceptors.

Given the difference between the calculated value of H_1 and that given by LH it is also necessary to obtain a value for the entropy change. The total change in entropy can be considered as the sum of two virtual entropies ;

(7.25) $$\Delta S_1 = \Delta S(1/2As_2, GaAs) + \Delta S(V_{Ga})$$

The entropy change $\Delta S(1/2As_2, GaAs)$ can be further broken down into different components as follows ;

(a) The change in entropy for the reaction,

(7.22) $${}^{1}/_{2}As_2(g) = As(g)$$

The experimental value is not available but an estimate can be obtained by considering the experimental values for dissociation

of group VI and group VII diatomic molecules. The entropy changes for these reactions all lie within 0.6k of each other, the average change being 6.5k. Hence this value was used for ΔS_{22}. Note that the entropy change in this case is positive.

(b) The configurational entropy change due to the mixing of the Ga and As atoms: This has been estimated by Swalin [7.14] to be approximately 2.2k. Again the entropy change is positive.

(c) The entropy change due to incorporation of a gas-phase As-atom into the solid lattice: There are two possible courses here. The first is to use the entropy difference between gaseous and solid Ge as an estimate. This has the disadvantage that while the entropy of vapourisation should be well approximated (due to Troutons' rule), the entropy of sublimation may be less so. This is not a problem however because the entropy of sublimation of GaAs has been measured experimentally by Lichter, and has been given in Arthurs' paper [7.11]. Hence, combining this with the entropy of vapourisation of Ge gives the following ;

$$\Delta S_{(As,GaAs)} = \Delta S^{vap(Ge)} + \Delta S^{sub(As,GaAs)}$$

$$= -17.51 \text{ k}$$

Combining all of the above component entropies gives a value for $\Delta S(1/2As_2,GaAs)$ of 8.8k. This in turn results in ΔS_1, equal to 7.7k.

This value is in close agreement with that given by LH (ΔS_1 = 7.88 k). Note that the above values correspond to the reaction taking place at 298K. However, since the defect concentrations require to be calculated at a variety of temperatures, it was not thought necessary to recalculate ΔS or ΔH. Any variation with temperature will be small and in any case will probably be masked by the uncertainties introduced by the above approximations. When estimating the entropy change for reaction (7.1)b, strictly speaking an average of the values appropriate to Si and Ge should be used. However, an estimate of the entropy of fusion of the

AlAs is also required (as against the experimental value available for GaAs). Again it was decided that this would make no significant difference to the results and so the entropy change appropriate to reaction (7.1) was used for reaction (7.1)b. The final set of values used in the calculations are collected together in Table 7.1.

7.3 Derivation of the Mathematical Model

The types of defect considered in the present calculation are the same as those considered by Blom. The relative concentrations are governed by the electroneutrality condition ;

$$(7.26) \qquad n + [V_{III}^{-}] + 2[Ga_{As}^{2-}] + 2[Al_{As}^{2-}] = p + [V_{As,Al}^{+}] + [V_{As,Ga}^{+}] + 2[As_{III}^{2+}]$$

Note that $[V_{III}^{-}]$ includes $[V_{Ga}^{-}]$ and $[V_{Al}^{-}]$ which are indistinguishable in AlGaAs. However, the concentrations are still calculated separately and weighted according to the AlAs mole fraction. The same applies to $[As_{III}^{2+}]$. As in Bloms' calculations there are a total of nine different defects to be considered, i.e., six neutral and charged vacancies (V_{III}^{x}, V_{III}^{-} , $V_{As,GaAs}^{x}$, $V_{As,AlAs}^{x}$, $V_{As,GaAs}^{+}$, $V_{As,AlAs}^{+}$) and three antisite defects ($As_{III}v^{2+}$, Ga_{As}^{2-}, Al_{As}^{2-}). The antisite defects are assumed to be fully ionised. The concentrations are obtained in terms of the equilibrium constants using equations (7.7) - (7.12) (and analogous ones for AlAs). Substitution of these expressions into the electroneutrality equation gives a fourth order polynomial in the electron concentration n ;

$$(7.27) \qquad A'n^4 + (1+B')n^3 - (n_i^2+C')n - D' = 0$$

where,

$$(7.28) \qquad A' = 2[(1-X_{AlAs})A^{Ga} + X_{AlAs}A^{Al}]$$

$$(7.29) \qquad B' = (1-X_{AlAs})B^{Ga} + X_{AlAs}B^{Al}$$

GaAs	AlAs
ΔH_1 = 0.87 eV	0.39 eV
ΔS_1 = 7.7 k	7.7 k
ΔH_2 = 4.62 eV	4.84 eV
ΔS_2 = 2.2 k	2.2 k
$\Delta H_3 = \Delta H_4$ = 3.62 eV	4.84 eV
$\Delta S_3 = \Delta S_4$ = 12.7 k	12.7 k
$\Delta H_5 = \Delta H_6$ = 0.327 eV	0.476 eV
$\Delta S_5 = \Delta S_6$ = 6.35 k	6.45 k

Table 7.1 Final values used for the Enthalpies and Entropies.

(7.30) $C' = (1-X_{AlAs})C^{Ga} + X_{AlAs}C^{Al}$

(7.31) $D' = 2[(1-X_{AlAs})D^{Ga} + X_{AlAs}D^{Al}]$

and,

(7.32) $A^{Ga} = [Ga_{As}^{2-}]/n^2 = (N_v^2 K_3 K_2 N')/(K_1^2 p_{As2} n_i^4)$

(7.33) $B^{Ga} = [As_{Ga}^{2+}]n^2 = (K_4 K_1^2 p_{As2} N_c^2 N')/K_2$

(7.34) $C^{Ga} = [V_{As}^{+}]n = (K_6 K_2 N_c N')/(K_1 p_{As2}^{1/2})$

(7.35) $D^{Ga} = [V_{Ga}^{-}]/n = (K_5 K_1 p_{As2}^{1/2} N_v N')/n_i^2$

with analogous expressions for AlAs. The polynomial coefficients are calculated using the ΔH_i and ΔS_i already given. The polynomial is then solved numerically to obtain a value for n, which is then used to calculate the concentrations of the different defects.

The factor N' in the above equations is simply a constant to convert the units of calculated defect density from mol^{-1} to cm^{-3}. It is given by ;

$$N' = Nd/M$$

Where N is Avogadros' number, d is the density of the material and M is its molecular weight. Another point worth noting is the appearance in these equations of the valence and conduction band densities of states, N_v and N_c respectively. These also appear in the expressions obtained by Blom but are not used by, for example, Munoz-Yague et.al. [7.7] or Chiang and Pearson [7.13]. Consider the reaction for the formation of an electron-hole pair;

$$e^- + e^+ = 0$$

Application of the law of mass-action to this reaction gives ;

$$[e^-]\,[e^+] = \exp(-\Delta E_{cv}/kT)$$

E_{cv} is the fundamental band gap and is a free energy change. The electron and hole concentrations, n and p respectively, are related through the following;

$$np = N_c N_v \exp(-\Delta E_{cv}/kT) = n_i^2$$

Hence;

$$[e^-][e^+] = (n/N_c)(p/N_v)$$

A more detailed exposition is given by Kroger [7.10]. Expressions for N_c, N_v and E_{cv} for AlAs molefractions up to 0.45 are given by Anthony [7.15].

The effect of shallow donors or acceptors on the defect concentrations is simply taken account of by adding N_D^+ or N_A^- to the electroneutrality condition.

7.4 Deep Traps in GaAs and AlGaAs

Before discussing the relevance of the foregoing vapour phase defect concentration calculations to MBE, a brief word on the deep traps thought to be associated with native defects observed in GaAs and AlGaAs is appropriate. More detailed compilations are found in the recent reviews by Mircea and Bois [7.16] and by Milnes [7.17]. It is important to note that the assignment of specific native defects to observed deep states is in the majority of cases very tentative. Deep states associated with transition metal impurities are the easiest to characterise.

Probably the most extensively characterised deep state in GaAs known to be associated with a native defect is the electron trap EL2. Even in this case, however, there is still controversy concerning the detailed microscopic structure. The one thing which can be said with reasonable confidence is that the EL2

state involves an As-antisite defect. Lagowski et. al. [7.18] have presented evidence to show this but claim that the As_{Ga} is part of a complex, probably with an As-vacancy. Bhattacharya et. al. [7.19] have studied EL2 in VPE material and found that its concentration increases with increasing As-overpressure. They deduced that EL2 is linked to the presence of Ga-vacancies. However, the results of Lagowski et. al. [7.18] show that EL2 is eliminated by the presence of shallow donors and so As_{Ga} would appear more likely.

The only method available at present for obtaining direct information on electronic structure is Electron Paramagnetic Resonance (EPR). This technique has been used to demonstrate the existence of P_{Ga} in GaP [7.20] and As_{Ga} in GaAs [7.21]. For As_{Ga} two donor levels were identified at E_c-0.77 eV and at E_c-1.0 eV, the first of which agrees closely with the DLTS and DLOS values for EL2. The results obtained from DLOS [7.22] are the most reliable for comparison with photo-EPR data. They show that there is a negligible Franck-Condon shift for EL2. Worner et. al. [7.21] have also demonstrated that there are no associated defects in the first shell around As_{Ga}. Hence if this defect is identified with EL2 then the As_{Ga}-V_{As} complex is incompatible with the EPR data. The EPR data of Weber et. al. [7.23] was obtained from plastically deformed GaAs. In agreement with this, Ishida et. al. [7.24] have reported the enhancement of EL2 after plastic deformation of GaAs.

Another objection against the As_{Ga}-V_{As} model is the stability of $(As_{Ga}-V_{As})^{2+}$. Reineke [7.25] obtains a binding energy of 0.9 eV for the neutral complex. However, the interaction energy of the doubly ionised complex would most likely be repulsive (EL2 has been shown to be a double donor).

Theoretical calculations of the energy levels associated with the As_{Ga} antisite are also inconclusive. Lin-Chung and Reineke [7.26] obtain a level 0.27 eV below the conduction band which they claim is too high for this to be EL2. However, Bachelet et. al. [7.27] obtain results which they say are compatible with the

EPR data. In particular, they obtain excellent agreement with the experimental energy splitting between the two donor states.

Although there is much disagreement as to the exact nature of EL2 the results of Lagowski taken with the EPR results strongly indicate that As_{Ga} is involved. Hence in the remainder of this chapter it will be assumed that the concentration of the EL2 defect is dependent on the concentration of the As_{Ga} (or As_{Al}) antisite. This does not preclude the association of the As_{Ga} with, say, a Ga-vacancy due to post-growth migration of defects. (The Ga-vacancy is an acceptor and would be a second-nearest-neighbour). If EL2 is due to a complex of As_{Ga} and another defect then its concentration will be dependent on the concentration of both defects. The Ga-vacancy is the only other native defect which is compatible with a high As-overpressure. The above discussion illustrates the fact that there is still much controversy as to whether the As-antisite is isolated or not.

Another native defect which has been identified in GaAs with some confidence is the Ga-antisite which was observed in PL studies on bulk material grown from a Ga-rich melt [7.28]. This defect gives rise to two acceptor levels at 77 meV and 230 meV. According to Worner et. al. [7.21] detection of Ga_{As} using EPR will probably require the application of uniaxial stress. In any case, observation of both As_{Ga} and Ga_{As} in the same sample would be unlikely since the former requires As-rich growth while Ga_{As} is observed in samples grown Ga-rich.

The presence of isolated vacancies in as-grown GaAs or AlGaAs has not been demonstrated , although Lang et. al. [7.29] claim that their results on electron-irradiated GaAs are compatible with the isolated Ga-vacancy. This is not to say that vacancies do not exist in as-grown material but rather that they exist in complexes with other native defects or with impurities.

Deep traps in AlGaAs are less well characterised than those in

GaAs. One point to note is that traps on the group III sublattice will tend to have parameters similar to the same defect in GaAs due to the nearest neighbours being As atoms in both cases. One example of this is the E6 trap identified by Hikosaka et. al. [7.30] in MBE AlGaAs which has an almost identical trap-signature to EL2 in GaAs. More rigourously, native defects on the group III sublattice will lead to gap states which are derived mainly from the conduction band.

7.5 Effect of Growth Technique on Trap Concentration

The type of growth technique used has a significant effect on the native defects and impurities incorporated into the grown layer. Apart from variations caused by the different growth mechanisms, the main factor distinguishing different techniques is the stoichiometry. For example, LPE growth takes place from a Ga-rich melt and consequently has a Ga-rich stoichiometry. LPE GaAs layers are distinctive in that the concentration of electron traps is normally below the detection limit, the trap concentration present being due to two hole traps which are unique to LPE layers [7.16]. As a result of this, LPE material has always been the purest available although recent improvements in VPE and MBE has resulted in comparable quality material. Given the Ga-rich stoichiometry the two hole traps are probably As-vacancy related.
Increasing the AlAs molefraction does not introduce any new traps or significantly increase the total trap concentration in LPE layers.

The trap concentration in VPE GaAs is normally dominated by the electron trap EL2. The concentration of this trap has been shown to be stongly dependent on the stoichiometry of the vapour-phase, being higher when the vapour is As-rich. Other levels which have been reproducibly observed are two hole traps at E_v + 0.35 eV and E_v + 0.31 eV. These have been observed in organometallic VPE (OMVPE) along with an electron trap at E_c-0.36 eV which is thought to be due to residual trimethylaluminium in the system. As the AlAs molefraction is increased this trap increases rapidly

in concentration being dominant for $X_{AlAs} > 0.1$. EL2 is found to be independent of AlAs molefraction. This rapid increase in total trap concentration is another difference between VPE and LPE material. MBE GaAs also has electron traps present, although mostly different ones from those observed in VPE. One exception is the level at E_c-0.36eV which is also found to increase rapidly with increasing AlAs molefraction. The deep traps observed in MBE material will be discussed in more detail in section 7.7.2.

7.6 Calculated Defect Concentrations

7.6.1 Defect Concentrations versus AlAs Molefraction

The concentrations of charged native defects versus AlAs molefraction at 970K for three different As overpressures are given in Figs. 7.1 to 7.3. (The concentration of neutral defects is very much smaller at this temperature). 970K was chosen because this is the normal growth temperature used in the experimental studies reported in chapters 8 and 9. Comparison of the results with those obtained by Blom reveals significant differences in the general trends. The vapour-phase calculations show an increase in the concentrations of all the defect types except group III antisites (the behaviour of which is seen to be more complex). In the liquid-phase calculations only the vacancies increase in concentration, that of both types of antisite decreasing.

In the case of As-vacancies, simple vapour-pressure arguments would lead to the conclusion that $[V_{As}]$ should be less in AlGaAs than GaAs. However, the calculated concentrations show the opposite behaviour. Closer examination of the results show that the overall stoichiometry of the AlGaAs is indeed more As-rich. However, the extra As does not reduce $[V_{As}]$ but rather increases the concentration of As-antisite defects. This is a very interesting result which will be discussed in relation to diffusion in chapter 8.

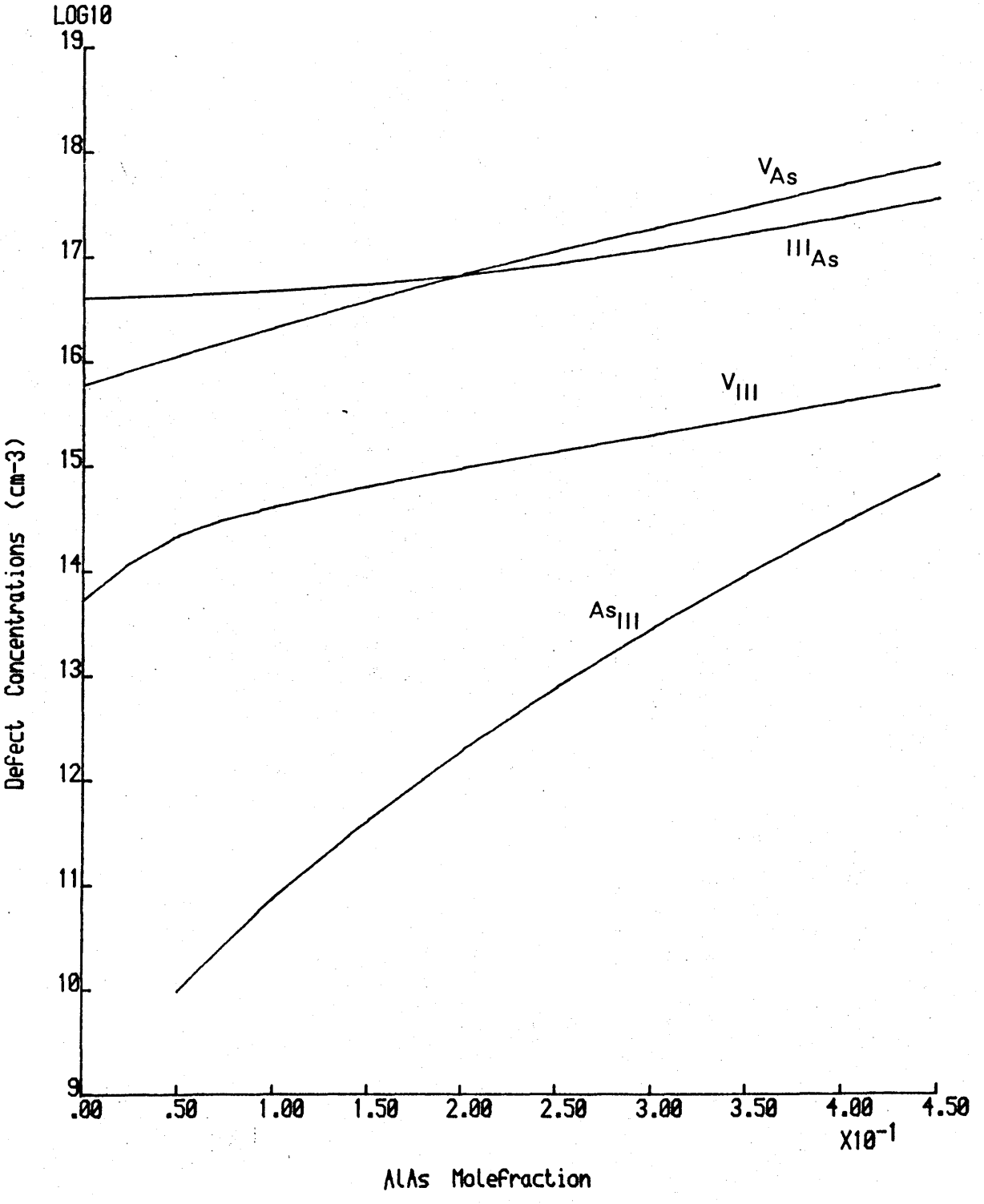

Figure 7.1 Native defect concentrations versus AlAs molefraction for T = 970K and $p_{As2} = 5 \times 10^{-10}$ atm.. Note that $[As_{III}]$ is zero for GaAs.

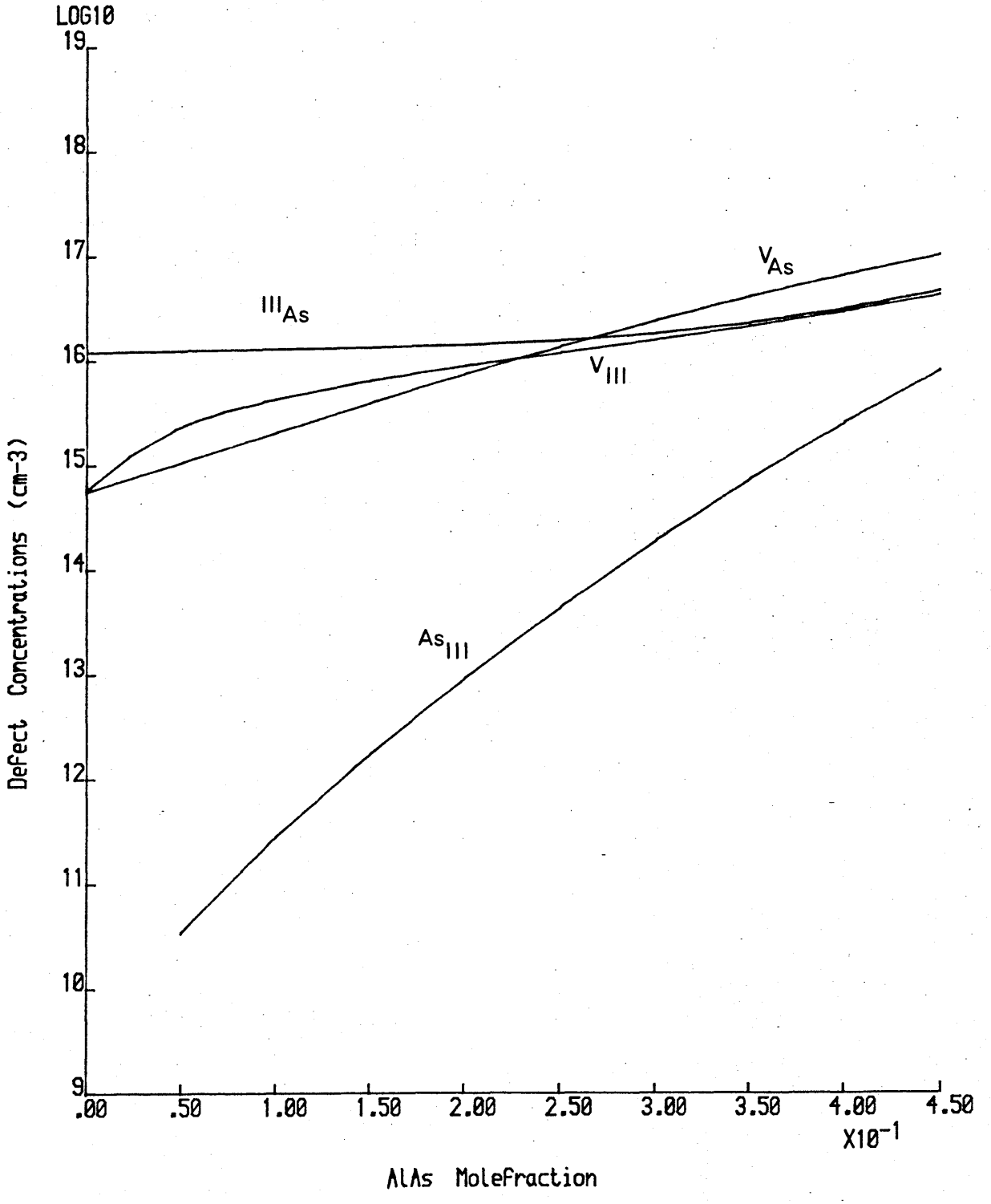

Figure 7.2 $p_{As2} = 10^{-8}$ atm., T =970K.

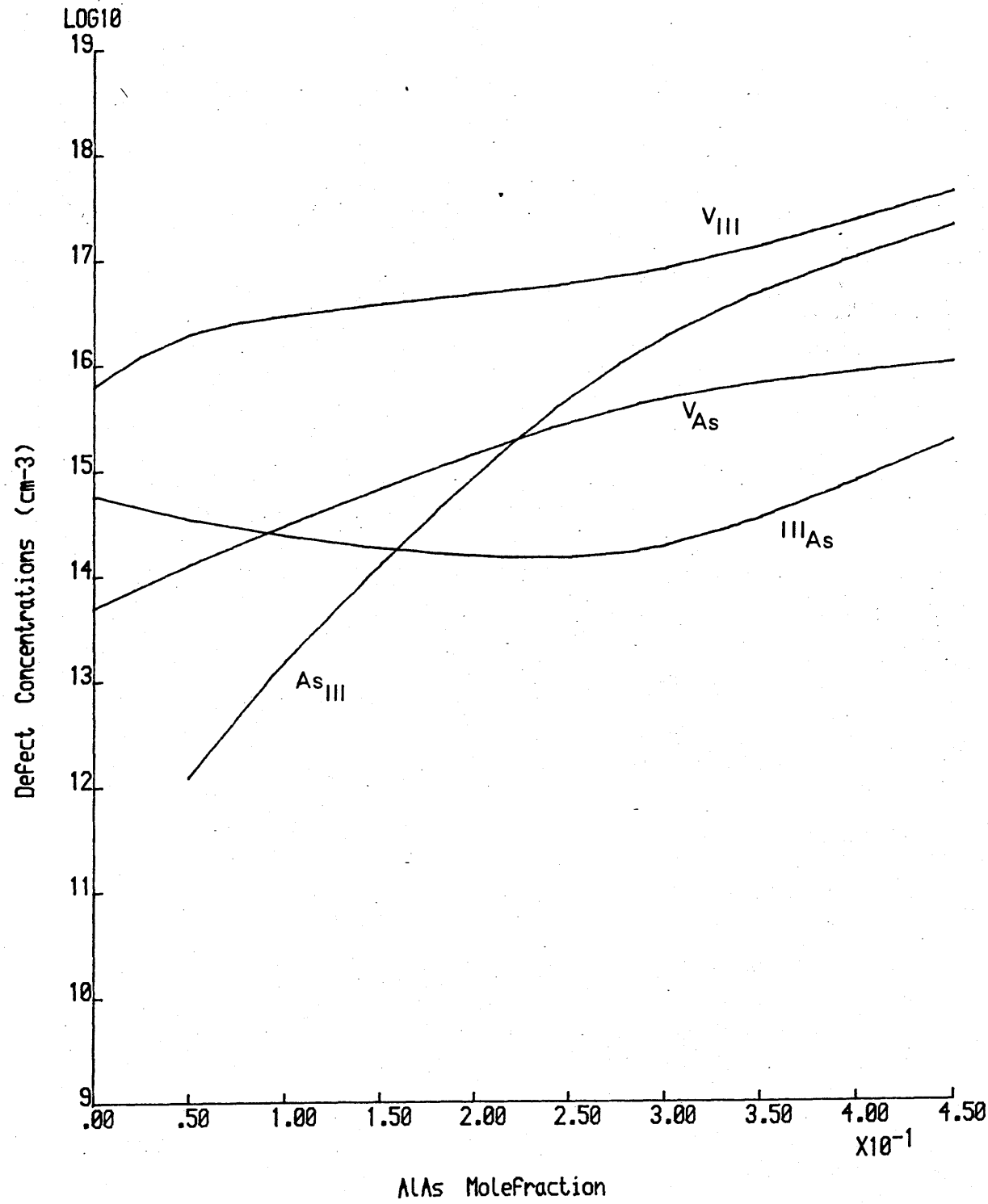

Figure 7.3 $p_{As2} = 5 \times 10^{-7}$ atm., T = 970K.

7.6.2 Defect Concentrations versus Temperature

The variation of defect concentration vs. temperature for GaAs and $Al_{0.3}Ga_{0.7}As$ is shown in Figs. (7.4) and (7.5) ($p_{As2} = 10^{-8}$). Once again there are qualitative differences with the liquid-phase results where both the total and individual defect concentrations increase with temperature. For the vapour-phase only As-vacancies and group III-antisites increase significantly with temperature, while the concentration of As-antisites decreases. This is the behaviour which would be intuitively expected for MBE growth from consideration of the surface lifetime of the As. However, it would appear to be adequately described within a thermodynamic framework. The concentration of V_{III} would be expected to decrease with increasing temperature. However, the results obtained show its behaviour to be more complex, falling and then rising again for $Al_{0.3}Ga_{0.7}As$.

The effect of a fixed concentration of dopants and acceptors is illustrated by the results shown in Figs. (7.6) and (7.7). As expected, donors suppress donor-type defects (i.e. As_{Ga} and V_{As}) and similarly for acceptors (i.e. Ga_{As} and V_{Ga} are suppressed). Note that the total defect concentration initially decreases with increasing temperature, passes through a minimum, and then increases. This behaviour was also obtained (for undoped material) by Munoz-Yague et. al. [7.7] in their study of vacancy concentrations.

7.7 Discussion

7.7.1 Stoichiometry

In liquid phase growth the stoichiometry is determined by the composition of the melt. In vapour-phase growth the stoichiometry is a complex function of temperature and As-overpressure, as is demonstrated by the results presented above. These show a transition from As-rich to Ga-rich material as the pressure decreases, with a crossover around $p_{As2} = 5 \times 10^{-8}$ atm. This raises the question of the applicability of these results to

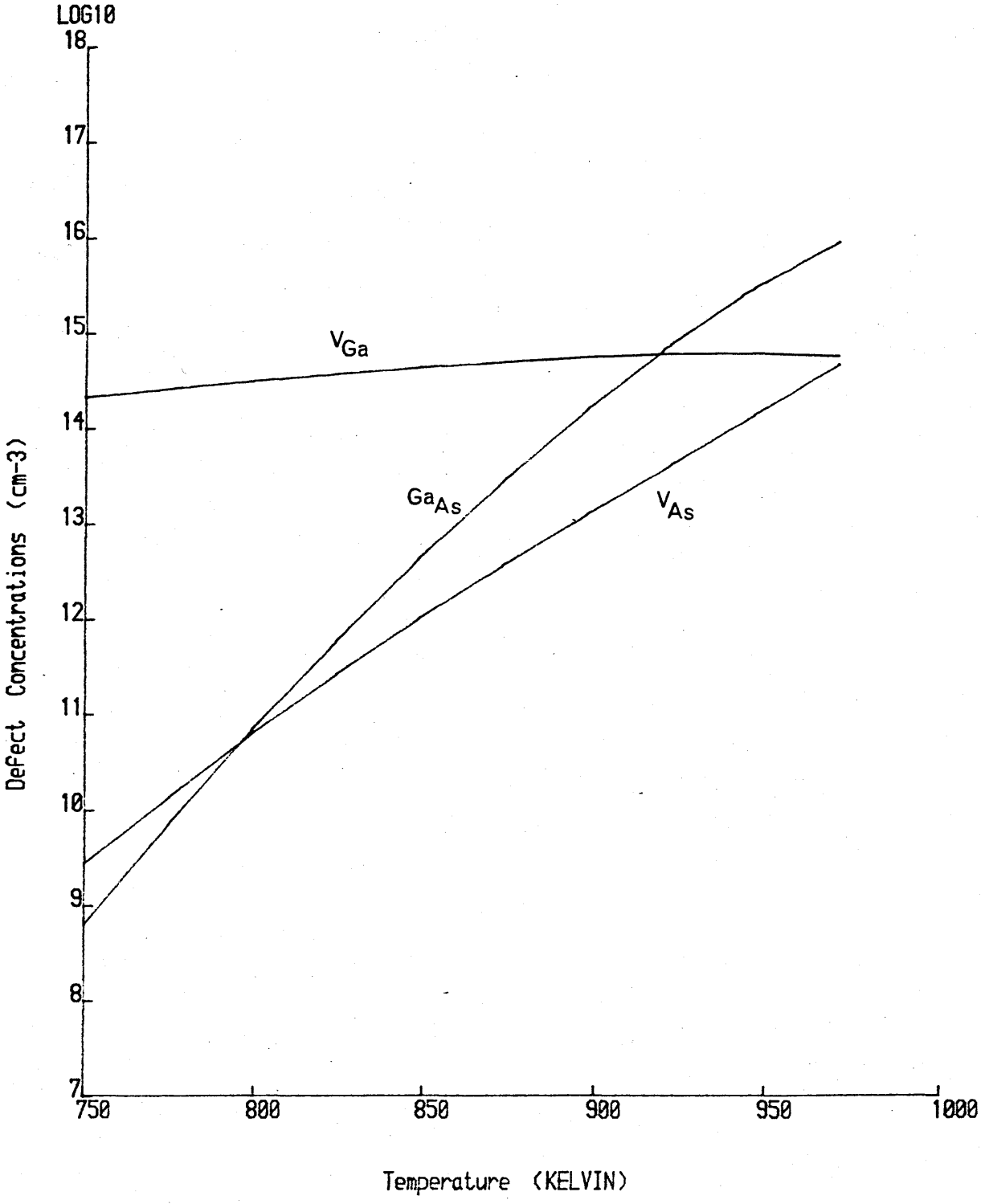

Figure 7.4 Native defect concentrations in GaAs versus temperature, $p_{As2} = 10^{-8}$ atm..

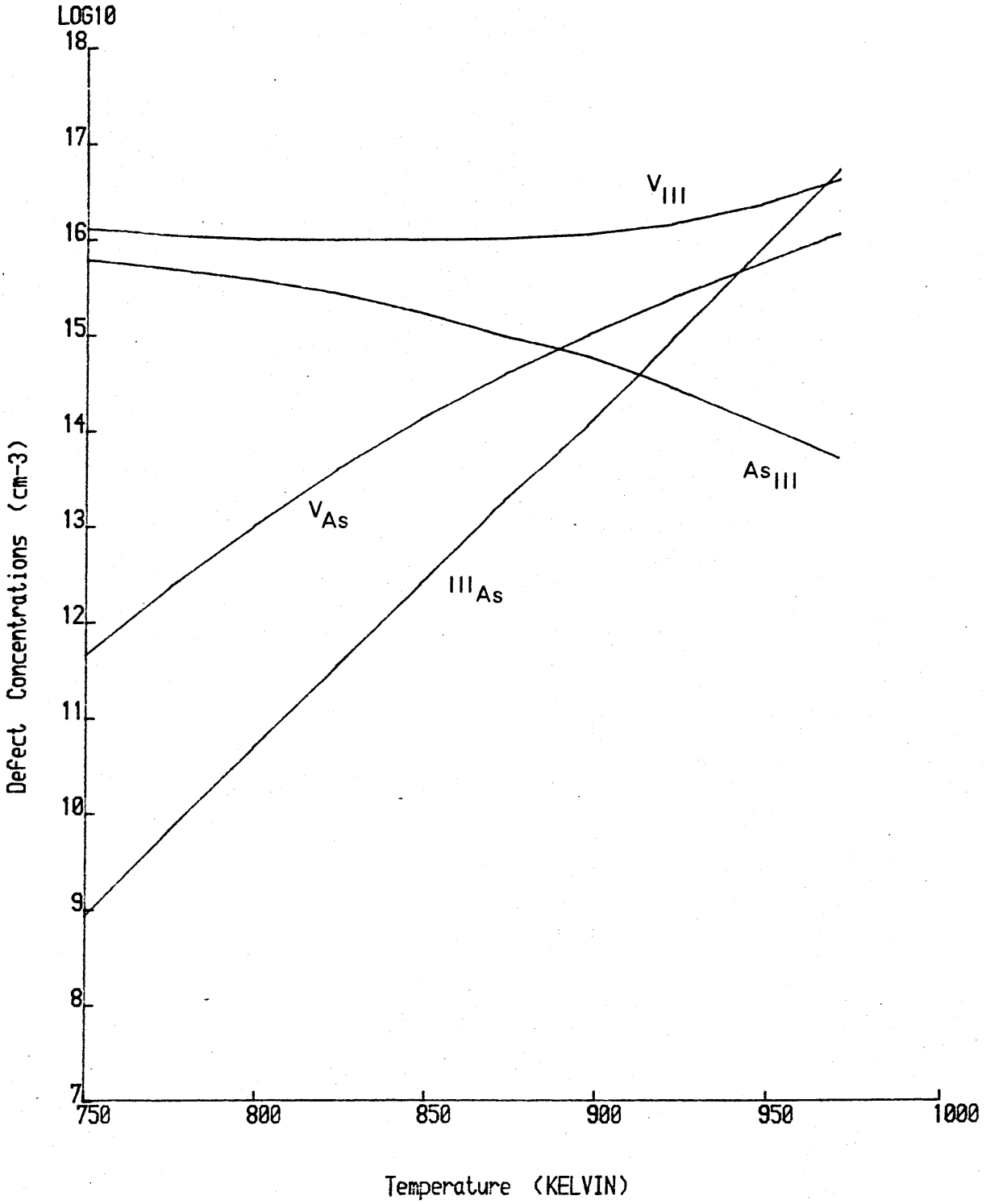

Figure 7.5 Native defect concentrations in $Al_{.3}Ga_{.7}As$ versus temperature, $p_{As2} = 10^{-8}$ atm..

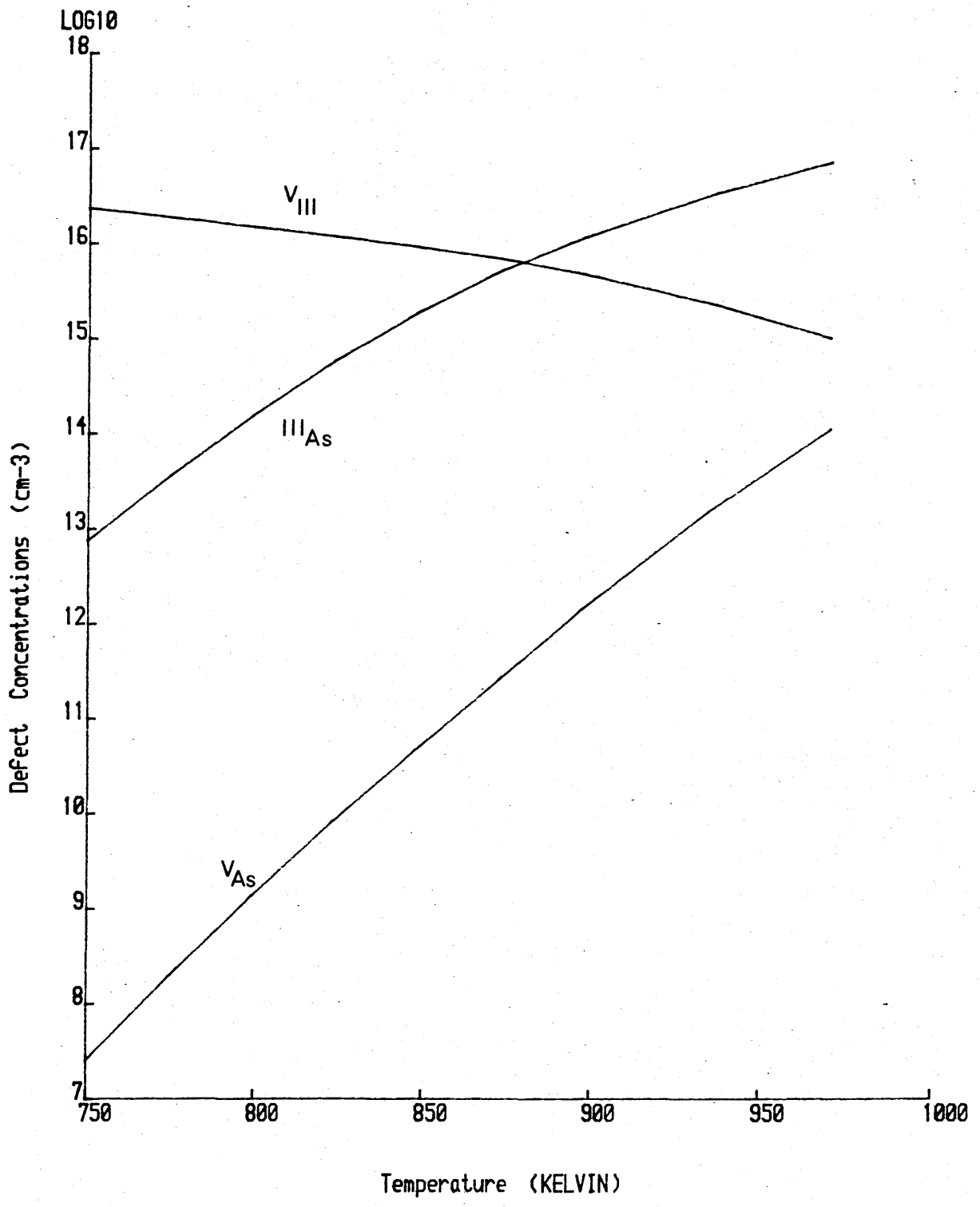

Figure 7.6 Native defect concentrations in GaAs versus temperature in the presence of a background of 1×10^{17} cm^{-3} donors, $p_{As2} = 10^{-8}$ atm..

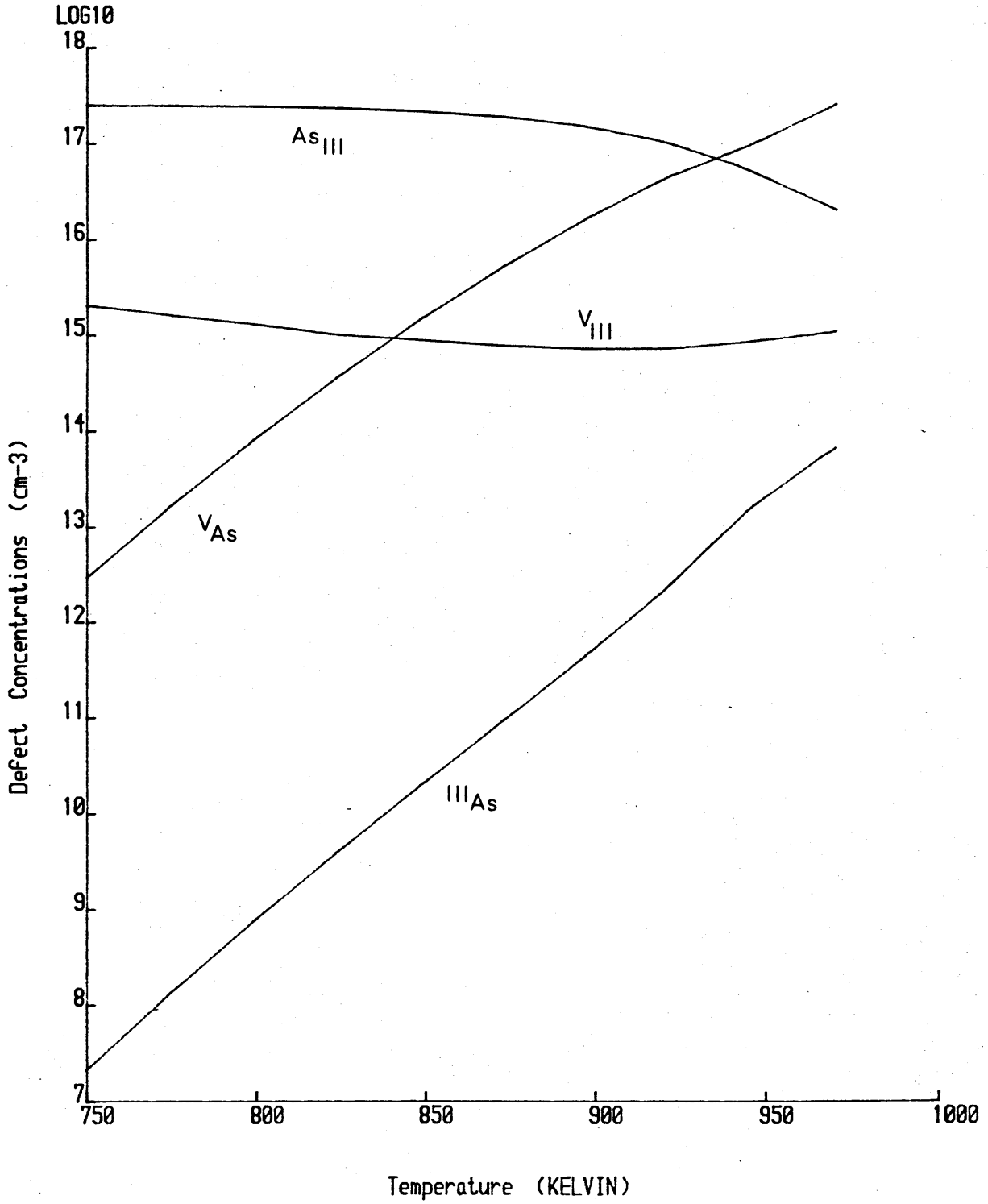

Figure 7.7 Native defect concentrations in $Al_{.3}Ga_{.7}As$ versus temperature in the presence of a background of 5×10^{17} cm^{-3} acceptors, $p_{As2} = 10^{-8}$ atm..

MBE growth and of the stoichiometry of MBE material.

Heckingbottom and Davies [7.32] use the vapour pressure data of Arthur to imply that MBE growth is Ga-rich. However, inspection of the phase diagram and vapour-pressure curves in chapter 2 shows that most of the partial pressure of As_2 on the Ga-liquidus is due to the GaAs itself. On the As-rich side of the liquidus line the large As partial-pressure is required to maintain equilibrium with the pure As in the melt. Hence, this phase diagram gives no information on the stoichiometry of the GaAs itself.

From Arthurs' data [7.11] the equilibrium partial pressure of As_2 on the Ga-rich side of the liquidus line is given by ;

$$p_{As2} = \exp(28.7)\exp(-4.0/kT)$$

At 970K the equilibrium partial pressure of As_2 over GaAs is therefore approximately 5×10^{-9} atm.. The As-overpressures normally encountered in MBE are of the order of 10^{-7} atm., i.e. significantly higher than the equilibrium value. For an As-overpressure of 5×10^{-7} atm., the defect calculations give an As-rich stoichiometry, which would seem to imply that MBE-grown material is As-rich. In practice, however, the situation is further complicated by the need to incorporate the growing film into the model. The model described here is a crude first approximation since it describes only the equilibrium between the vapour and the bulk. In practice sufficient As must be supplied to stabilise the surface phase, i.e. the growing film. Hence, as pointed out by Madhukar [7.33], consideration of the equilibrium state of the entire system must include vapour + substrate + growing film. Note, however, that some of the more dominant thermodynamic features of MBE growth should still be describable.

The stoichiometry of MBE layers has not been directly obtained experimentally. However, some insight can be gained by studying the behaviour of deep traps as the growth temperature is varied. As has already been pointed out, different growth techniques and

conditions introduce native defects in different relative concentrations. Hence the total defect concentration may be dominated by one particular type and may increase or decrease with temperature. However, providing the calculated trends for individual defects are followed in practice then reasonable deductions may be made as to the type of defect associated with a particular trap.

7.7.2 Deep Traps in MBE GaAs

The most detailed study of the behaviour of deep traps in MBE GaAs has been carried out by Blood and Harris [7.34]. They have examined the behaviour of five electron traps which they label M1, M2, M2', M3 and M4. The two growth parameters varied were temperature and the ratio of the As and Ga fluxes and from the results obtained the following conclusions can be made : Trap M2 only occurs for growth at 650°C and above and hence is probably an As-vacancy complex. M1 and M4 decrease with increasing growth temperature and at first glance this would indicate that As-vacancies are not involved. However, they also decrease with increasing As:Ga flux ratio and hence the most likely explanation is that they are As-vacancy/impurity complexes with the temperature dependence being dominated by the desorption of impurities. From the flux ratio dependence of M2' and M3 it would appear that they involve Ga-vacancies (assuming a negligible concentration of As_{Ga}). Note though that the temperature dependence of M3 is unusual in that it passes through a maximum at about 550°C. Hence M3 may be a complex involving both As and Ga-vacancies. The increase from 500°C to 550°C may be due to the availability of extra As-vacancies from M1 and M4 and extra Ga-vacancies from M2' (assuming the decrease in all these traps is dominated by impurity desorption).

The main conclusion of this discussion is that the dominant traps in the temperature range 500°C to 650°C would appear to involve As-vacancies. This therefore implies that MBE GaAs is always Ga-rich for an As: Ga ratio of 5:1 at 550°C. However, increasing the flux ratio leads to a crossover at 7:1, i.e., As-rich

material can be obtained for high As-overpressures. As the growth temperature is increased this becomes more difficult to achieve due to the dominance of the temperature dependence. This is in agreement with the rapid increase in $[V_{As}]$ with temperature observed in Figs. (7.4) and (7.5).

7.7.3 Qualitative Trends in the Calculated Concentrations

The results in Figs. (7.1) to (7.3) show that both $[V_{As}]$ and $[V_{III}]$ increase with increasing AlAs molefraction. Unfortunately, however, the available studies of traps in MBE AlGaAs are not detailed enough to allow conclusions on stoichiometry to be drawn. An interesting point is the effect of $[V_{III}]$ on the diffusion of group II elements such as Zn and Be. The experimental and theoretical results obtained indicate that AlGaAs is more As-rich than GaAs and hence has a higher concentration of group III vacancies. This is difficult to reconcile with the incorporation reaction usually invoked for interstitial-substitutional diffusion, and this point will be discussed further in chapter 8.

The antisite defects are potentially the most reliable indicators of defect trends since they have been ascribed to particular traps with reasonable confidence. Consider first the Ga_{As}-antisite in GaAs, which has been identified with the 77 and 230 meV acceptor levels in MG GaAs. The results obtained indicate that Ga_{As} should be present in MBE GaAs and the PL results of Bhattacharya et. al. do indeed show a series of unidentified levels between 70 and 100 meV. The presence of these levels would appear to be strongly dependent on the growth conditions since they are not observed in other published PL spectra.

By a fortunate coincidence the other native defect which has been ascribed to a deep trap, i.e., As_{Ga} to EL2, is the one which shows the most dramatic behaviour as the AlAs molefraction is increased in the calculated defect concentrations. This is in fact observed in practice since EL2 has never been detected in MBE GaAs while it is, however, detected in MBE AlGaAs. This

would suggest that these vapour-phase calculations do indeed qualitatively describe the native defect variation with AlAs molefraction. Hikosaka et. al. [7.30] have shown, however, that the concentration of E6 (EL2) is virtually independent of AlAs molefraction (excluding GaAs) while the theoretical results suggest that it should continue to rapidly increase.

A possible explanation for this behaviour is as follows : The main factor affecting the concentration of As-antisites would appear to be the ease with which cation vacancies are formed. The above calculations reflect the fact that formation of V_{Ga} rather than As_{Ga} is more favourable. The calculated trend for As_{Ga} will only be observed in practice, however, if the concentration of cation vacancies is maintained at it's equilibrium level. During MBE growth the surface will be a better source of As-vacancies than of cation vacancies and hence there exists the possibility of a frozen-in concentration of the latter (which will be dependent on the growth conditions). The concentration of EL2 will then be fixed by the concentration of cation vacancies (in fact if it is a complex it may require the participation of, for example, a V_{Ga}-V_{Ga} divacancy).

Hence a concentration of cation vacancies in GaAs greater than the equilibrium value may lead to the formation of As-antisites. This is supported by the observation that annealing of Si_3N_4-capped MBE-GaAs leads to the creation of EL2 [7.36]. This has been attributed to the out-diffusion of Ga, and hence formation of Ga-vacancies. The dependence on AlAs molefraction of $[V_{III}]$ will be much weaker than $[As_{Ga}]$ although there should still be some variation. Again, however, this variation will only be observed under conditions where thermodynamic equilibrium is maintained.

The results in Fig. (7.5) indicate that the concentration of EL2 should decrease with increasing growth temperature. This behaviour was in fact observed by McAfee et. al. [7.37] in their study of MBE AlGaAs.

A final important point which should be mentioned here is the discrepancy between the calculated total defect concentration (> 10^{15} cm^{-3}) and the concentrations observed by DLTS (10^{12}-10^{13} cm^{-3}). Although this might be ascribed to growth effects, Blom has noted that the defect concentrations obtained from TEM studies are often at variance with the DLTS results. The reason for this is still unclear, although there is a school of thought which attributes clusters of defects as being the cause of each trap. Certainly the results obtained for the temperature variation show that the total defect concentration decreases with temperature and in practice this may be achieved through the formation of complexes.

7.7.4 Effect of Variation of Enthalpies

Given the distinct behaviour of the As-antisite a test of the effect of varying the enthalpies of reaction was carried out. Within the confines of the present model the most likely source of error is in the enthalpy for reaction (7.1) (and reaction (7.1)b). Calculations carried out using values of ΔH_1, and $\Delta H_1'$ both 50% smaller and larger showed no differences in the qualitative trends although the absolute levels were obviously altered. The only way in which a significant concentration of As_{Ga} could be introduced into GaAs was by making ΔH_1 negative, i.e., an exothermic reaction. This further illustrates the dependence of the As_{Ga} concentration on the formation of cation vacancies since a negative ΔH_1 obviously means that they will be easily formed. Varying the enthalpy for reaction (7.4) by plus and minus 50% also had no effect on the qualitative behaviour.

The effect of varying ΔH_2 and $\Delta H_2'$ by +/-10% was also examined and again there was observed to be no change in the qualitative trends. The antisite defects were virtually unaffected while the change in vacancy concentration was at most one order of magnitude.

7.7.5 Growth Mechanisms and Surface Effects

The behaviour observed for the As-antisite emphasises the important effect which the growth mechanisms have since EL2 is observed in both VPE and MG GaAs. Consider vapour phase growth using AsH_3. The defect reaction involving As-vapour and V_{Ga} (i.e. equivalent to reaction (7.1)) is :

$$AsH_3 = As_{As} + {}^3/_2H_2 + V_{Ga}$$

A simple calculation shows the enthalpy change to be positive in this case also, and so As-antisites would not be formed.

Three possible ways by which EL2 might form in VPE GaAs are :
(i) An above-equilibrium concentration of cation vacancies, as discussed earlier,
(ii) A different defect reaction leading to formation of As-antisites.

With regard to the latter a possible reaction may involve direct incorporation from the vapour phase, i.e.

$$AsH_3 = As_{Ga} + {}^3/_2H_2 + V_{As}$$

It would appear to be direct incorporation which gives rise to the As-antisite in Melt-Grown GaAs as evidenced by Bloms' calculations. In MBE the detailed surface reactions will probably mitigate against direct incorporation from the vapour. This would probably require insertion of an As-atom into the surface dimer and it is a well established fact that the impinging As-molecules bond only to surface Ga atoms. This may be yet another example of kinetic effects hindering a possible outcome favoured by thermodynamics. Surface effects in MBE are also apparent in the difference between material grown using As_2 and As_4 [7.38], where use of the latter leads to a higher concentration of the M1, M3 and M4 traps. (Note that the increase in the M3 concentration is additional evidence that it involves an As-vacancy).

Yet another possibility is formation via the reaction ;

$$As_i + V_{Ga} = As_{Ga}^{2+} + V_i + 2e^-$$

where V_i denotes an interstitial "vacancy". This does not lead to As-antisites in MBE GaAs because the concentration of As_i is likely to be very small. However, it may be the preferred mechanism for VPE growth, rather than direct incorporation.

7.7.6 AlGaAs/GaAs Heterojunctions

The quality of such heterojunctions grown by MBE has been observed to be strongly dependent on whether the GaAs is grown on top of the AlGaAs or vice-versa, the former leading to HJs with poorer optical and transport properties. Various suggestions have been put forward to explain this including surface roughness of the AlGaAs [7.39], strain due to the (small) lattice mismatch [7.40] and impurities on the growing surface [7.41]. It has also been suggested [7.42] that the cause may be an equilibrium build-up of native defects in the AlGaAs as the GaAs grows on top and hence the present calculations should provide some information on this. The results do indeed show that there is a native defect which increases rapidly with increasing Al-content, i.e. the As-antisite. However, in a study of DH lasers, McAfee et. al. [7.37] have ruled out the E_c-0.78 eV trap (also observed by Hikosaka et. al. [7.30] and attributable to As_{III}) as being the cause of the poor laser performance. Hence, further experimental work is required in this area.

7.8 Conclusions

The concentration of native defects in the grown film is generally regarded as being a critical test of the closeness of approach to equilibrium of the growth. Growth of GaAs at temperatures above about 650°C gives deep trap densities of the order of 10^{12} which is far lower than the concentrations calculated in this chapter. Hence from this alone it is not possible to elucidate the relative influences of kinetics and

thermodynamics in the film growth. As well as this it is difficult to draw any conclusions regarding the relative concentrations of the different native defects in MBE material. The calculations suggest the group III-antisite while the DLTS studies of Blood and Harris [7.34] suggest the As-vacancy. However, comparison of the calculated concentrations with experimental results suggests that certain qualitative features of the variations with temperature, As-overpressure and AlAs molefraction are reasonably well reproduced.

An interesting point which is clearly illustrated is the danger in using simplistic arguments to justify trends in defect concentrations. For example, it has often been stated in the literature that the vacancy concentrations will be lower in AlGaAs due to the greater lattice binding energy. The calculations show that this is not the case.

The model also illustrates the effect of the choice of defect formation reactions, in particular that for the As-antisite. For example, direct incorporation into GaAs leads to a measureable concentration of As_{Ga} (c.f. Melt-Grown GaAs and Bloms' results) while incorporation via a vacancy reaction is unfavourable.

A factor which has not been considered in the above discussion is the effect of kinetics in the formation of the defects. This is obviously outwith the scope of this chapter.

CHAPTER 8

BERYLLIUM DIFFUSION IN MBE GaAs AND AlGaAs

8.1 Introduction

A significant advantage of MBE over other growth methods has been the low level of interdiffusion at interfaces due to the lower growth temperatures. For GaAs and AlGaAs, however, it has become apparent that growth at temperatures as high as 700^{o}C often leads to superior quality material (in respect to both transport and optical properties). This involves growth in a temperature range where significant diffusion effects, e.g. involving dopants, might take place during growth. This chapter deals with one particular case where diffusion of a dopant has in fact been observed, namely that of Be-doping in GaAs and AlGaAs. This has great technological importance due to the fact that Be is the only suitable p-type dopant available for these materials. This diffusion effect also has potential value as a probe of the defect properties of MBE - grown material.

The aims of this chapter do not include the assimilation and analysis of quantitative diffusion data (for reasons which will be discussed later). Rather, its aims are two-fold ; (i) From a practical viewpoint it is neccesary to have a knowledge of the conditions under which diffusion of Be will occur in MBE. This is obviously of importance when growing multilayer structures where the doping has to be precisely controlled. (ii) The diffusion of atoms through a semiconductor is greatly influenced by the type and concentration of the native defects present. By examining the diffusion behaviour it may be possible to obtain some information on the defect structure peculiar to MBE, and perhaps on the growth processes themselves.

8.2 Diffusion of Zinc in GaAs

The diffusion of group II atoms in III-V semiconductors is still not yet fully understood, despite the large amount of

experimental work which has been carried out (principally on Zn diffusion in GaAs).

It is generally accepted that diffusion of Zn in GaAs takes place via an interstitial - substitutional mechanism [8.1]. Here it is assumed that the bulk of the Zn atom population resides on substitutional (Ga) sites, acting as acceptors, i.e. Zn_s^-. At the same time there is a very small concentration of interstitial atoms, Zn_i, which are usually assumed to act as single donors. The diffusion constant for the interstitial atoms is very much greater than that for substitutionals and hence they dominate the diffusion, despite having a very much lower concentration. Until recently the incorporation of interstitial atoms into substitutional sites was assumed to take place by the Frank-Turnbull (or Longini) mechanism [8.2] ;

$$(8.1) \qquad Zn_i^+ + V_{Ga} = Zn_s^- + 2e^+$$

where V_a denotes a Ga-vacancy. This process consumes Ga vacancies and hence, in order for the defect equilibrium to be maintained, there must be a source of Ga vacancies available.

The theoretical diffusion profile obtained is dependent on various assumed conditions, this being illustrated by considering the diffusion equations involved. The continuity equation for the Zn is given by (assuming a negligible diffusion coefficient for the substitutional atoms);

$$(8.2) \qquad \partial C_i/\partial t + \partial C_s/\partial t = D_i \, \partial^2 C_i/\partial x^2$$

and that for the Ga vacancies is ;

$$(8.3) \qquad \partial C_v/\partial t = D_v(\partial^2 C_v/\partial x^2) - \partial C_s/\partial t + k(C_v^{eq} - C_v)$$

where C_i and C_s are respectively the concentrations of interstitial and substitutional Zn, D_i is the diffusion constant for interstitial Zn, D_v that for Ga vacancies, C_v^{eq} the equilibrium concentration of Ga vacancies and C_v the non-

equilibrium value. The first term on the right-hand side of equation (8.3) represents vacancies gained by diffusion from the surface, the second represents loss of vacancies due to interstitial Zn going substitutional and the third represents production of vacancies in the bulk of the crystal, e.g, by dislocation climb. The rate of production in the bulk is simply assumed to be proportional to the deviation of C_v from its equilibrium value, the constant of proportionally being k.

In solving these equations the simplest approach is to consider special cases, the most obvious being that when vacancy equilibrium is maintained, i.e. $C_v = C_v^{eq}$. Within this regime there are two situations of interest here. The first of these is when the diffusing Zn dopes the material p-type, i.e. $C_s > n_i$, and hence $p=C_s$. Application of the law of mass-action to equation (8.1), followed by substitution in (8.2), gives the following approximate expression for the diffusion constant ;

$$D \approx (3KD_i/C_v^{eq})C_s^2 \qquad (8.4)$$

where K is the equilibrium constant for reaction (8.1), which is in turn given by ;

$$K = [Zn_i^+][V_{Ga}]/[Zn_s^-][e^+]^2 \qquad (8.5)$$

This gives a concentration-dependent diffusion constant, which is one of the distinguishing features of interstitial-substitutional diffusion. This is due to the fact that the Fermi level is not constant throughout the sample, being dependent on the concentration of Zn, i.e. C_s. The diffusion constant is dependent on the ratio C_i/C_s which is in turn dependent on the position of the Fermi level (since Zn_i is a donor and Zn_s an acceptor).

The second case of interest is when the intrinsic carrier concentration at the diffusion temperature is greater than the concentration of Zn, i.e. $p=n_i$. This is a situation where the Fermi level is fixed throughout the sample (in this case mid-gap)

and hence a concentration-dependent diffusion constant would not be expected.

The following expression for the diffusion constant is obtained ;

$$D^{intrin} = Kn_i^2 D_i / C_V^{eq} \qquad (8.6)$$

The diffusion profile obtained is described by the complementary error-function ;

$$C(x,t) = C^{surf}\ \mathrm{erfc}\{x/2(Dt)^{1/2}\} \qquad (8.7)$$

where C^{surf} is the surface concentration, x the distance from the surface and t is the diffusion time. When $C_s > n_i$ the continuity equation has to be solved numerically and the diffusion profile is no longer of the form given by (8.6).
The dependence of the incorporation on the Ga-vacancy concentration (equation (8.1)) leads to a diffusion constant which is inversely proportional to the As-overpressure, $p_{As2}^{-1/2}$ and $p_{As4}^{-1/4}$ for dimers and tetramers respectively.

Note that the above analysis takes no account of how the defect equilibrium is maintained, be it from the surface or the bulk. Ga-vacancy production from the surface is fixed by the diffusion constant, while that from the bulk is dependent on the density of suitable sources. If it is assumed that dislocation climb is the dominant mechanism then k in equation (8.3) will be a function of the density of the dislocations.

In addition to the special cases already considered there are those corresponding to (i) no production of vacancies in the bulk, i.e. k = 0, and (ii) finite production rate of vacancies in the bulk. Normally the only one of these which is of real interest is the case when k is large enough to almost maintain the vacancy equilibrium. This results in anomalous diffusion profiles as discussed by Tuck and Kadhim [8.3]. However, these profiles only become apparent at very high concentrations, i.e. outwith the range considered for Be in this chapter. Hence these

cases will not be discussed further here.

Although reaction (8.1) has successfully accounted for many of the characteristics of Zn diffusion in GaAs, its limitations have prompted the introduction of a new model. This is the kick-out mechanism of Gosele and Morehead [8.4]. The only difference between this and the previous model is in the way the Zn is incorporated into the substitutional sites, since the atoms are still assumed to diffuse interstitially. The basic equation describing the process is ;

(8.8) $$Zn_i^+ = Zn_s^- + Ga_i + 2e^+$$

where Ga_i denotes an interstitial Ga atom. Hence, for equilibrium, the rate at which Ga vacancies are supplied is determined by the rate at which the excess Ga interstitials can be annihilated at an appropriate sink, dislocations again being the most likely. It is when defect equilibrium is almost maintained (i.e. relatively large k) that the difference between the Frank-Turnbull and kick-out mechanisms becomes most apparent. During such a diffusion the profile will change with time, gradually approaching that appropriate to equilibrium conditions [8.3].

A linear time dependence for this process is obtained from the Frank-Turnbull mechanism while that for kick-out is $t^{0.25}$. The experimentally observed time dependence is given approximately by $t^{0.15}$-$t^{0.30}$, in agreement with the kick-out model. Van Ommen [8.5] has analysed equilibrium diffusion profiles obtained for different diffusion times and has also obtained better agreement using the kick-out model. Since dislocations are the likely bulk sink for Ga interstitials, the kick-out mechanism predicts that diffusion-induced dislocation loops should be of interstitial type. This has in fact been shown to be the case [8.6]. The characteric features of interstitial-substitutional diffusion, such as concentration-dependent diffusion and dependence on As-overpressure, are still present in the kick-out model. Note that interstitial Ga is likely to be a single donor and this requires

that Zn_i should be a double donor, if the square-law dependency on concentration is to be maintained. This is also required for equation (8.1) if the Ga vacancy is taken to be a single acceptor, as it normally is.

8.3 Microscopic Factors Affecting Diffusion

For diffusion of Zn in the low concentration regime the temperature dependence of the diffusion constant is given by ;

$$D = D_o \exp(-E_a/kT) \tag{8.9}$$

where E_a is the activation energy of diffusion. Since the diffusing flux has been shown to be predominantly due to the interstitial atoms then D can be identified with D_i in equations (8.4) and (8.6).

From Ficks' Law the diffusion constant for interstitial diffusion is found to be ;

$$D = C_1 \alpha^2 \omega \tag{8.10}$$

where C_1 is a constant whose value is dependent on the type of lattice, α is the jump distance and ω is the average jump frequency. In order to move from one site to another the atom must pass over a potential barrier. When the energy is at a maximum the diffusing atom forms part of an activated complex (see chapter 2). It is the temperature dependence of the fraction of atoms in activated complexes which leads to equation (8.9) above. If the diffusion takes place via a vacancy mechanism then D is also affected by the temperature dependence of the vacancy concentration.

The final expression obtained for interstitial diffusion is ;

$$D = C_1 \alpha^2 \ \omega_o \exp(\Delta S_m/k) \exp(-\Delta H_m/kT) \tag{8.11}$$

where ΔS_m and ΔH_m are the entropy and enthalpy change

respectively for the activated complex, and ω_o is usually taken to be the vibrational frequency of the atom in the interstitial site.

The temperature dependence of the effective diffusion constant for interstitial-substitutional diffusion is influenced by other factors (see equation (8.6)). Among these there is a dependence on the formation of Ga-vacancies (or annihilation of Ga-interstitials for the kick-out model). This is a property of the lattice alone and will affect different types of diffusing atom in the same way.

The factors which lead to differences between atoms are the equilibrium constant K for reaction (8.1) and the interstitial parameters described above. The activation energies for interstitial diffusion are usually of the order of 1 eV or less. However, the influence of the additional mechanisms in interstitial-substitutional diffusion dramatically reduces the effective diffusion constant.

8.4 Diffusion in the Presence of Ion-Pairing

The diffusion of Zn is complicated still further by the presence of this effect. It occurs due to the diffusing species (Zn_i) having an opposite charge to that of the atom in the lattice. The attraction between the two leads to a reduction in the diffusivity of the interstitial atoms. For $[Zn_i] \ll [Zn_{Ga}]$, the diffusion coefficient is ;

$$D = D_o/(1 + \Omega [Zn_{Ga}]) \qquad (8.12)$$

where Ω is an equilibrium constant defined by Tuck [8.1]. The denominator of (8.12) can be much larger than unity. Another way of regarding this effect is through consideration of the built-in field, a detailed discussion of which has been given by Casey and Pearson [8.7].

8.5 Diffusion of other Group II Atoms

As stated earlier most of the group II diffusion studies have involved Zn, data on other elements being relatively scarce. Diffusion of Mg into a GaAs substrate during LPE growth of GaAs has been studied by Small et.al. [8.8]. For the doping levels used, (2×10^{19} cm^{-3}), concentration-dependent diffusion would be expected. The abrupt diffusion profiles obtained suggest that this is the case, i.e. Mg also appears to diffuse by the interstitial-substitutional mechanism. Of more direct relevance to this chapter is the diffusion of Be. An early study of straight Be diffusion into GaAs exists [8.9] along with one involving Be diffusion into a GaAs substrate during LPE growth of $Al_{0.8}Ga_{0.2}As$ [8.10]. The latter of these has shown that for Be concentrations less than 6×10^{18} cm^{-3} the diffusion profile is given by equation (8.7). At higher doping levels the diffusion profile is characteristic of that for concentration-dependent diffusion, again indicating interstitial-substitutional diffusion. This is in qualitative agreement with the analysis given earlier. Note, however, that the transition concentration is rather higher than expected, given that the intrinsic concentration at 750°C is of the order of 10^{16} cm^{-3}. The reason for this discrepancy will be discussed later.

The diffusion of Mn in MBE InGaAs during both growth and post-growth anneals has been studied by Silberg et. al. [8.11]. Surprisingly it was found that low level diffusion took place even at the growth temperature, i.e. 500°C. From the annealing studies the diffusion coefficient was found to be of the order of 10^{-15} cm^2s^{-1} at 650°C. Note, however, that this corresponds to diffusion from an embedded junction, which usually gives a lower diffusivity as has been discussed by Tuck and Houghton [8.12]. From the results given it is not possible to determine if the diffusion mode is interstitial-substitutional.

8.6 Diffusion in AlGaAs

Relatively little work has been carried out on diffusion in AlGaAs. One study which has compared Zn diffusion into GaAs and AlGaAs is that of Blum et. al. [8.13]. They found the diffusivity of Zn in AlGaAs to be significantly greater than in GaAs if the AlAs molefraction is greater than 0.14. Any further increase has little effect, for reasons which are not clear. Yuan et. al. [8.14] have also studied this system and observed that the diffusivity increased regularly with increasing AlAs molefraction, up to $X_{AlAs} = 0.5$. They explained their results in terms of a lower vacancy concentration in the AlGaAs. This, however, assumes incorporation via reaction (8.1) and is at variance with the defect calculations in chapter 7. This will be discussed in more detail later.

8.7 Analytical Methods

8.7.1 Polaron Profiling

The main method of obtaining the Be-profiles from the layers considered in this chapter is via the use of a Polaron Profiler. The basic principle by which the carrier concentration is measured is simply the capacitance-voltage behaviour of a rectifying junction. This is a standard method whereby the gradient of a plot of junction capacitance versus junction voltage gives a direct measure of the carrier concentration. In the Polaron Profiler the rectifying junction is formed by bringing the semiconductor into contact with an electrolyte solution. When the junction is reverse-biased then a C-V plot can be obtained in the normal way. However, the electrolyte solution is chosen so that when a forward-bias is applied then etching of the semiconductor surface takes place. These procedures are alternately repeated and in this way a profile of the carrier concentration through the layer can be obtained. A more detailed exposition of the principles involved can be found in the original publication by Ambridge and Faktor [8.15].

One disadvantage of this type of profiler is that if the semiconductor is n-type then it must have a direct band-gap. This is because the etching process requires the presence of holes and these are produced by illuminating the sample.

8.7.2 Secondary Ion Mass Spectroscopy (SIMS)

This is a highly sophisticated technique of obtaining a profile of a particular element through a semiconductor layer which is carried out under UHV conditions. Basically it involves the sputtering of the material under study while at the same time analysing the elements ejected from the surface with a mass-spectrometer. It has the advantage over the Polaron in that the species of interest need not be electrically active in the lattice. It is, however, relatively time consuming to perform and requires expensive equipment. Fortunately in the layers grown in this study the Be is electrically active and so SIMS was used only to check any anomalous profiles and to profile samples with an indirect band-gap. Work carried out by the Philips group has shown that the Polaron Profiler is perfectly adequate in most cases, the profiles obtained closely corresponding to the SIMS results [8.16].

8.7.3 Surface Photovoltage

When a semiconductor surface is illuminated with light of a greater energy than the band-gap, then an electron-hole pair is produced. The electric field in the surface space-charge region causes the electron and hole to move away from one another. For example, if the bands bend upwards then the photoproduced electrons move away from the surface and the holes move towards it, the opposite being the case if the bands bend downwards. This movement of charge leads to a flattening of the bands at the surface and hence a change in the surface potential. By varying the wavelength of the incident light while monitoring the change in the surface potential, a relatively rapid measure of the AlGaAs band-gap is obtained. This is used in the present study

as an integral part of the polaron profiler to obtain the AlAs molefraction at any point in the profile studied.

8.8 Diffusion During Growth : Experimental Results

All of the layers were grown on Si-doped substrates ($n = 5x10^{17} - 1x10^{18}$ cm^{-3}) and, unless otherwise stated, were grown at a temperature of 700°C. At such a high temperature significant re-evaporation takes place, hence leading to lower thicknesses than those programmed into the growth system. In all cases, growth of the required heterostructure was preceded by growth of a GaAs buffer layer of at least 0.5 μm thick. A typical example is shown in Fig. (8.3).

8.8.1 Diffusion at Low Concentrations

Masu et. al. [8.10] have shown that the transition to concentration-dependent diffusion for Be occurs at around 6×10^{18} cm^{-3}. Hence the initial experiments in this study were carried out for concentrations less than 10^{18} cm^{-3}.

8.8.1.1 Diffusion in AlGaAs at Low Concentrations

Figs. (8.1) and (8.2) show Polaron profiles obtained from a typical AlGaAs sample with a schematic of the structure used shown in Fig. (8.3). Both As-deficient and As-rich conditions were obtained on the one sample by utilising the geometry of the MBE growth apparatus. Since the As-flux is incident on the sample at an angle significantly off-normal there is a large variation across the sample, giving conditions ranging from As-stable growth to Ga-droplets by choosing an appropriate flux. Fig. (8.1) was obtained from the As-stable region and Fig. (8.2) from the As-deficient region. From the results obtained three observations can immediately be made ; (i) diffusion occurs only in the region grown As-deficient, (ii) there is no diffusion back towards the growing surface and (iii) there is no evidence of concentration-dependent diffusion, in agreement with the observations of Masu et. al.. Note that results from other

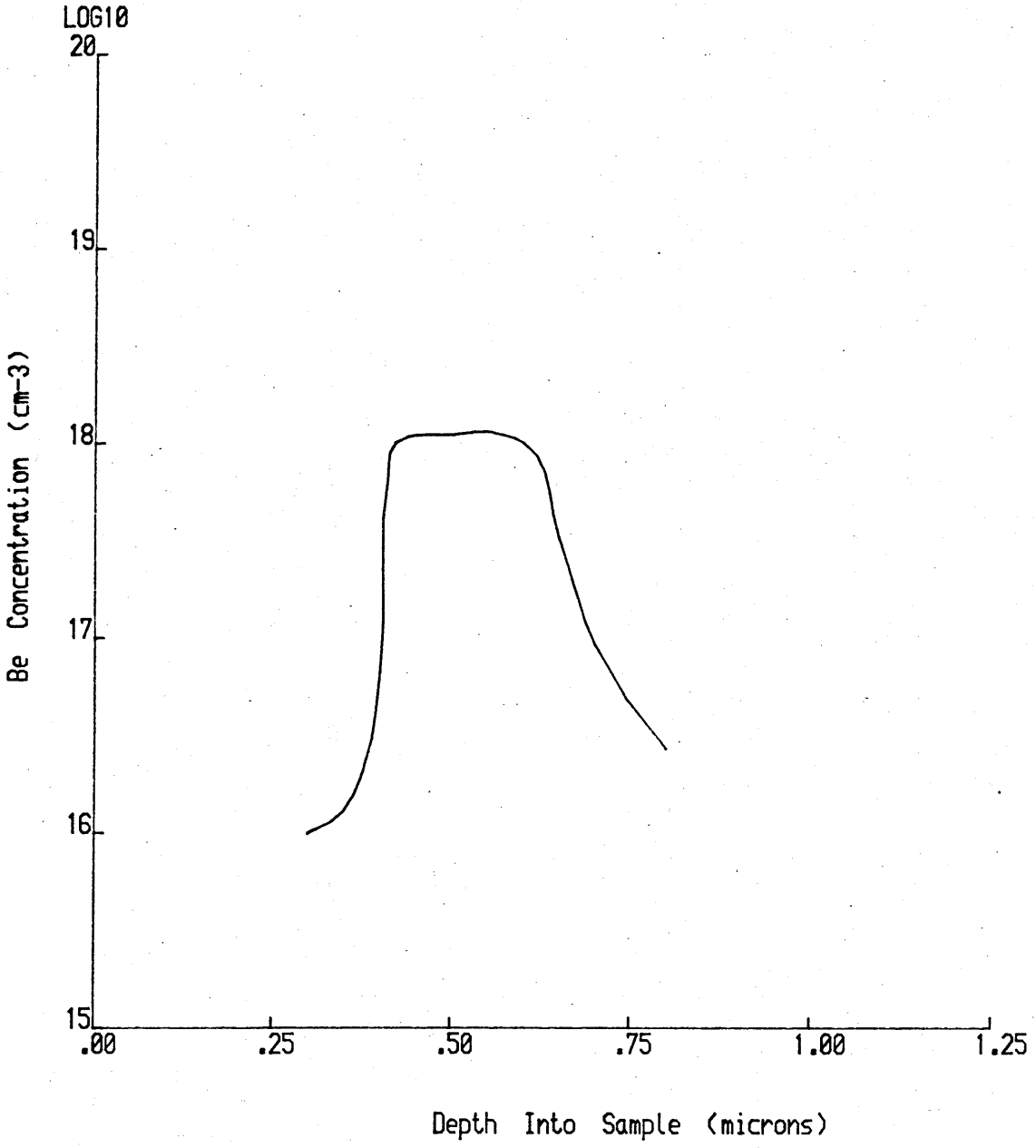

Figure 8.1 Be profile obtained from the As-rich area of an AlGaAs sample (X_{AlAs} = 0.29).

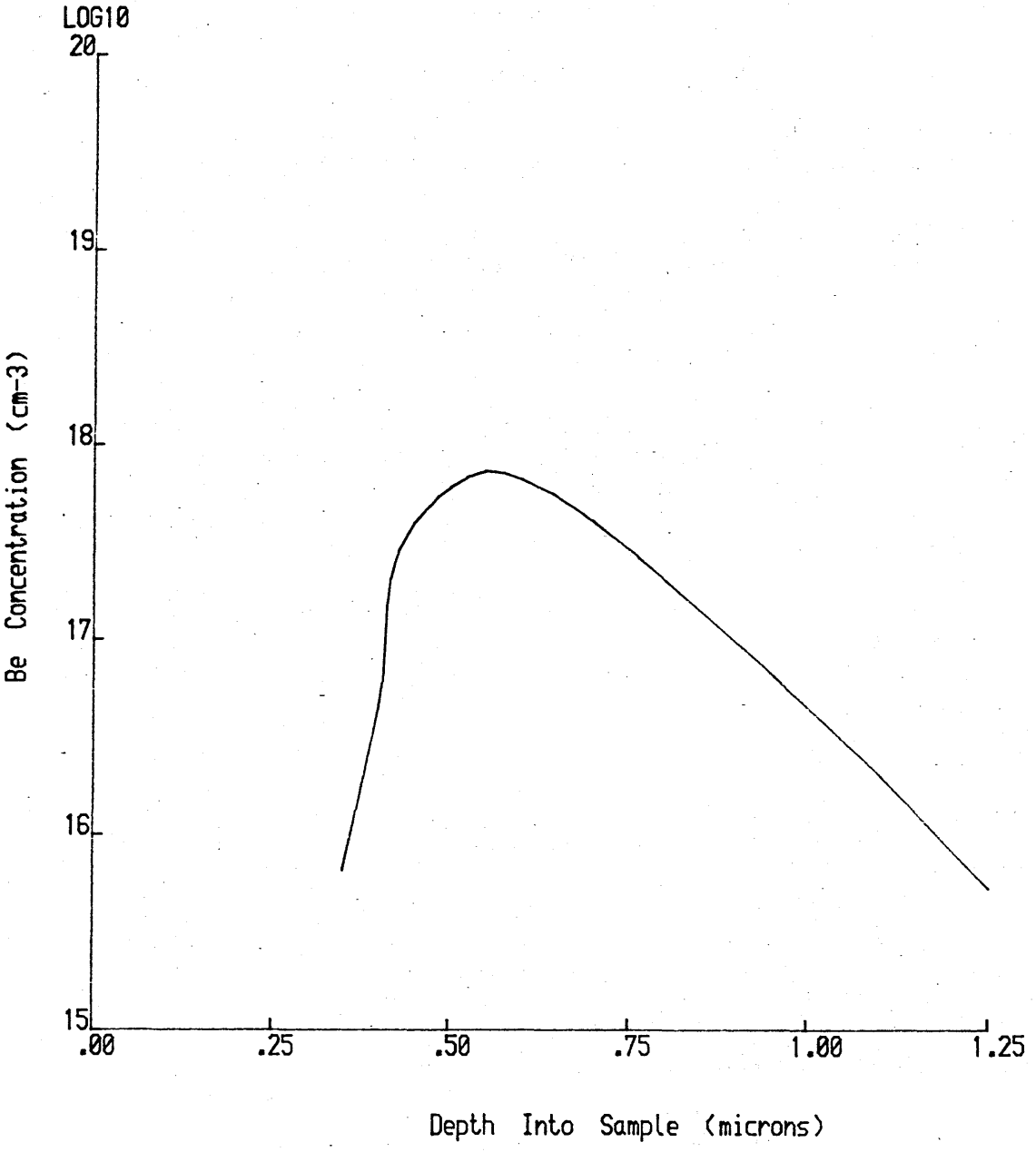

Figure 8.2 Be profile obtained from the As-deficient area of an AlGaAs sample (X_{AlAs} = 0.39).

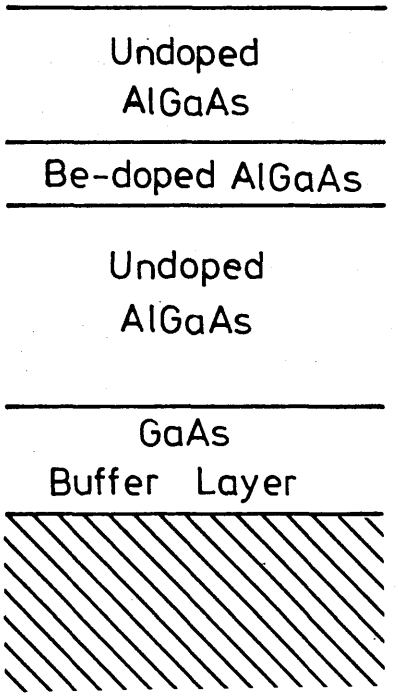

Figure 8.3 Schematic of basic heterostructure used for diffusion studies. Note that most samples were grown without the undoped capping layer.

layers rule out the slight difference in X_{AlAs} as being the cause of the different diffusivities.

The profile in Fig. (8.2) is close to that given by the complementary error-function (equation (8.7)). By fitting the profile to this equation at several points an average diffusion coefficient of $D = 2.2 \times 10^{-13}$ cm^2s^{-1} is obtained. Using the values given by Masu et. al. the diffusion coefficient at 700°C is 1.7×10^{-13} cm^2s^{-1}, i.e. close to that obtained for the MBE layers. Note, however, that their results are for diffusion in GaAs, suggesting that the value obtained for MBE AlGaAs is not unusually high. In fact, given the generally higher diffusivity in AlGaAs, the results would suggest that the diffusivity in the As-rich area is anomalously low.

The above experiment does not allow any conclusions to be drawn regarding the diffusion mechanism. Although the interstitial-substutional mechanism is the most obvious, another possibility is a Be-vacancy complex. This will be discussed in more detail later.

8.8.1.2 Diffusion in GaAs at Low Concentrations

From the work reported in the literature a much lower diffusivity should be expected for the GaAs layers. In fact, a repeat of the structure shown in Fig(8.3) with the AlGaAs replaced by GaAs showed no apparent diffusion in either the As-rich or As-deficient regions of the sample. This is at variance with the results obtained by Masu et. al.. Note, however, that the conditions of their experiment were different in two respects (i) diffusion took place across a heterojunction and (ii) growth was by LPE, which may favour a higher concentration of interstitial Be in equilibrium with the Be in the melt, or may affect the way the Be atoms enter the lattice.

The effect of a heterojunction on the Be will be discussed in more detail in a later section, suffice to say for the present that this can be ruled out as the cause of the diffusion.

Note that the results presented in this and in the previous section consider only two values of AlAs molefraction, i.e. X_{AlAs} = 0 and 0.4. The behaviour observed indicates that the transition to high diffusivity is likely to be abrupt. Although the value of X_{AlAs} at which this occurs has not been determined in the present study, it must lie between X_{AlAs} = 0 and 0.3.

8.8.2 Diffusion at High Concentrations

The following experiments are concerned with Be concentrations from about 5 x 10^{18} cm^{-3} up to a maximum of about 4 x 10^{19} cm^{-3}. These values span a regime where concentration - dependent diffusion behaviour would normally be observed. In contrast to the growth conditions employed for the low-concentration experiments, most of the layers described below were grown under high As-overpressure, maintaining As-stable conditions.

8.8.2.1 Diffusion in GaAs and AlGaAs at High Concentrations

Figs. (8.4) to (8.6) show profiles obtained from three GaAs samples, each with a different Be concentration. From these it is apparent that there is a transition concentration, above which extensive diffusion of the Be occurs. Note that these profiles were all obtained from As-rich samples and hence indicate radically different behaviour from that observed in the low concentration regime. From Fig. (8.5) it is observed that the diffusion starts to become apparent in GaAs at a Be concentration of about 5 x 10^{18} cm^{-3}.

Shown in Figs. (8.7) and (8.8) are two profiles obtained from AlGaAs samples. Although the profile in Fig. (8.7) has a higher concentration than the GaAs profile in Fig. (8.5), there is no sign of any diffusion. This suggests that the transition concentration is slightly higher in AlGaAs. Figs. (8.6) and (8.8) involve similar concentrations ($\sim$ 2 x 10^{19} cm^{-3}) and, as expected, the diffusivity is seen to be significantly greater in the AlGaAs. Although not shown here, other samples have shown

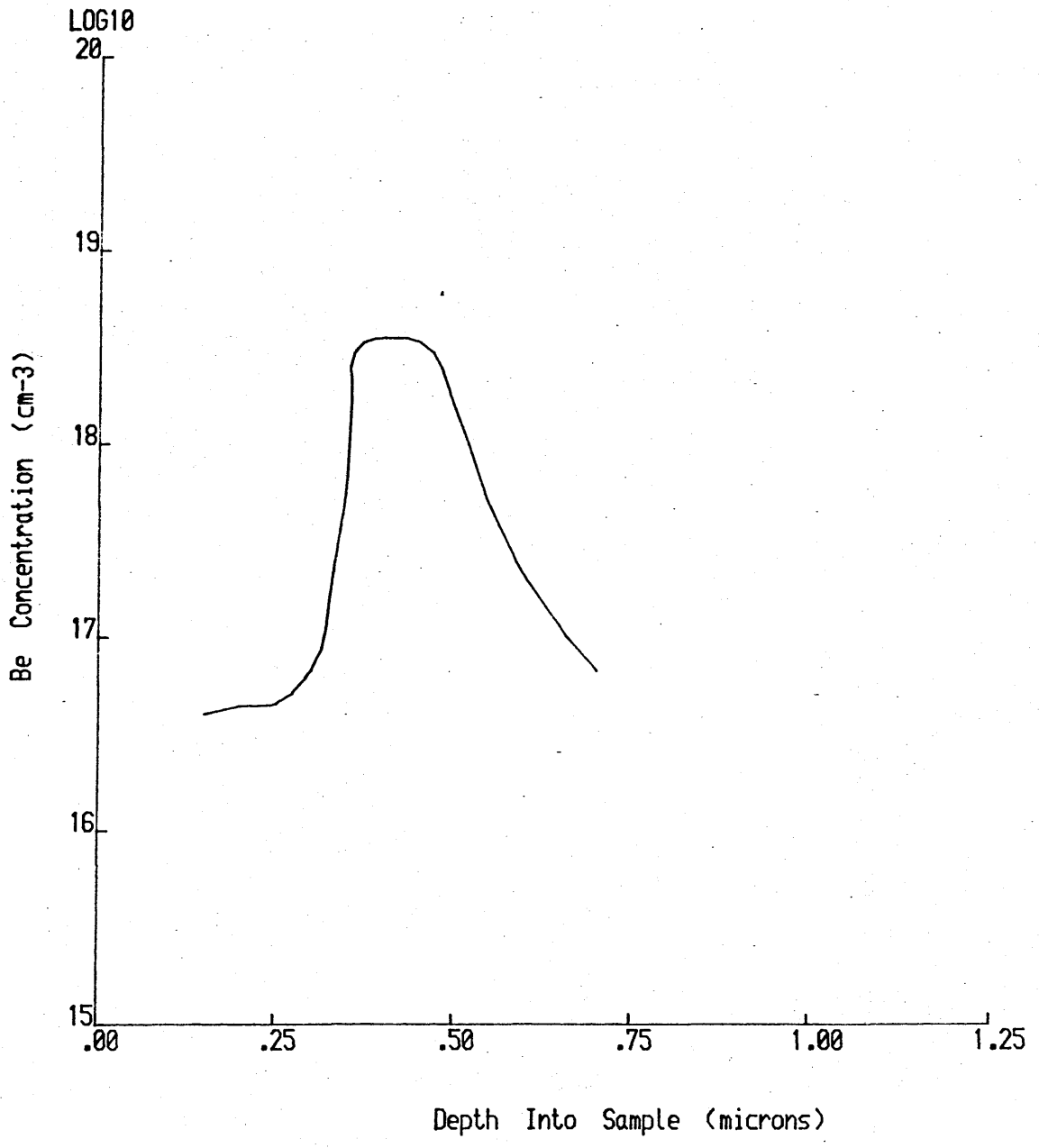

Figure 8.4 Be profile obtained from GaAs exhibiting no sign of any diffusion.

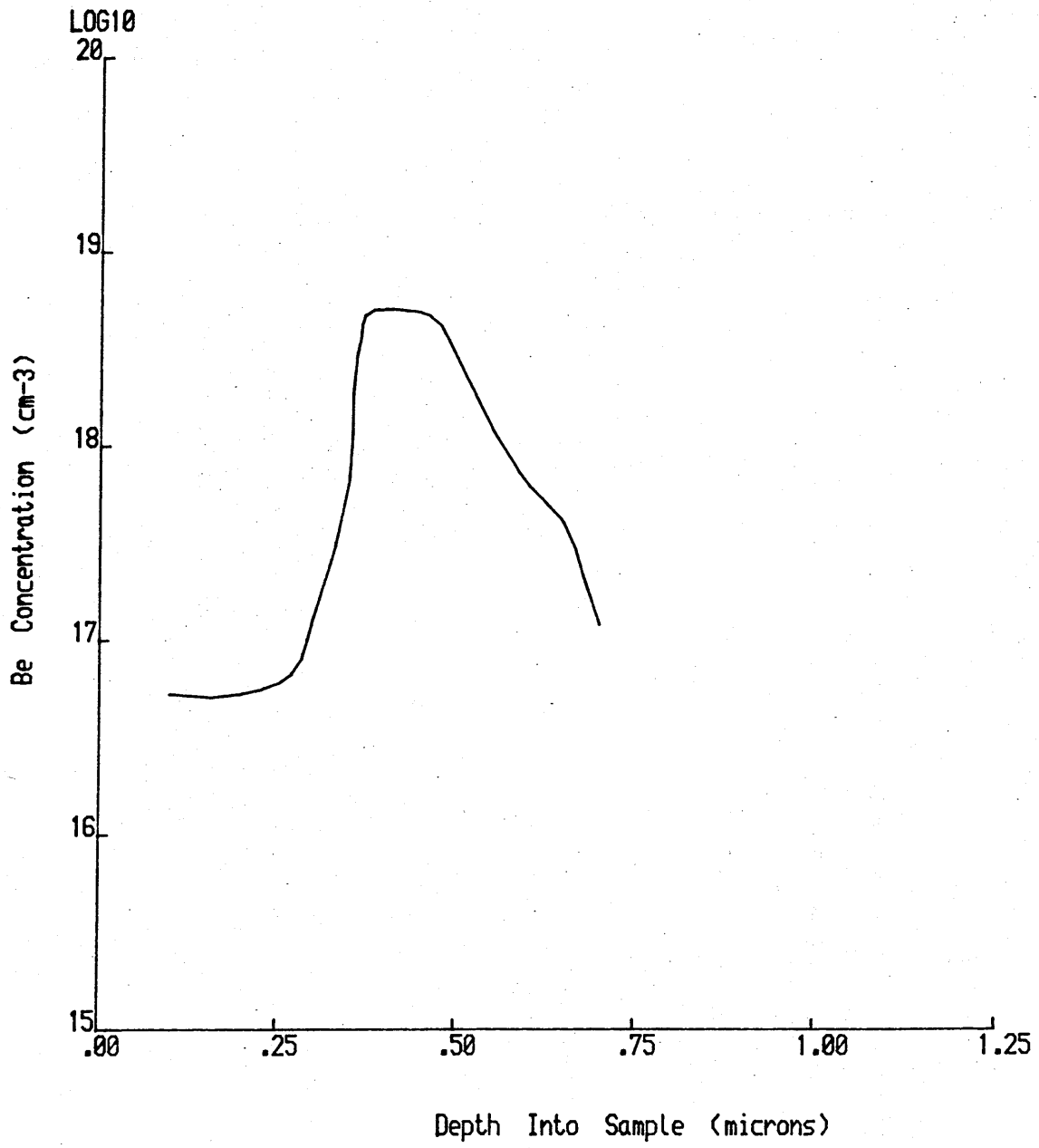

Figure 8.5 Be profile obtained from GaAs with some diffusion apparent on the falling edge.

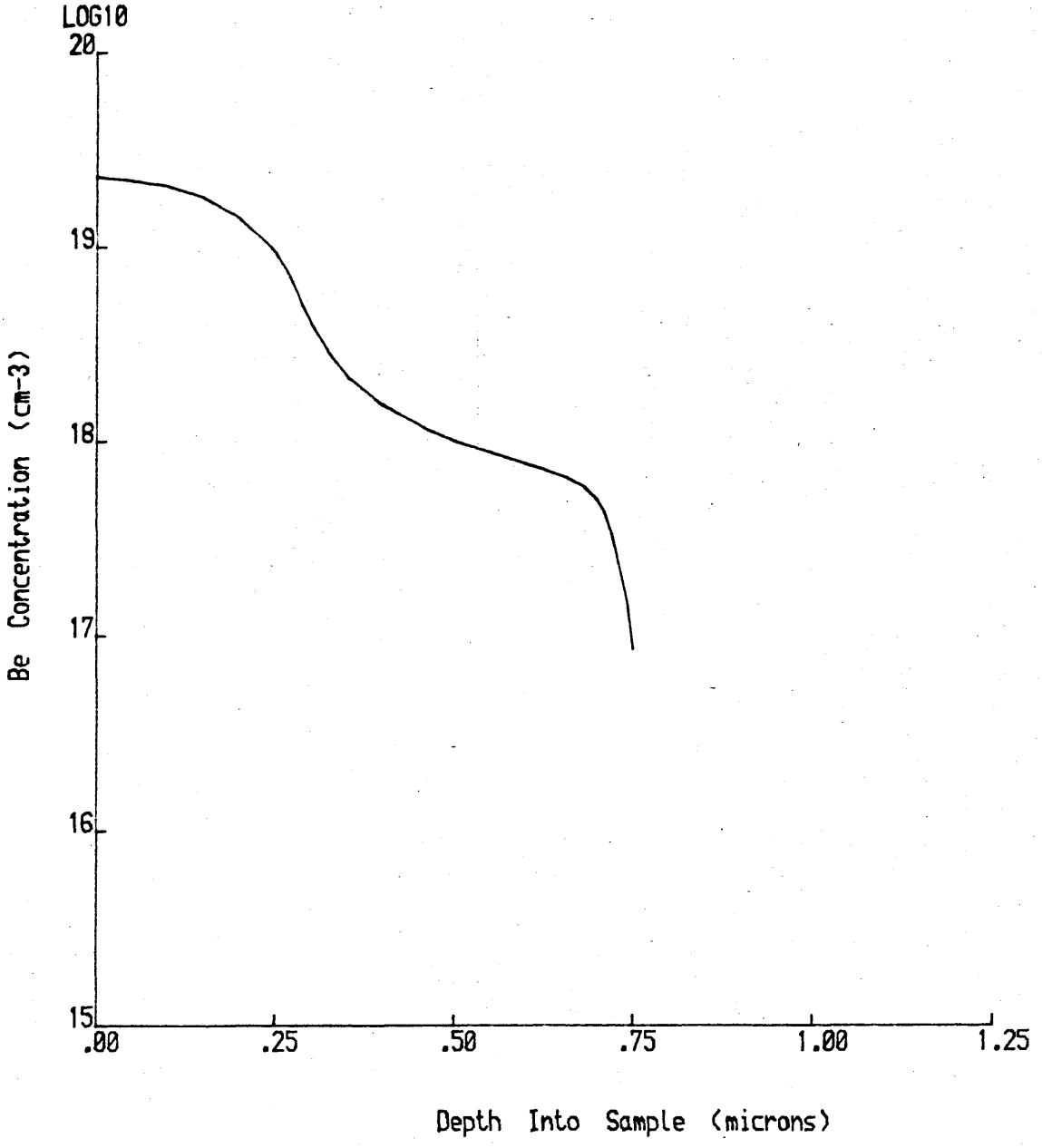

Figure 8.6 Be profile obtained from GaAs exhibiting significant diffusion. Note that this sample does not have an undoped capping layer.

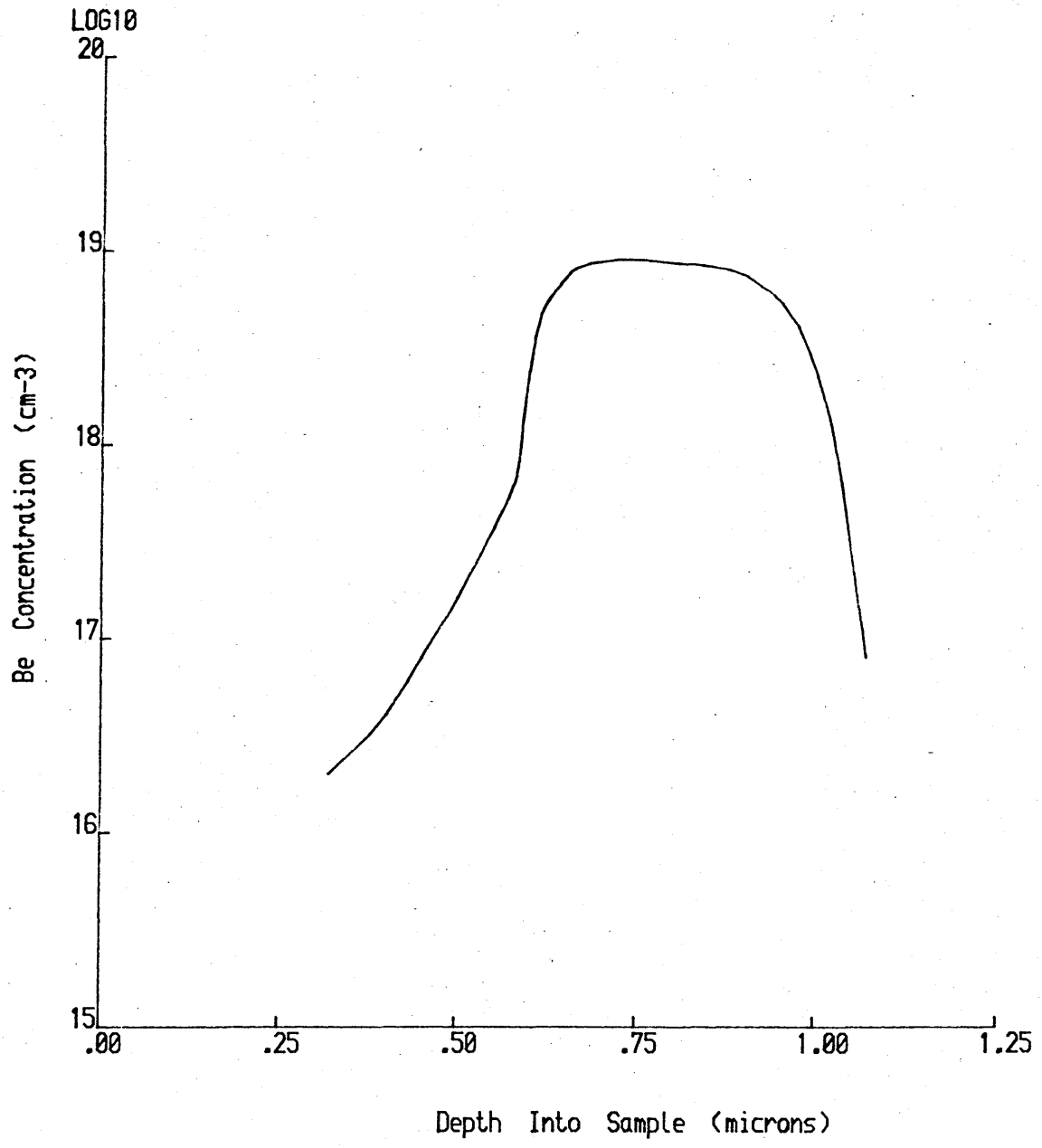

Figure 8.7 Be profile obtained from AlGaAs exhibiting no sign of any diffusion (X_{AlAs} = 0.27).

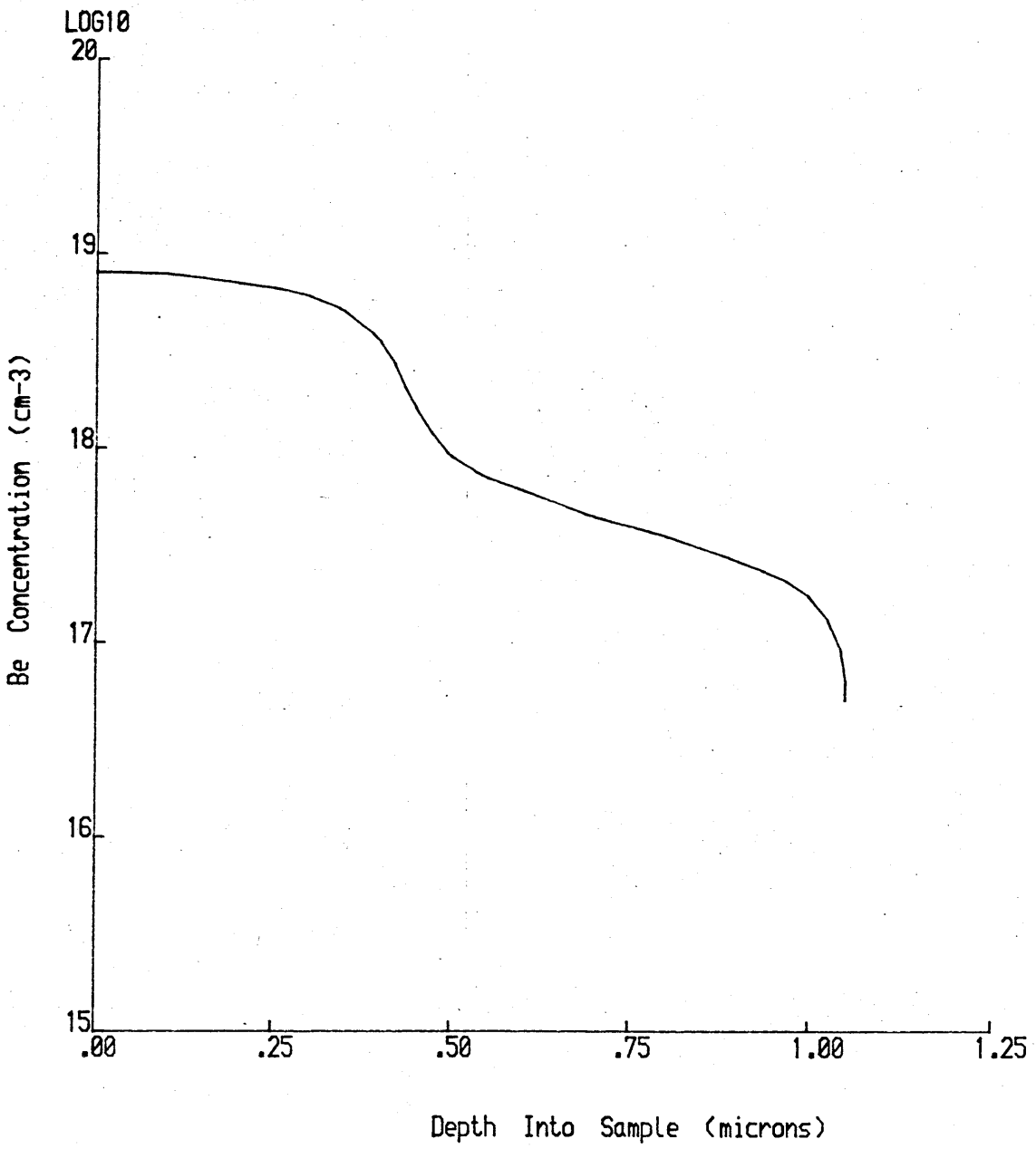

Figure 8.8 Be profile (polaron) obtained from AlGaAs sample exhibiting significant diffusion (X_{AlAs} = 0.36).

the diffusion to be extensive for concentrations of the order of 1.5×10^{19} cm^{-3} in both GaAs and AlGaAs. Concentrations of this order are used in the diffusion experiments described in the following chapter.

Note that the profile in Fig. (8.4) shows no sign of any diffusion, although the fall-off is less abrupt than for, say, the AlGaAs profile in Fig. (8.1). This is purely due to the variability and limitations of the polaron profiler when profiling layers with rapid changes in carrier concentration. Note that the rising edges of the doping spikes are shown as being more abrupt. On the falling edge the polaron detects p-type conductivity from the sides of the etch crater.

The structure of Fig. (8.8) was repeated at a growth temperature of 650°C from which diffusion was still apparent, although obviously to a reduced degree. It would appear that growth temperatures of the order of 600°C are required if diffusion at high concentrations is to be avoided.

Possible causes of the transition concentration will be discussed in more detail in a later section.

8.9 Diffusion at Heterojunctions

Most of the structures grown using MBE involve at least one heterojunction (HJ) and hence it is important to gain an understanding of their effect on the Be diffusion. A useful advantage of studying GaAs/AlGaAs HJs is the absence of any complicating factors due to lattice mismatch. Again, it is convenient to discuss the low and high concentration regimes separately, since a possible outcome may be the illustration of any differences in the diffusion modes of the two regimes.

8.9.1 Low Concentration at AlGaAs/GaAs HJ

In this case the Be-spike must be within the AlGaAs region since it has already been shown that diffusion cannot be induced in

GaAs at low concentrations. The doping profile obtained from the As-deficient area of a sample is shown in Fig. (8.9). An obvious difference from the profile presented in Fig. (8.2) is the completely different shape, the HJ profile being significantly more abrupt. This behaviour is characteristic of a single diffusing species moving to a region of lower diffusivity [8.17], and hence suggests that the diffusion mode is not interstitial-substitutional.

8.9.2 High Concentrations

The range of different HJs which can be examined in the high concentration regime is obviously much greater, and shown in Figs. (8.10) and (8.11) are profiles which illustrate the two types of characteristic behaviour observed.

Consider first the diffusion from AlGaAs into GaAs (Fig. (8.10)), i.e. from a higher to a lower diffusivity region. Initially it would appear that up-hill diffusion has occurred. However, this is caused by the diffusion mode involving two different species, i.e. the profile of the interstitial Be, which dominates the diffusion, will decrease in the normal way. Comparing this profile with that obtained for a low concentration (Fig. (8.9) suggests a different diffusion mechanism for the two cases.

Fig. (8.11) shows the profile obtained for diffusion from GaAs into AlGaAs. In this case the diffusing flux through the AlGaAs is limited by the rate of supply from the GaAs region. This leads to a characteristic step in the profile at the interface.

A profile from a structure involving two HJs is shown in Fig. (8.12). Note that this profile was obtained using SIMS since AlAs is involved. This profile shows that, as well as the high concentration diffusion, there is also a low level diffusion which penetrates deep into the sample (this has also been observed on many other samples). This is a rather puzzling observation which will be discussed in more detail later. Note, though, that the behaviour exhibited at the HJs is qualitatively

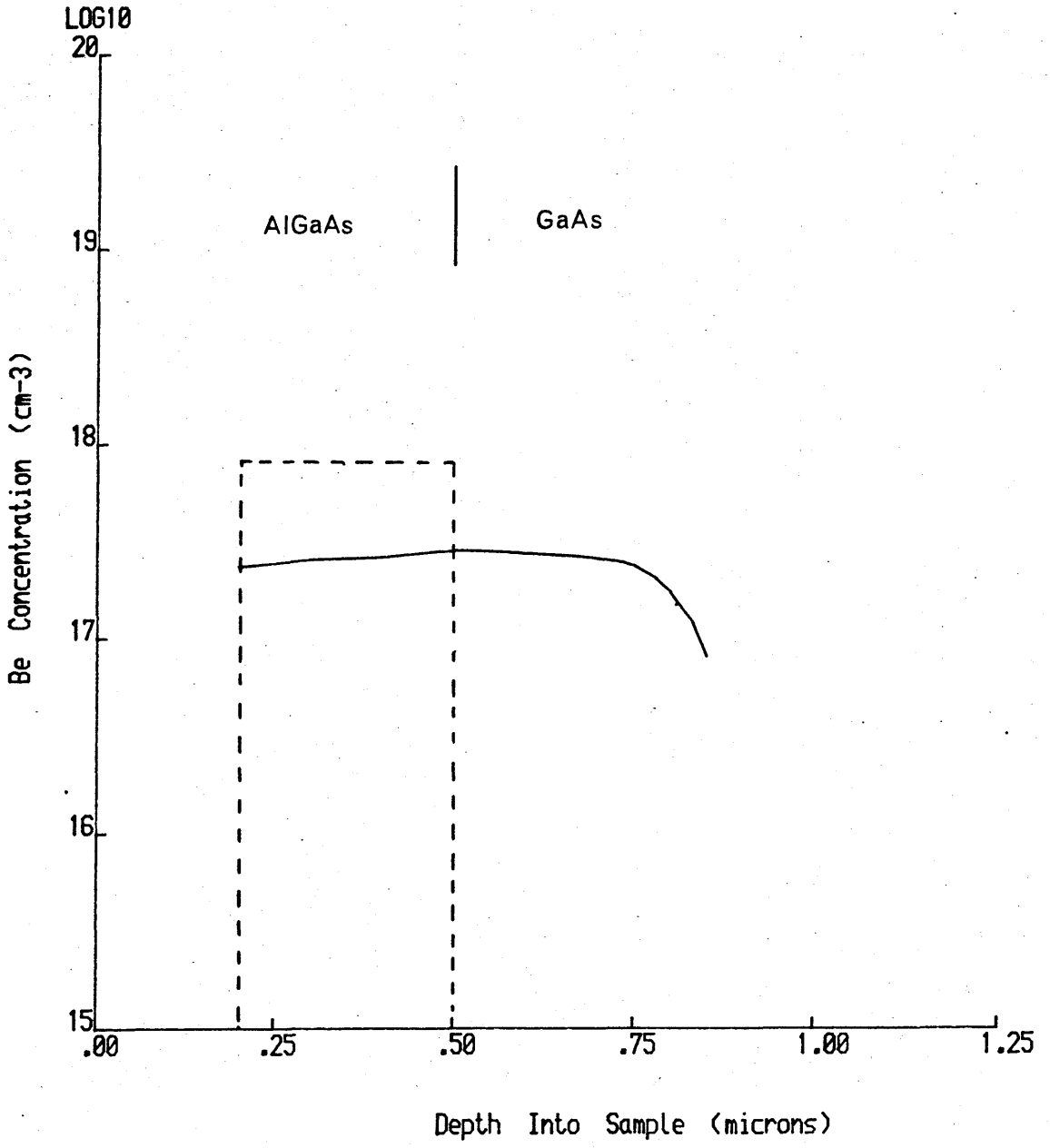

Figure 8.9 Be profile (polaron) obtained from As-deficient region of heterojunction structure.

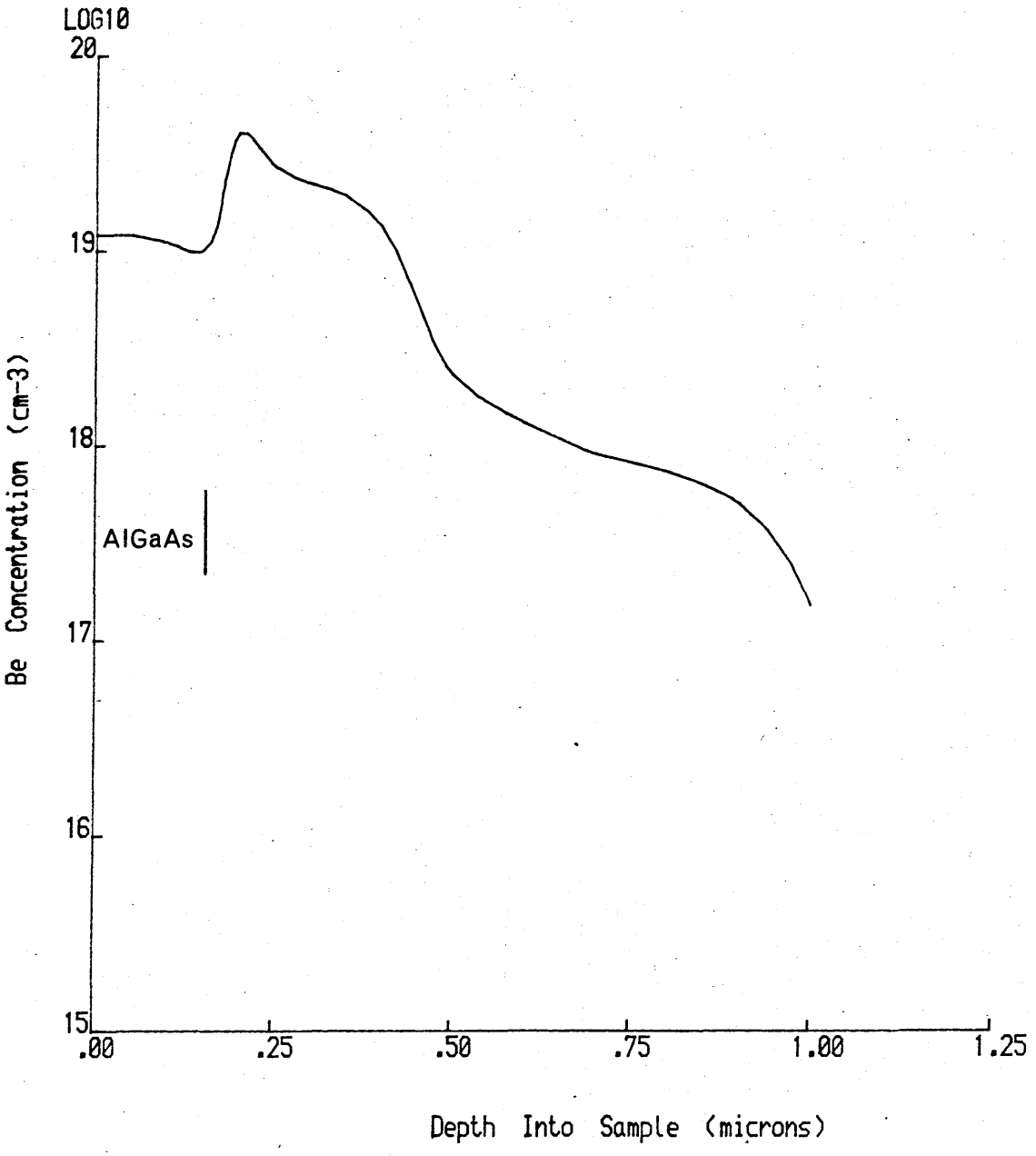

Figure 8.10 Be profile (polaron) obtained for diffusion from $Al_{.36}Ga_{.64}As$ into GaAs.

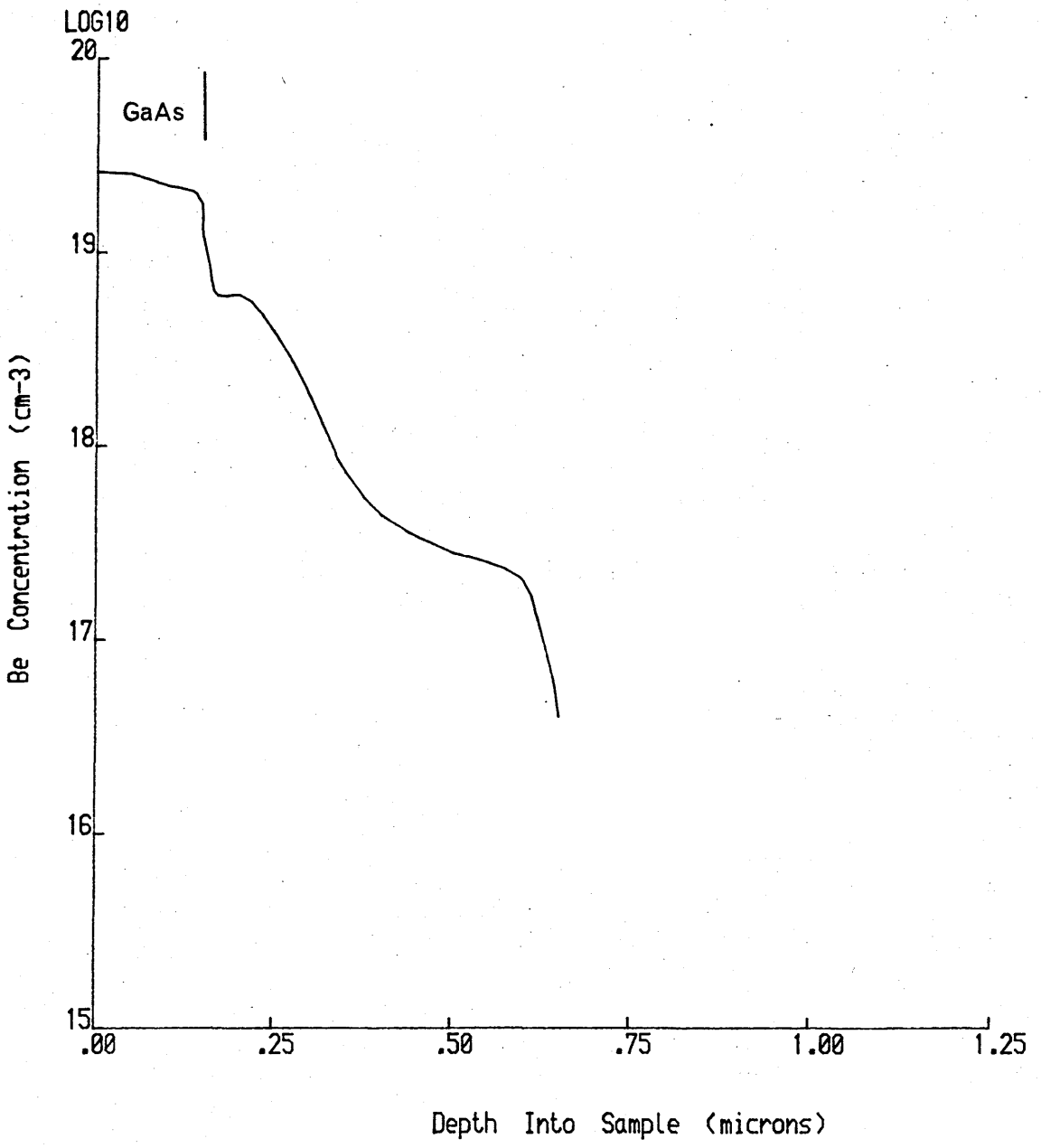

Figure 8.11 Be profile (polaron) obtained for diffusion from GaAs into $Al_{.36}Ga_{.64}As$.

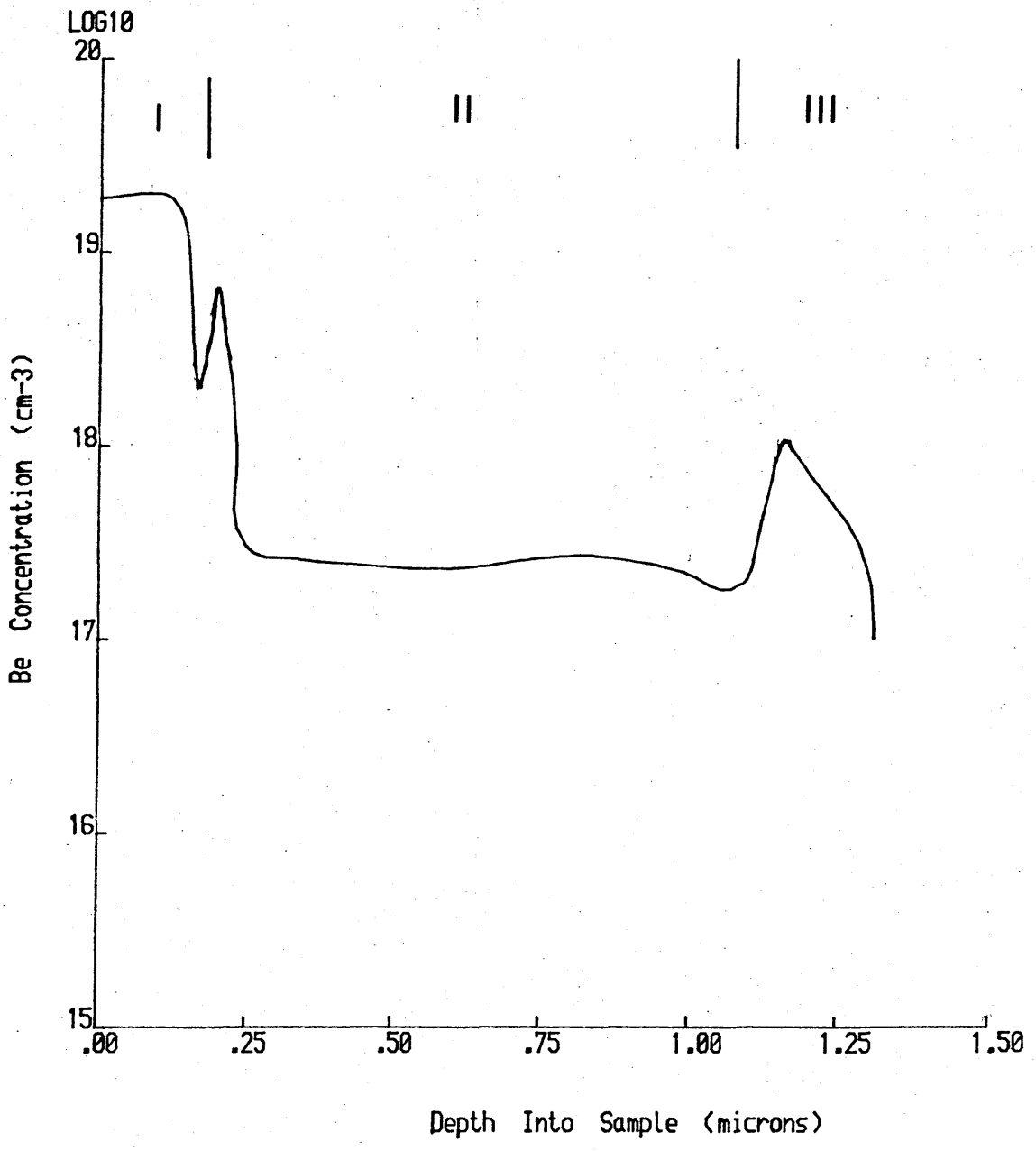

Figure 8.12 SIMS profile exhibiting low-level rapid Be diffusion through two HJs. Region I, $Al_{.3}Ga_{.7}As$: Region II, AlAs : Region III, GaAs. The source of the spike between regions I and II is unclear.

the same as that for the high concentration diffusion, suggesting the same diffusion mode.

8.10 Effect of Dopant Spikes

In analogy with the work of Silberg et. al. [8.11], the diffusivity of the Be through a dopant spike, in this case Si, was examined. The resultant Polaron profile is shown in Fig. (8.13). The abrupt rise in the Be concentration marks the position of the Si-spike, from which it is observed that a reduction in the diffusivity has occurred, in agreement with Silberg et. al..

8.11 Discussion

The results presented in the foregoing sections raise several points which require explanation, these being (i) the role of the As-overpressure in determining the diffusivity in AlGaAs at low concentrations, (ii) the cause of the different behaviours observed in GaAs and AlGaAs at low concentrations, (iii) the cause of the large diffusivity at high concentrations (iv) the difference in behaviour of low and high concentration regimes at a HJ and (v) the effect of AlAs molefraction on the diffusivity at high concentrations. The last of these is, of course, not a novel observation. However, it is an effect which has never been adequately explained.

8.11.1 Low Concentration Regime

Consider first the cause of the observed diffusion in the low concentration regime. The most obvious explanation for the difference between the As-rich and As-deficient regimes is that involving the usual As-overpressure dependence of interstitial-substitutional diffusion. This effect operates via alteration of the native defect concentration in the bulk. Regardless of whether the Frank-Turnbull or Kick-Out mechanisms are assumed the dependence of the effective diffusivity, D_{eff}, on As-overpressure is ;

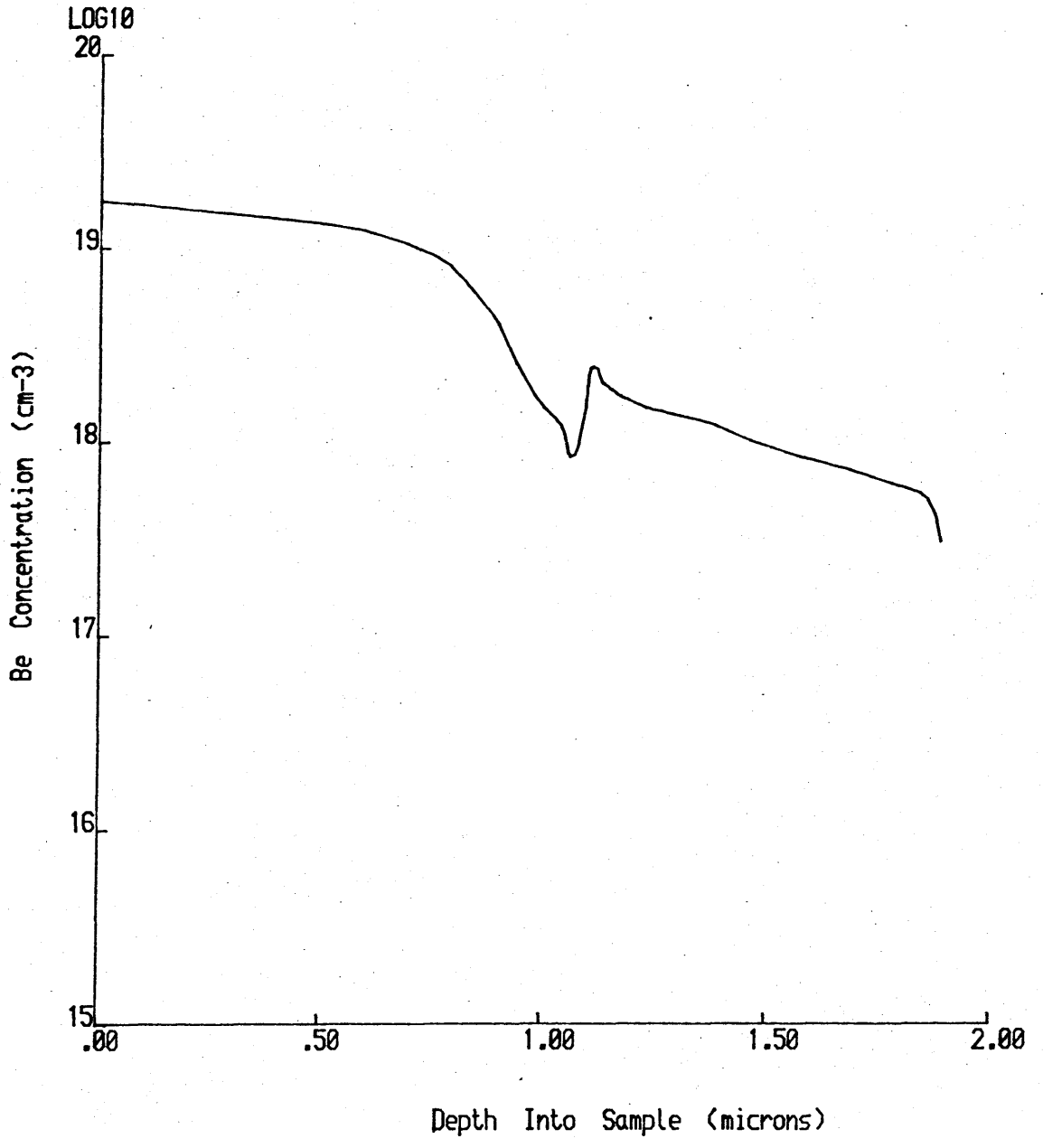

Figure 8.13 Be diffusion through a Si dopant spike (Polaron, $X_{AlAs} = 0.33$).

(8.13) $$D_{eff} \propto p_{As2}^{-1/2}$$

i.e. assuming growth using dimers. The variation in As-overpressure across the sample is unlikely to be greater than an order of magnitude and hence D_{eff} will change by about a factor of three, at most. The observed change in diffusivity is at least two orders of magnitude and hence this explanation can be ruled out.

Another possibility may be that the use of As-deficient conditions leads to a larger number of Be atoms being forced interstitial from the surface. This might occur due to Be adsorption at the site of an As surface vacancy, as was discussed in chapter 6 for Zn. It is difficult for this model to account for the low diffusivity in GaAs, and hence it seems unlikely.

The preceding models have been based on the assumption that the diffusion mode is interstitial-substitutional. This may not be the case, however, since a vacancy complex is also a possibility, being consistent with the low As-overpressure. The most likely contender is the $V_{As}Be_SV_{As}$ complex, which is directly analogous to the $V_PZn_SV_P$ complex proposed by Tuck and Hooper for Zn diffusion in InP [8.18]. Note, however, that Tuck and Hooper concluded that this complex led to electrically inactive Zn in the lattice. Yamada et. al. [8.19] have also studied Zn diffusion in InP and have observed a low concentration erfc profile which cannot be explained using the interstitial-substitutional model. They attribute this to a Zn_S-V_P complex, which they postulate to be a deep acceptor. This complex is, reasonably enough, assumed to be virtually immobile in the lattice, the diffusion taking place via an interaction with another P-vacancy, i.e. a $V_PZn_SV_P$ complex.

The strict control over growth conditions which is required for MBE results in limitations in the range of diffusion conditions which can be studied, hence making quantitative studies difficult. For example, one possible method of determining the

diffusion mode is to measure the diffusivity versus temperature, hence obtaining the activation energy for diffusion, E_a. The activation energy for diffusion of a vacancy complex is usually greater than that for interstitial-substitutional diffusion and therefore one or the other can often be ruled out [8.20]. This is difficult in MBE layers, however, due to the restricted temperature range which can be studied.

As a result of this, more indirect methods have to be used. An obvious approach in the present study is to compare the behaviour of the two different regimes, i.e. high and low concentrations. The most striking difference (apart from the different diffusion profiles, which can be explained from the concentration dependence) is the absence of any diffusion in GaAs at low concentrations. Assuming that a vacancy-complex is indeed responsible for the low-concentration diffusion, this would suggest that the equilibrium concentration of As vacancies is greater in AlGaAs than in GaAs. This is a conclusion which would appear to be supported by the defect calculations in chapter 7. This does not require that the vacancy-complex be formed in the bulk, but indicates that a high concentration of As vacancies would be stable in AlGaAs.

It may be that the As vacancies are formed on the surface. Hence, the difference between GaAs and AlGaAs would be explained by an ability to push the surface of the latter more group III stable before the onset of metal clustering.

The most direct evidence for there being two different diffusion modes for the low and high concentration regimes, however, comes from the results obtained for the AlGaAs/GaAs HJs.

8.11.2 High Concentration Regime

The first point to note is that the transition concentration lies well below the solubility limit of Be in GaAs, as is apparent from the fact that hole concentrations well above 10^{19} cm^{-3} can be obtained [8.21]. In fact, it is observed that the transition

concentration is close to that given by Masu et. al. for concentration-dependent diffusion. This concentration-dependence, however, does not explain the large enhancement observed since an extrapolation back to lower concentrations should still exhibit a significant diffusivity.

As was mentioned in section 8.2 the Fermi level plays a crucial role in determining the diffusivity through its influence on the ratio $[Be_i]/[Be_s]$. The two regimes considered were (a) intrinsic material (due to the high temperature) and (b) p-type material, i.e. Be concentrations above the intrinsic value. The diffusivity is greater for the latter of these due to the increase in the $[Be_i]/[Be_s]$ ratio. If, however, the semiconductor is n-type the diffusivity will be reduced. A way in which this might be achieved is through the native defects which are formed as the crystal grows. MBE grown layers typically exhibit deep trap concentrations of about 10^{14} cm^{-3} or less. However, as was discussed in chapter 7, this is not necessarily an accurate guide to the concentration of native defects in the layer, since complexes form as the crystal cools. Also, there is evidence to show that the dominant defect in MBE GaAs grown at 650°C is the As vacancy (see chapter 7). Growth at 700°C will increase the concentration still further (by about an order of magnitude according to the calculations in chapter 7) and hence a concentration of As-vacancies of about 10^{18} cm^{-3} during growth seems perfectly feasible. Since As-vacancies are known to be donors, this would result in n-type material and hence lead to the observed behaviour for the Be.

Some evidence that this is the case is provided by the different transition concentrations obtained for GaAs and AlGaAs, the latter being slightly higher. This suggests that the concentration of As vacancies is greater in AlGaAs, in agreement with the defect calculations in chapter 7. Note that this model also explains the discrepancy observed for the transition to concentration-dependent diffusion discussed in section 8.6.

A logical conclusion of this is that the diffusivity should be strongly affected by the presence of n-type dopants. The Si-spike experiment in section 8.10 does indeed suggest that the diffusivity of the Be has been reduced. However, the profile is just as readily explained by the effect of the p-n junction. This has been discussed in detail by Anthony [8.22].

Consider now the low-level rapid diffusion shown in Fig. (8.12). The diffusion is so rapid that it must be interstitial, yet without the added complications which normally reduce the diffusivity. Although the bulk of the Be will be incorporated into substitutional sites in the lattice, it would appear that there is also a non-equilibrium concentration of interstitial Be.

Diffusion of the substitutional Be occurs through movement to an interstitial site, the factors affecting the rate at which this occurs having already been discussed. A non-equilibrium concentration of Be will be relatively unaffected by the rest of the Be in the lattice, and hence will diffuse rapidly until incorporation occurs. Therefore the activation energy for diffusion will be that appropriate to interstitially diffusing species, i.e. of the order of 1 eV.

This still leaves unresolved the question as to how this population comes about. One possibility is that some of the Be may bond to a surface site which leads to rapid diffusion into the lattice. Such anomalous diffusion has been observed during Mg deposition onto GaAs [8.23]. Alternatively, an activation barrier for incorporation, discussed in chapter 6, may be to blame. Although any activation barrier for Be will be relatively small, there will be a certain concentration which is not incorporated into a substitutional site. Instead, these may be incorporated into an interstitial site.

8.11.3 Diffusivity versus AlAs Molefraction

The increase in the diffusivity of group II atoms with increasing AlAs molefraction is now well established, although it has never been adequately explained. This section is concerned with the description of a model which explains the trends observed. In order to obtain the essential details of the model, it is necessary to consider only the diffusivity under concentration-independent conditions. Depending on whether the Frank-Turnbull or Kick-Out mechanisms are assumed, two expressions for the diffusivity are obtained ;

$$D^{intrin} = K_1 n_i^2 D_i / C_V^{eq} \qquad (8.6)$$

for the Frank-Turnbull mechanism and ;

$$D^{intrin} = K_8 n_i^2 D_i / C_I^{eq} \qquad (8.14)$$

for the Kick-Out mechanism. K_1 is the equilibrium constant for reaction (8.1) and K_8 that for (8.8), the convention used being given in section 8.2. C_V^{eq} and C_I^{eq} are the equilibrium concentrations of group III vacancies and interstitials respectively.

From these equations it is observed that there are two temperature-dependent terms, K and D_i. The latter of these is the diffusion constant for the interstitial atoms, the value of which will be determined mainly by the atom's charge state and the crystal's lattice parameter. The charge state of both Zn_i and Be_i is assumed to be constant for the III-V materials discussed here and so only the effect of the lattice parameter will be considered (InP is a possible exception). It is generally accepted that, all other things being equal, an increase in lattice parameter leads to an increase in D_i.

The terms which present difficulties, as regards elucidation of trends among different materials, are the equilibrium constants $K_{1,8}$ and the defect concentrations $C_{I,V}$. Whereas D_i is the same

irrespective of the incorporation mechanism, this is obviously not the case for either $K_{1,8}$ or $C_{I,v}$.

Consider first the equilibrium constant for the Kick-Out mechanism, with Zn the diffusing species (no quantitative data exists for Be and the qualitative features are expected to be the same for both elements). The enthalpy change for reaction (8.8) can be written as the sum of two separate enthalpies ;

$$\Delta H_8 = \Delta H(Ga,Zn) + \Delta H_{cv} \qquad (8.15)$$

The $\Delta H(Ga,Zn)$ term arises from the difference in energy between a Zn-As bond and a Ga-As bond. Although these will be similar in strength (the Zn-As being slightly weaker), the Zn atom has only two electrons to contribute to the valence band and this is the source of the ΔH_{cv} term. Hence, as it stands, equation (8.15) gives a positive value of ΔH_8 for the reaction going from left to right.

Qualitatively, an increase in diffusivity with increased X_{AlAs} would therefore be expected due to the interstitial atoms finding it more difficult to displace the group III atoms ($\Delta H_{cv}(AlAs) > \Delta H_{cv}(GaAs)$). The AlGaAs system is ideal for studying the effect of ΔH_{cv} due to there being no change in the lattice constant as X_{AlAs} increases.

The situation is, however, more complicated as is illustrated by the results of Arseni et. al. [8.24] from their study of Zn diffusion in GaAsP. Here it was observed that the diffusivity decreased as the band-gap increased (i.e. increased X_{GaP}). GaP has an indirect bandgap and GaAsP becomes indirect at $X_{GaP} = 0.4$. The results of Arseni et. al. are reproduced in Fig. (8.14) from which it is observed that there is a discontinuity in the diffusivity curve at the direct-indirect transition. At this point the increase in band-gap becomes less rapid, and at the same time the diffusivity starts to fall more rapidly. This is direct evidence that an increased band-gap enhances the diffusivity. In the case of GaAsP, however, the decrease in the

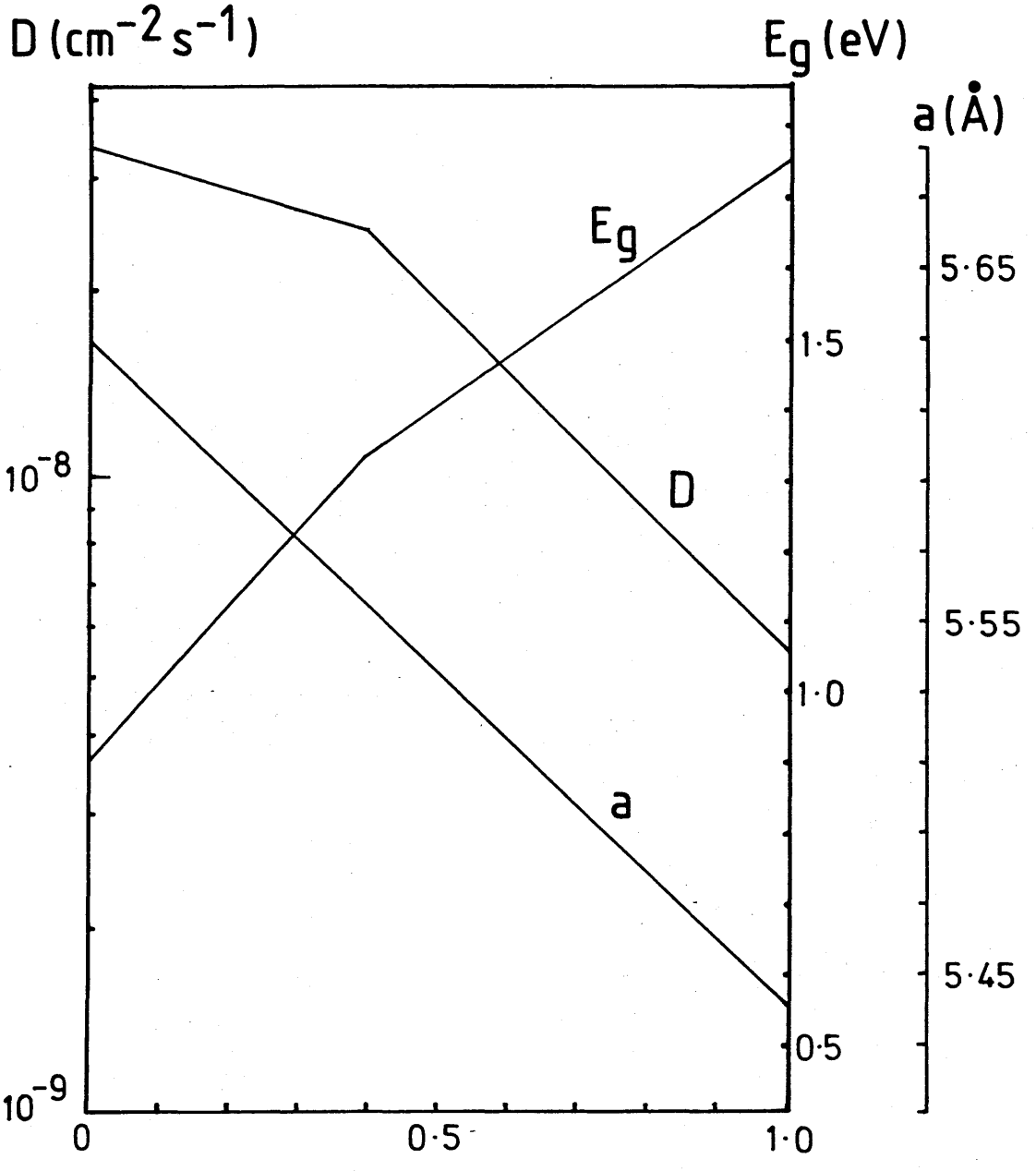

Figure 8.14 Reproduction of results of Arseni et. al. [8.24] showing variation of diffusion constant D, band-gap E_g and lattice constant a versus composition for GaAsP.

lattice constant is dominant and this leads to an overall reduction in the diffusivity. The dominance of the lattice constant is unexpected, given that going from Si to Ge normally leads to a reduction of only a few tenths of an eV in the activation energy of interstitially diffusing species.

A factor which has not yet been taken into account is the effect of the entropy change for reaction (8.8). The entropy of ionisation of defects in semiconductors is still poorly understood and hence obtaining an accurate value for ΔS_8 is not possible. However, it is reasonable to assume that the entropy change will be negative from right to left, and that it will be dependent on ΔS_{cv}. The equilibrium constant for reaction (8.8) is ;

$$(8.16)\quad K_8 = [Zn_i^+]/[Zn_s^-][Ga_i][e^+]^2 = \exp(\Delta S_8/k)\exp(-\Delta H_8/kT)$$

Examination of this expression shows that an increase in band-gap will increase the effect of the entropy term and hence reduce the diffusivity. Therefore this accounts for the reduced effectiveness of ΔH_{cv} in increasing the diffusivity.

The enthalpy change change for reaction (8.1) also includes a contribution due to ΔH_{cv} (other reactions of this type are those leading to the formation of As- and Ga-antisite defects in GaAs). In this case, however, no Ga atom needs to be displaced from the lattice and a significant amount of energy can be gained from the formation of the Zn-As bonds. This bond energy will probably dominate over the ΔH_{cv} term and hence ΔH_1 will be negative for the reaction moving from left to right. As for the kick-out model, an increase in band-gap will lead to an increase in the diffusivity. Hence, from this property alone it is not possible to determine which of the incorporation mechanisms is operative.

In interstitial-substitutional diffusion it is normally assumed that the concentration of Zn_i is much less than that of Zn_s. Inspection of (8.16) shows that the entropy factor must dominate to a large degree in order for this to be the case. In practice,

however, the situation will be further complicated by the presence of other reactions in the solid. This is illustrated by the results obtained in chapter 7 where it was shown that the behaviour of a particular defect cannot be determined from consideration of a solitary reaction. Hence, although the Frank-Turnbull mechanism would appear to be energetically more favourable, this does not preclude the existence of the kick-out mechanism in the semiconductor. As has already been discussed in section 8.2, there is a large body of experimental evidence to support the latter. One possibility is that both mechanisms in fact operate simultaneously, with one dominating over the other.

The discussion so far has taken no account of the role played by the defect concentration. This is crucial and is often the factor which determines the actual shape of the diffusion profile. It is usually assumed that the dislocations in the solid maintain the defect equilibrium, either by the emission of vacancies or the absorption of interstitials. The diffusivity of interstitial Ga atoms will be greater than that of Ga vacancies, hence favouring the kick-out model.

Despite the high complexity of the diffusion process the above discussion has shown that the band-gap of the semiconductor plays a crucial role in determining the diffusivity.

8.12 Conclusions

The study has shown that extensive Be diffusion readily takes place under certain conditions (particularly at high concentrations) during MBE growth of GaAs and AlGaAs. Evidence has been presented which suggests that there are two different diffusion modes for the high and low concentration regimes.
This diffusion has important practical implications since many device structures utilise high concentration Be-spikes. The experiments performed do not readily suggest any way of reducing the diffusion at high concentrations. However, one possible approach may be the use of background doping, as has been studied by Silberg et. al. [8.11] and discussed in section 8.11.2.

CHAPTER 9

IN-SITU DIFFUSION OF Be THROUGH A SUPERLATTICE

9.1 Introduction

In recent years the availability of MBE has resulted in a wide range of experiments being carried out on Superlattice (SL) structures, a SL being simply a structure composed of many alternating layers of two different materials (normally lattice matched). The effect of dopant diffusion through these SL structures is one of the topics which has come under study. The most striking observation from these experiments has been the enhanced intermixing of the two component materials due to the presence of the diffusing dopant, an effect which was first observed for Zn diffusing into a GaAs/AlAs SL [9.1]. In this case the diffusion leads to the formation of compositionally disordered AlGaAs, the composition being dependent on the relative widths of the AlAs and GaAs layers. Zn is not the only dopant which displays this behaviour, similar experiments involving Si diffusion having also resulted in enhanced intermixing [9.2] [9.3].

This type of enhanced intermixing is not restricted to the cation sublattice since a GaP-GaAsP SL has also been disordered in this way [9.4]. Similar results have also been obtained for other III-V compound SLs, including InGaAs-GaAs [9.5], GaAsSb-GaAsP and InGaAs-GaAsP [9.6].

Another effect which has been studied is the role played by the SL period (taken to be the sum of the thicknesses of two adjacent layers) in determining the diffusivity of the dopant [9.7].

The studies which have been carried out so far have all involved post-growth diffusions, a method in which difficulties are often encountered regarding accurate control of the diffusion conditions and hence reproducibility of results. Given that Zn causes disordering it seems reasonable to assume that Be will

also, since it is another group II element and diffuses by the same mechanism. It has been shown in chapter 8 that Be-diffusion can be obtained during MBE growth of GaAs and AlGaAs by suitable choice of growth conditions. This property was utilised in the present chapter to provide a controllable source of diffusing Be for SL studies, with the principal advantage that a post-growth diffusion could thus be avoided.

The two areas of study already mentioned are considered in this chapter, i.e. (a) to determine if diffusing Be leads to disorder of the SL and (b) the effect of the SL period on the Be diffusivity. Most of the work described in the literature has concentrated on the extent of the disordering. The emphasis in this chapter is on (b) above, although the disordering mechanism will also be discussed.

9.2 Properties of AlAs/GaAs Superlattices

Before describing any experimental results a brief description of the properties of the AlAs/GaAs SL is in order. Shown in Fig. (9.1)a and (9.1)b respectively, are the electronic structures of a single quantum well and a 1:1 SL. Note that these electronic structures are shown greatly simplified, and that band-bending at the interfaces has been ignored. As the width of the GaAs layers is reduced the states in the well split off from the conduction band-edge and, for an isolated well, give discrete energy levels as shown in Fig. (9.1)a. The transition to quantum-well-type behaviour occurs at about 500 Å. As the width of the AlAs layers is reduced the quantised states in the GaAs wells increasingly overlap, and eventually form SL sub-bands. From this it is apparent that the conduction and valence band discontinuities, ΔE_c and ΔE_v, are fundamental in determining the properties of the SL.

The calculation of the energies and dispersions of the bands is non-trivial, and is a subject which is being widely investigated at the present time. One of the most commonly used approaches is the envelope-function method which has been developed by Bastard

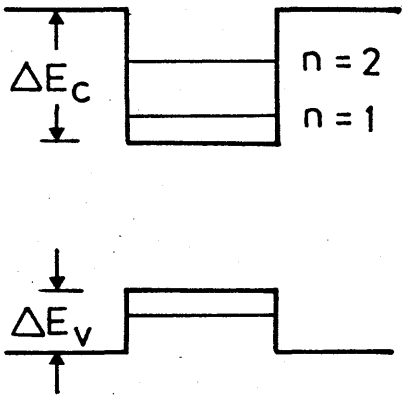

(a)

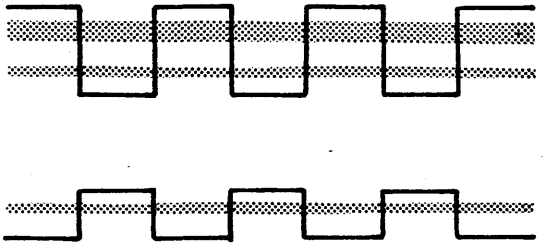

(b)

Figure 9.1 Electronic structures of (a) single quantum well and (b) 1:1 superlattice.

[9.8]. If the AlAs barriers are sufficiently wide, i.e. > 250 Å [9.9], then the states can be obtained using the simple three-dimensional rectangular well model, as described by Dingle [9.10].

9.3 Experimental Results

9.3.1 Disordering of Superlattice

The study of Lee and Laidig (LL) [9.7] has shown that the concentration of Zn must be greater than about 10^{18} cm^{-3} in order for disordering to occur. For this reason the following experiments all utilise Be concentrations of 10^{19} cm^{-3} and above. In the previous chapter a range of As-overpressures was obtained on a single sample by utilising the off-normal geometry of the molecular beam. This method is used in this study to obtain a variation in Be concentration across the sample, while keeping the growth As-stable at all points.

Shown in Fig (9.3) is the Polaron profile for the structure shown in Fig (9.2), taken from the area of the sample with the higher Be concentration. Note that the GaAs well width used here is narrow enough for quantum-well behaviour, and that some coupling between the wells is also expected since the barrier width is narrow. The double-hump structure in Fig. (9.3) is due to the undoped layer of AlGaAs between the Be-spike and the SL. Note that the Be concentration at the other end of the sample (7 x 10^{18} cm^{-3}) is below the concentration required for anomalous diffusion.

From the profile in Fig (9.3) alone it is not possible to determine if the superlattice has been disordered (although in certain cases it is possible, as will be described later). The techniques most commonly used by other workers to determine the extent of the disordering are cross-sectional Transmission Electron Microscopy (TEM) and/or photoluminescence [9.1]. The method used in these studies to determine if the SL has in fact been disordered is the Surface Photovoltage measurement described in the previous chapter. There, the method was used to determine

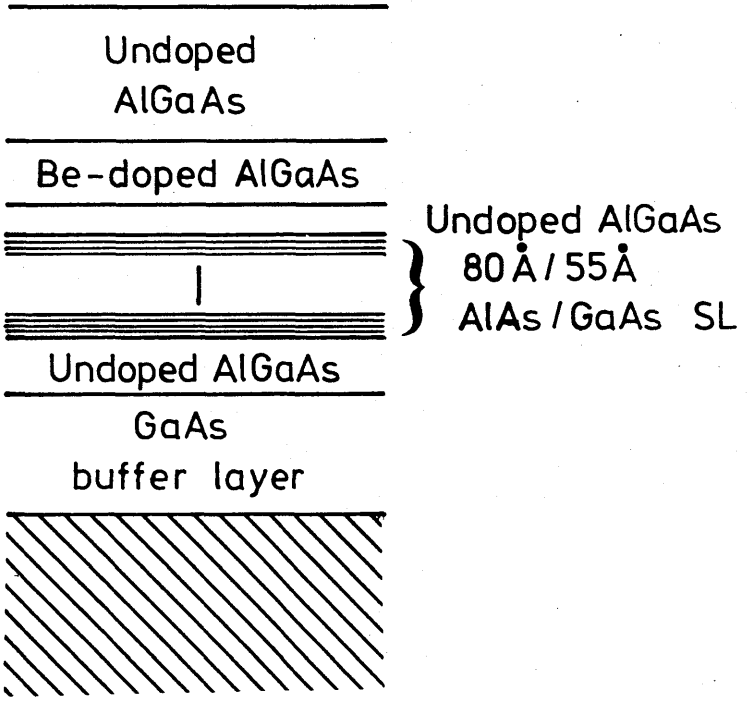

Figure 9.2 Schematic of structure used for SL diffusion studies.

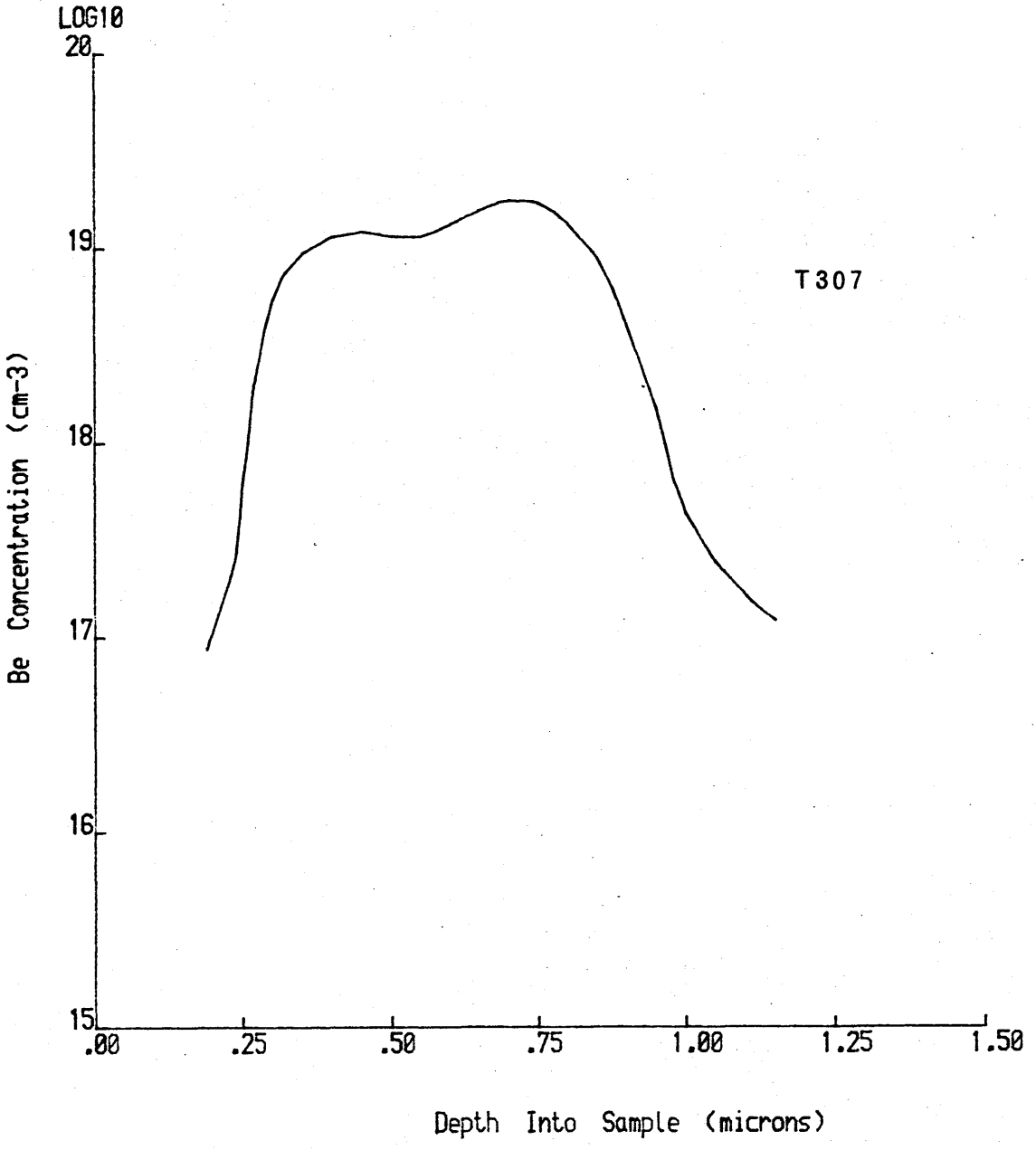

Figure 9.3 Be profile obtained after diffusion through structure shown in Fig. (9.2).

the bandgap and hence AlAs molefraction of the AlGaAs. In the same way, the presence or otherwise of a SL can be checked for by examination of the SPV spectra. It is important to realise that only SLs with narrow wells and barriers can be studied in this way since at least one well must be within the depletion region.

The SPV spectrum obtained from the area of the sample with the lower Be concentration, taken after removal (by etching) of the top AlGaAs layer, exhibited a transition due to the SL with a wavelength of about 800 nm. This is less than that for bulk GaAs due to the higher energy of the quantum-well states. The corresponding profile taken from the diffused area of the sample did not exhibit such a transition, hence indicating the presence of the disordering effect.

9.3.2 Diffusion in SLs of Different Periods

The only other work which has considered the effect of SL period is that of LL [9.7]. Only three different SLs were studied with total periods of 1100, 630 and 320 Å, all having equal barrier and well widths. In the present study a wider range of structures was examined, including SLs with total periods ranging from 1000 to 40 Å with equal barrier/well widths. The basic structure used is similar to that shown in Fig. (9.2) but without the spacer between the SL and the Be-spike, or the top undoped AlGaAs layer. Note that for the basic diffusion studies the top layer with the Be-spike is usually AlGaAs ($X_{AlAs} \approx 0.4$). Note also that the time taken to grow this doped layer, and hence the diffusion time, is typically about 4 min.. The expected diffusion depth is therefore relatively small.

Polaron profiles obtained from SLs with total periods of 200 and 40 Å are shown in Figs. (9.4) and (9.5). Note that both of these layers have total integrated Be concentrations of about 1.5×10^{19} cm^{-3} for the peak doping level of the spike. It is important to maintain a constant value for all the samples in order to minimise any concentration-dependence effects. Note

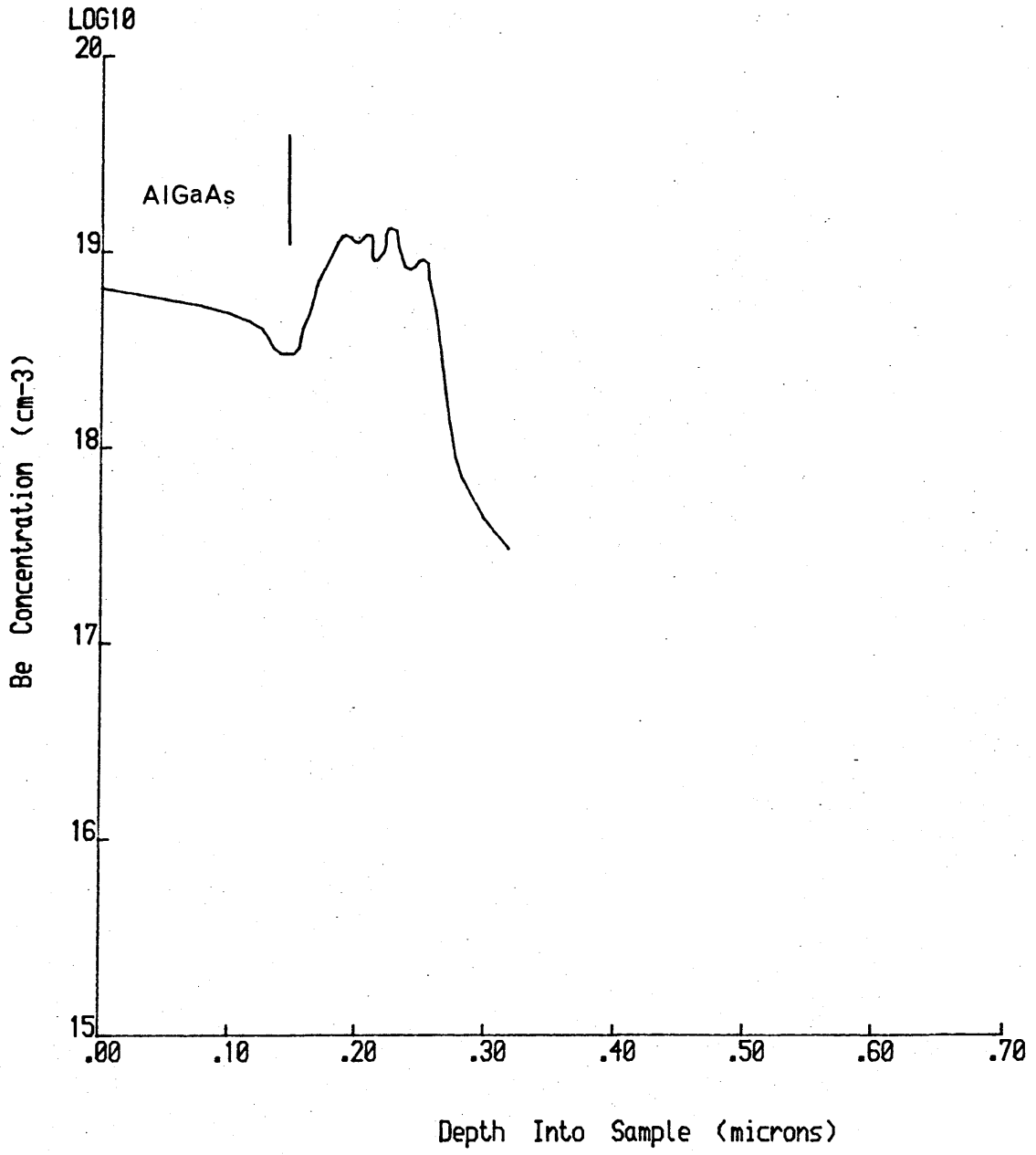

Figure 9.4 Diffusion profile obtained from 200 A SL.

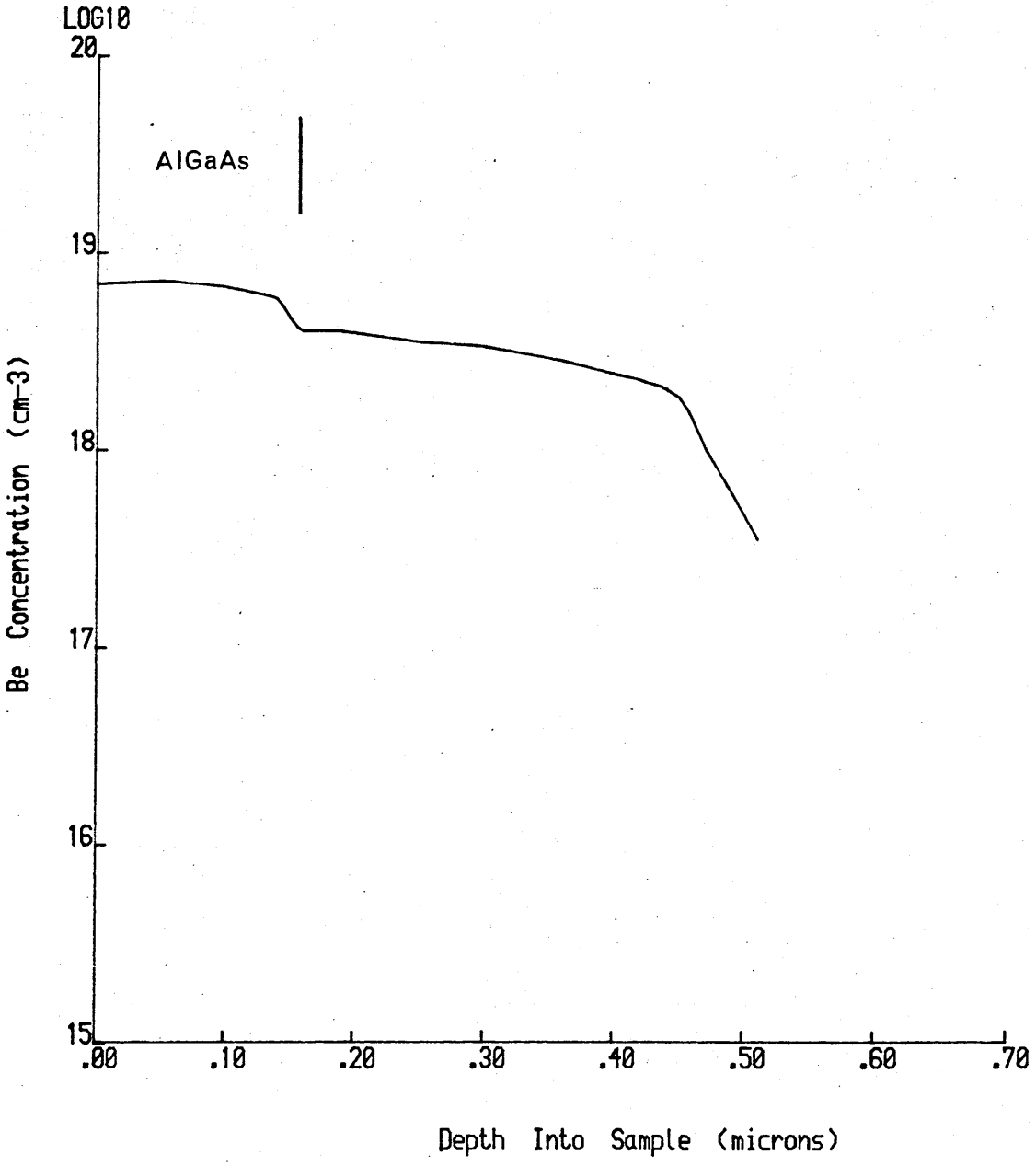

Figure 9.5 Diffusion profile obtained from 40 A SL.

also that the widths of the Be-spikes should be as similar as possible.

In agreement with the conclusions of LL it is observed that the diffusivity of the Be increases with decreasing SL period. However, the trend in diffusivity vs. SL period observed in the present study is markedly different from that of LL and this will be discussed in more detail later. Shown in Fig. (9.6) is the Polaron profile of a 100 Å SL with a slightly lower Be concentration ($\sim$1.0 x 10^{19} cm^{-3}) than those shown in Figs. (9.4) and (9.5). Fig. (9.7) shows a SIMS profile obtained from a 600 Å SL and Fig. (9.8) a SIMS profile from the 40 Å SL. Note that the latter of these is from a different part of T322 having a higher Be concentration. Comparison of Figs. (9.5) and (9.8) shows that all of the Be is electrically active. The different diffusion depths of these two profiles suggests that the diffusivity is highly sensitive to concentration.

A characteristic feature which is worth noting at this point is the modulation of the Be concentration in the wider-period SL structures (examination of the SIMS profile in Fig. (9.7) shows that the modulation is a real effect). This is simply a result of the diffusivity being less in the GaAs layers as was noted in the previous chapter. The modulation of the Be concentration can be used to gain an idea of the extent of the disordering as is illustrated by the profile for the 100 Å SL in Fig. (9.6).

The presence of the modulation leads to very different profile shapes, e.g. compare T318 and T322 in Figs. (9.7) and (9.8). Visual inspection gives the impression of a greater diffusion depth for T322, but quantitative comparisons are more difficult. The measure of the diffusion depth which has been chosen here is the point at which the Be concentration drops to 10^{18} cm^{-3} (as was used by LL). For a profile such as that of T318, this requires an averaging of the Be peaks, keeping in mind the logarithmic scale.

The step-like change in the concentration on going from the Be-

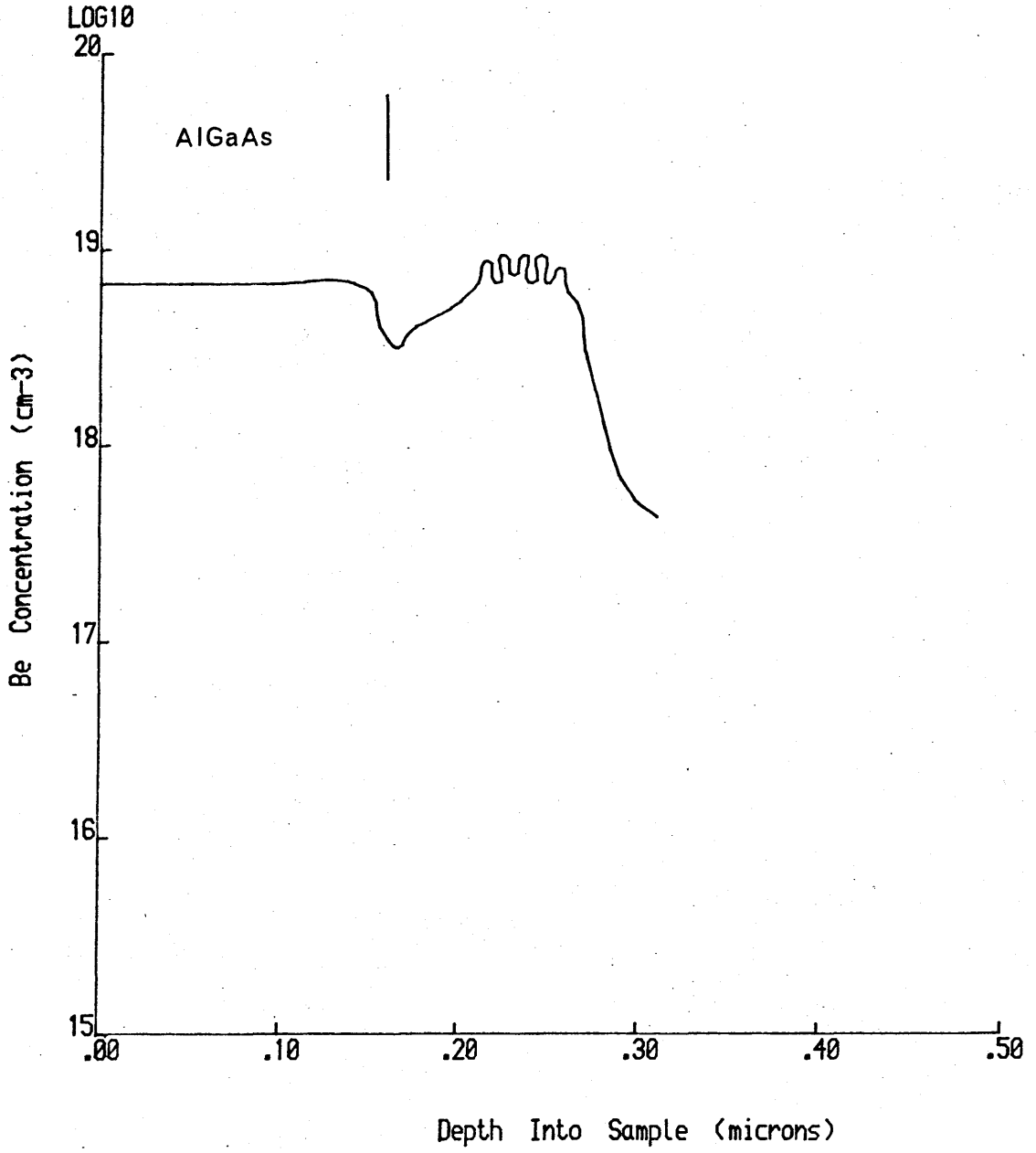

Figure 9.6 Diffusion profile obtained from 100 A SL.

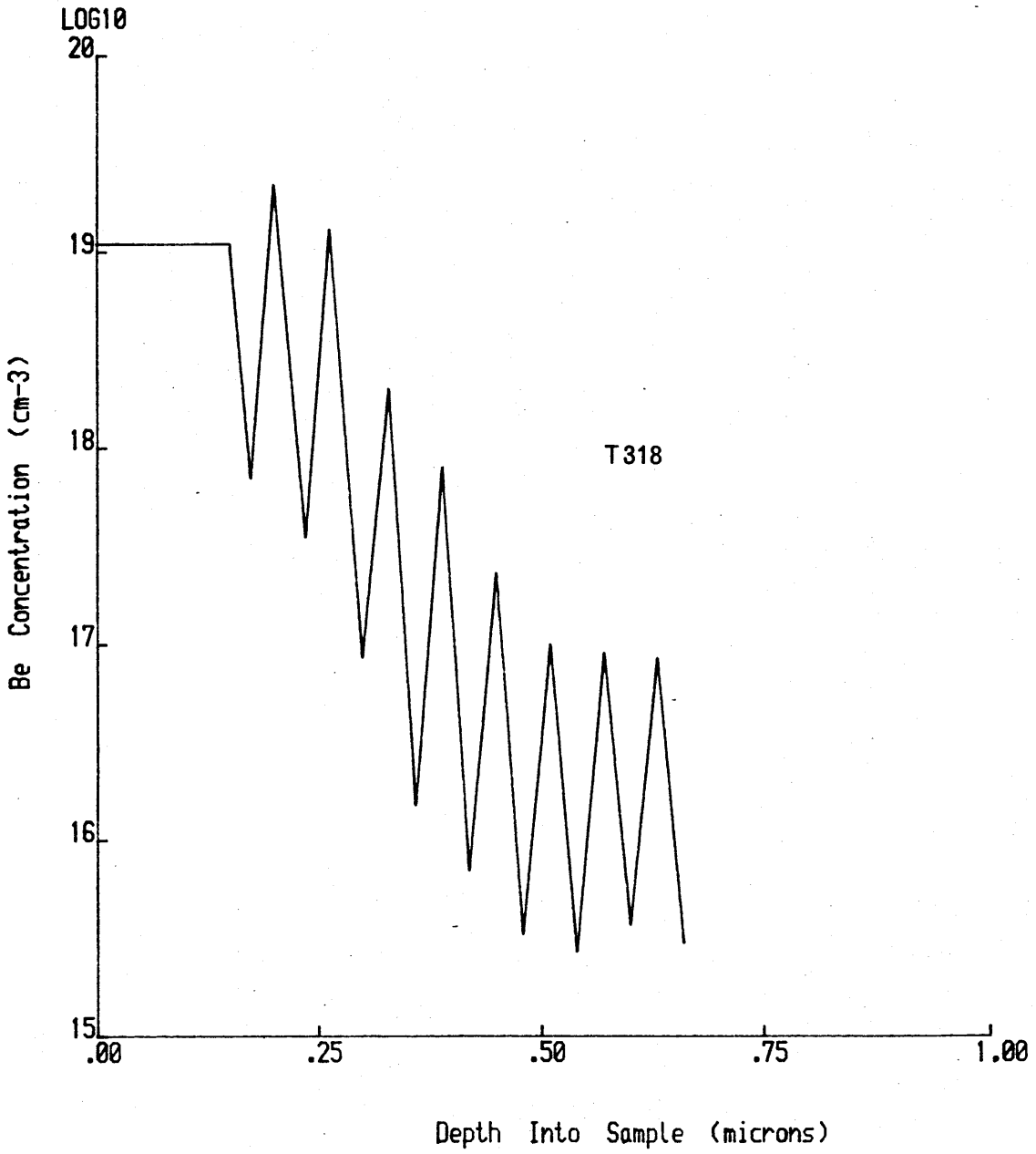

Figure 9.7 Diffusion profile obtained from 600 A SL (SIMS).

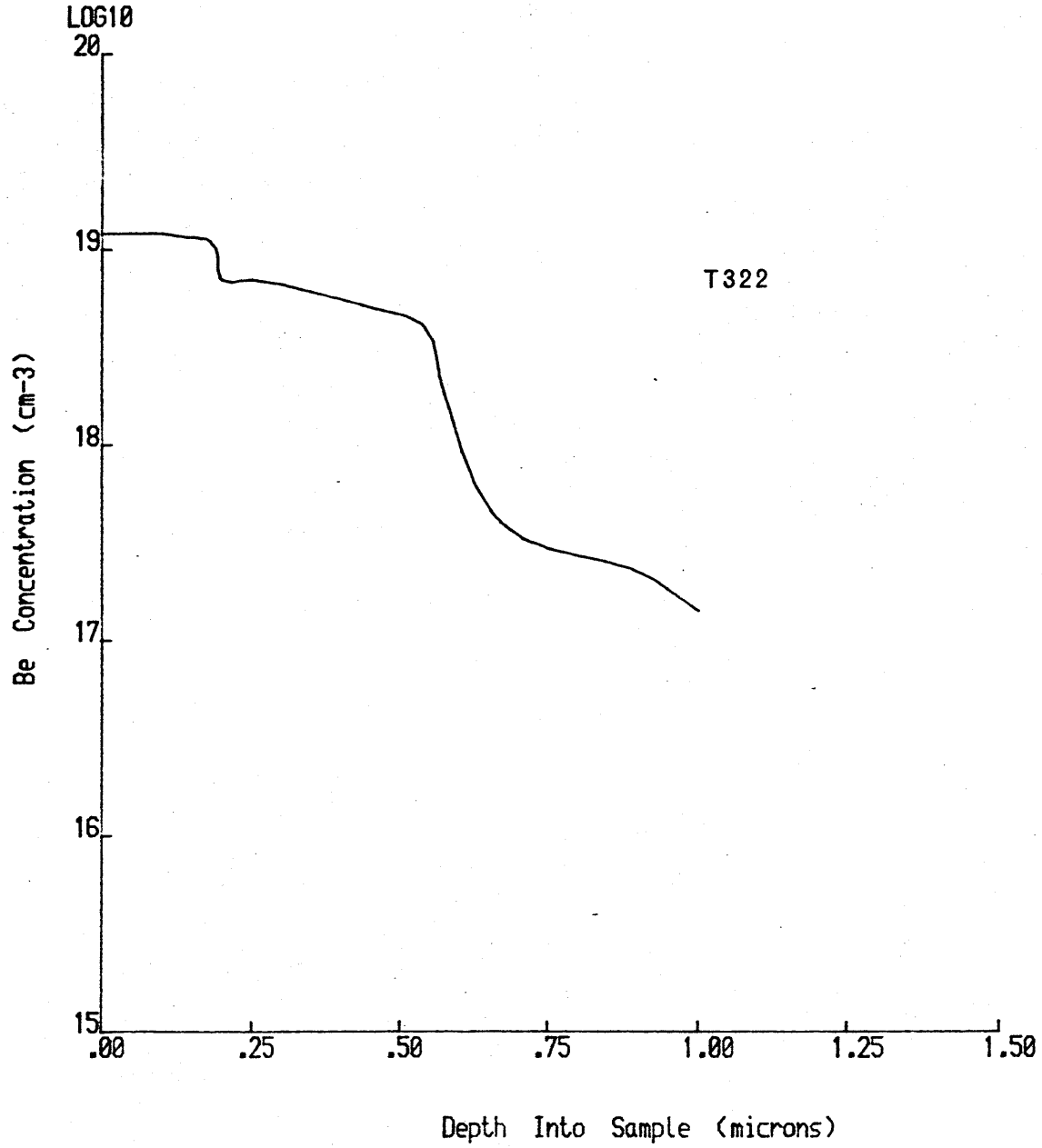

Figure 9.8 Diffusion profile obtained from 40 A SL (SIMS).

doped layer to the SL is due to diffusion into a region of higher diffusivity (the first layer of the SL is AlAs) as was discussed in section 8.9.2 of the previous chapter.

9.4 Discussion

9.4.1 Disordering Mechanism

The details of the mechanism leading to the disordering are as yet unclear, although the models proposed so far have in common an important role played by vacancies. Laidig, et. al. [9.1] have proposed a model where the Zn diffuses as part of a (Zn_i, V_{III}) pair-complex, the presence of the vacancy enhancing the Al-Ga interchange. Two other possible explanations have been suggested by Van Vechten [9.11] which differ from the above model in that they involve anion vacancies, either singly or as divacancies. Camras et. al. [9.4] claim that their results for the GaP-GaAsP, in which anion intermixing takes place, rule out the divacancy model. However, as pointed out by Van Vechten [9.11], the magnitude of the enhancement is not known since data for the Zn-free interdiffusion rate is not available.

At this point it is worth noting that the enhanced intermixing of the AlAs/GaAs SLs is observed in structures grown by both MOCVD [9.1] and MBE [9.7]. This is interesting because, as has been discussed in chapter 7, the relative concentrations of the different native defects are very different for these two growth methods.

The models discussed above all assume that the Zn is incorporated into the lattice via the Frank-Turnbull mechanism, discussed in chapter 8. Also discussed was an alternative incorporation method, i.e. the kick-out mechanism. It was shown that there is substantial experimental evidence in favour of this model, the relevant reaction being repeated here;

(9.1) $$Zn_i^+ + Ga_{Ga} = Zn_s^- + Ga_i + 2e^+$$

The implications of this for intermixing are obvious since there now exists a large population of highly mobile interstitial group III atoms. The intermixing will take place via the reaction ;

$$(9.2) \qquad Ga_i + Al_{Al} = Ga_{Al} + Al_i$$

There are, however, certain experimental observations which require explanation, and these will be discussed in the following three subsections.

9.4.1.1 Si-Disordering of a SL

As was mentioned in the introduction the diffusion of Si has also been shown to lead to disordering of AlAs/GaAs SLs. Given that Si does not diffuse by the interstitial-substitutional mechanism, the intermixing is obviously not due to a reaction analogous to that for Zn given above. A mechanism whereby Si enhances intermixing has been proposed by Van Vechten [9.12], and hence the formation of cation interstitials is not required. Note, however, that the experiments carried out by Coleman et. al. [9.2] involved ion-implantation of the Si, a process which would be expected to result in an increased concentration of interstitials. The results of Meehan et. al. [9.3] were obtained from conventional diffusion of Si. Although no detailed comparison of the enhancement with that for Zn was carried out, it would appear that Si is less efficient than Zn in disordering a SL.

Hence Si would appear to disorder the SL by a different mechanism from either Zn or Be.

9.4.1.2 Disordering on the Anion Sublattice

While the single anion-vacancy model of Van Vechten leads to disordering on the anion sublattice, it is not immediately obvious how this could occur via reaction (9.1). Recalling from chapter 7, however, that both anion and cation antisite defects are stable in GaAs and GaP, then the following reaction might

occur ;

(9.3) $$Ga_i + As_{As} = Ga_{As}^{2-} + As_i + 2e^+$$

and similarly for GaP. This will in turn lead to anion intermixing via the reaction ;

(9.4) $$As_i + P_P = As_P + P_i$$

i.e. for the GaP-GaAsP SL.

If the kick-out mechanism is indeed the dominant diffusion mode for group II atoms, then the effects of reactions such as (9.3) and (9.4) should be apparent after a conventional Zn diffusion into bulk GaAs. Initially, GaAs would appear to be the best choice for such an investigation since, as was discussed in chapter 7, both Ga_{As} and As_{Ga} have been identified with reasonable confidence. Unfortunately, however, the high concentrations normally encountered in diffusion experiments mitigates against the use of the two methods used to identify the Ga_{As} and As_{Ga} defects, i.e. photoluminescence and DLTS respectively (see chapter 7).

One possibility is a PL study on the Be-diffused layers described in the previous chapter, where diffused concentrations as low as mid-10^{18} cm^{-3} can be obtained.

Besides these, there are also more indirect methods of assessing the types of defects present during the diffusion. One of these has already been mentioned in chapter 8, namely Transmission Electron Microscrope examination of diffusion-induced dislocation loops, which were observed by Ball et. al. [9.13] to be of interstitial-type. Of more direct relevance to disordering of an anion sublattice is their observation of triangular stacking faults. They suggest that this is due to the presence of Zn allowing the addition of As-interstitials onto the faulted layer. This, however, presupposes the existence of the As-interstitials in the lattice. Another possible explanation is that the

presence of the Zn actually causes the formation of the As-interstitials through reactions (9.3) and (9.4). Hence the anion intermixing would appear to be reconcilable with the kick-out model.

9.4.1.3 Depth of the Disordering

This is a topic which was extensively studied by LL, who observed that the depth of the disordering was strongly dependent on the SL period, being greater for shorter period SLs. The depth of the disordering is obviously partly determined by the diffusion depth, but not wholly so as is clear from an examination of LLs results presented as Fig. 7 of their paper. Comparison of the 320 Å SL diffused at 550°C with the 1100 Å SL diffused at 575°C shows that the diffusion depth is similar yet the extent of the disordering is far less in the latter of the two. Assuming that disordering is caused by interstitial group III atoms, the depth of the disordering will obviously be less for a large period SL due to the greater diffusion distance. Note, however, that defining a measure of disordering is very difficult and essentially qualitative measures have been used by Lee and Laidig.

9.4.2 Effect of Superlattice Period on Diffusion Depth

The increase in diffusivity with decreasing SL period, observed by LL, has been discussed by Van Vechten [9.12] who has proposed that it is due to the presence of interface states. These states help achieve this by accommodating excess electrons during the diffusion step, the electrons being created as a result of the change of charge state of the Zn atom.

The interface states are formed as a result of the change in bonding at the junction of the two materials. This is similar to the situation encountered for surfaces which was discussed in chapters 4 and 5. Interface states can also arise due to defects which might be caused, for example, by lattice mismatch. Despite the many studies which have been carried out on interfaces grown

by different methods, the presence of these states in grown layers has not yet been unequivocally proven.

Van Vechten's analysis predicts that the presence of the states will lead to a reduction in the activation energy for diffusion, E_a, of about 1 eV. LL do in fact obtain such a variation from their results. However, as pointed out by Van Vechten himself, such a large change in E_a is inconsistent with the relatively small increase in diffusion depth. Van Vechten also pointed out that the situation is further complicated by the destruction of the interfaces by the disordering, hence removing the alleged source of the increased diffusivity.

Examination of the results obtained from the Be-diffusion structures reveals an important difference from LLs results, namely that there is no significant increase in the diffusion depth on going from a 600 Å to a 200 Å SL. Decreasing the SL period still further, however, does lead to an increase in the diffusion depth. Another observation is the decrease in the dopant modulation as the SL period decreases. Hence, it would appear that for the thicker SLs the overall diffusivity is strongly limited by the diffusivity through the GaAs layers. As the period is reduced the effect of the GaAs would appear to be lessened, hence leading to greater diffusion depths.

In section 8.11 of the previous chapter it was demonstrated that the band-gap of a semiconductor plays a significant role in determining the diffusivity of Zn and Be. In the same way, it seems reasonable that the SL electronic structure should also strongly affect the diffusivity. Recalling the diagram of Fig. (9.1) and the discussion of section 9.2, the higher diffusivity in the short period SLs can therefore be explained by the rise in energy of the quantum-well states.

Shown in Fig. (9.9) is a plot of the electron-heavy hole (e-hh) transition energy versus SL period for AlAs/GaAs SLs with equal barrier and well widths. The energies were calculated using Bastard's envelope-function approach [9.9] [9.14] and are

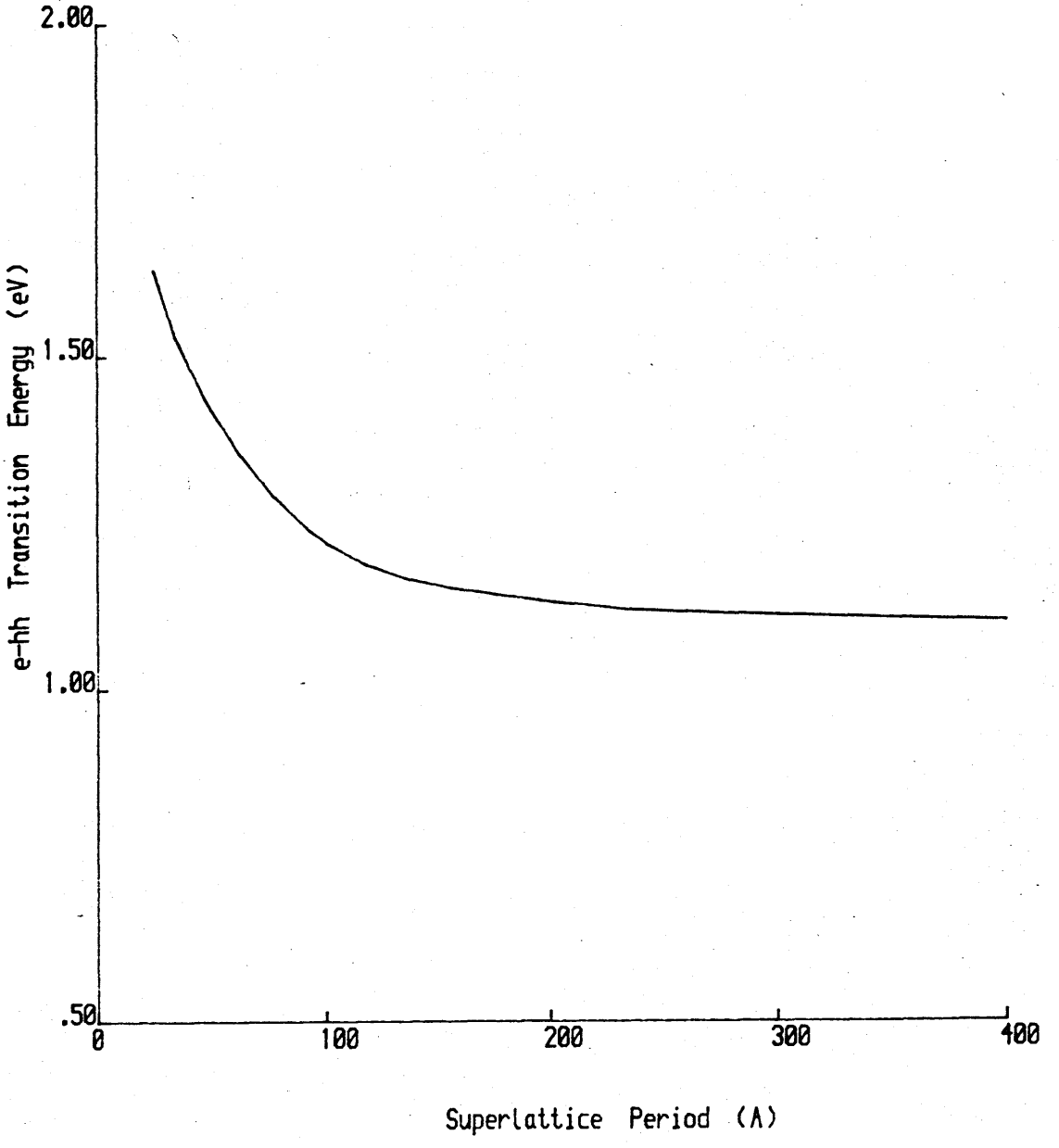

Figure 9.9 Plot of electron-heavy hole transition energy versus total period for the 1:1 AlAs/GaAs SL.

appropriate to a temperature of 970K. The valence and conduction band discontinuities are taken to be 0.48 eV and 1.12 eV respectively, i.e. a 70:30 split in the band-gap difference, ΔE_g.

This data demonstrates that there is no significant rise in the quantum well states until a well width of about 50 Å is reached, and that there is large rise by the time 20 Å is reached. This is in good agreement with the experimental results presented in Figs. (9.4) to (9.8), and suggests that the diffusivity is governed predominantly by the quantum well states, rather than by interface states. Note that the lower than expected diffusivity for the 100 Å SL (Fig. (9.6)) can be attributed to the lower Be concentration.

It remains to explain why LL observed an increase in diffusivity on going from a 1100 Å to a 300 Å SL. The most important difference between LLs experiments and those in the present study is that the former involved a post-growth diffusion. Two factors combine to make the interpretation of the data more prone to error, (i) high sensitivity to dopant concentration, and, (ii) shallow diffusion depths coupled with large SL periods.

In the present experiments the total concentration of Be in the layers can be kept constant. Hence it is not necessary to maintain an equilibrium with a source of atoms outside the sample. The effect of the concentration can be seen by comparing the profile in Fig. (9.5) with that shown in Fig. (9.8), from which it is apparent that the diffused depth increases with the concentration. This illustrates the extreme caution which must be exercised when evaluating diffusivities of such structures, given that the increase in Be concentration is relatively modest. Note, however, that even the highest concentration, large-period SL does not exhibit as much diffusion as that shown in Fig. (9.5), as is apparent from comparison with Fig. (9.7).

9.4.3 Factors Affecting the Overall Profile Shape

The diffusion profile obtained from the SLs is complicated by the destruction of the quantum wells. Hence, the diffusivity is a function of both position and time. Due to the short diffusion times utilised in the present study the thicker SLs remain intact. This is not the case for the 100 Å SL which is observed to be disordered over a large part of the diffusion profile (Fig. (9.6)) and will not be the case for the 40 Å SL which is likely to be disordered over most of the profile (remembering that it is difficult to define an accurate measure of the extent of the disordering).

Assuming this to be the case, a comparison of the diffusivity at the diffusion front with that closer to the surface can be obtained. The band-gap of $Al_{0.5}Ga_{0.5}As$ is 1.7 eV and the transition energy for the 40 Å SL is 1.5 eV (at a temperature of 970K). Qualitatively, the profile would therefore be expected to be more abrupt since the atoms nearer the surface will diffuse more rapidly. This is observed to be the case (see Figs. (9.5) and (9.8)). Note, however, that the diffusion depth will still be determined by the quantum well states ahead of the diffusion front (these will be the lowest energy states available since the material behind the diffusion front is obviously p-type).

9.5 Conclusions

The work described in this chapter has provided evidence that the diffusivity of group II atoms in SLs is determined to a large degree by the quantum well states. Several points still require clarification, in particular the behaviour of Si and the role of the kick-out mechanism.

CONCLUSIONS

The overall aim of the thesis has been to identify some of those aspects of MBE growth which are governed by kinetic factors as well as the role played by thermodynamic factors. Obviously the overall growth process is extremely complex and any modelling is very difficult. Work is, however, being carried by various groups and factors such as those considered in this thesis need to be properly understood if the growth models are to be valid.

For example, chapter 6 has shown that closed-shell systems are likely to have some activation barrier associated with their incorporation into the lattice. Another example of this may be the competition between group V species observed in the growth of III-V-V ternaries. This chapter, along with that on the surface dimer, have also demonstrated the utility of MO methods in understanding reactions on solid surfaces. This is an area where much further work could be carried out and applied to the MBE growth models.

The chapter on native defects has highlighted some aspects of MBE which do appear to be adequately described by thermodynamics, while at the same time showing the limitations of the method. One of the main unresolved problems is the disparity between the calculated and observed (by DLTS) defect concentrations. Useful information has, however, been obtained on the effect of the AlAs molefraction.

Finally, the diffusion chapters have resolved some problems while again demonstrating the complexity of the processes involved in growth. In particular, the role of the electronic states in determining the diffusivity has been illuminated.

REFERENCES

Chapter Two

[2.1] C.T. Foxon et.al., Int. J. Mass Spec. and Ion Phys., 21 (1976) 241

[2.2] C.T. Foxon and B.A. Joyce, Current Topics in Materials Science, 7 (1981) Chapter 1

[2.3] K. Ploog in "Crystals : Growth, Properties and Applications", Vol. 3, Springer, Berlin, 1980

[2.4] M.B. Panish, J. Crystal Growth, 27 (1974) 6

[2.5] W. Koster and B. Thomas, J. Metallic, 46 (1955) 293

[2.6] J.R. Arthur, J. Phys. Chem. Solids, 28 (1967) 2257

[2.7] R.M. Logan and D.T.J. Hurle, J. Phys. Chem. Solids, 32 (1971) 1739

[2.8] C.T. Foxon et.al., J. Phys. Chem. Solids, 34 (1973) 1693

[2.9] J.R. Arthur, Surf. Sci., 43 (1974) 449

[2.10] J.R. Arthur, J. Appl. Phys., 39 (1968) 4032

[2.11] C.T. Foxon and B.A. Joyce, Surf. Sci., 64 (1977) 293

[2.12] R. Heckingbottom et. al., Surf. Sci., 132 (1983) 375

[2.13] J.H. Neave et.al., Appl. Phys. Lett., 36 (1980) 311

[2.14] C.T. Foxon et.al., J. Crystal Growth, 49 (1980) 132

[2.15] C.E.C. Wood et.al., Inst. Phys. Conf. Ser., 45 (1979) 28

[2.16] J.H. Neave et.al., Appl. Phys., **A32** (1983) 195

[2.17] J.H. Neave and B.A. Joyce, J. Crystal Growth, **44** (1978) 387

[2.18] R. Ludeke, IBM J. Res. Dev., **22** (1978) 304

Chapter Three

[3.1] L. Salem, "Electrons in Chemical Reactions", Wiley-Interscience, 1982

[3.2] W.G. Richards and D.L. Cooper, "ab-initio Molecular Orbital Calculations for Chemists", (2nd Ed.), Oxford Science Publications, 1983

[3.3] G. Klopman in "Chemical Reactivity and Reaction Paths", Chapter 4, (Ed. G. Klopman), Wiley-Interscience, 1974

[3.4] R.G. Pearson, "Symmetry Rules for Chemical Reactions", Wiley-Interscience, 1976

[3.5] R.B. Woodward and R. Hoffmann, "The Conservation of Orbital Symmetry", Academic Press, New York, 1970

[3.6] J.A. Pople and D.L. Beveridge, "Approximate Molecular Orbital Theory", McGraw-Hill, New York, 1970

[3.7] I.N. Levine, "Quantum Chemistry", (3rd Ed.), Alyn and Bacon, 1983

[3.8] W.A. Goddard and T.C. McGill, J. Vac. Sci. Tech., **16** (1979) 1308

[3.9] K. Wittel and S.P. McGlynn, Chemical Reviews, 77 (1977) 745

[3.10] R. McWeeny, "Coulsons' Valence", (3rd Ed.), Oxford Univ. Press, 1979

[3.11] (i) R.C. Bingham, M.J.S. Dewar and D.H. Lo, J. Am. Chem. Soc., 97 (1975) 1285

[3.12] (i) M.J.S. Dewar and W. Theil, J. Am. Chem. Soc., 99 (1977) 4899

[3.13] J.K. Burdett in "Structure and Bonding in Crystals", Chapter 11, Academic Press, 1981

[3.14] J.S. Binkley and L.R. Thorne, J. Chem. Phys., 79 (1983) 2932

[3.15] K. Fukui in "Molecular Orbitals in Chemistry, Physics and Biology", (Ed. P.O. Lowdin and B. Pullman), Academic, New York, 1964

[3.16] P.K. Larsen et. al., Phys. Rev. B, 26 (1982) 3222

Chapter Four

[4.1] F. Forstmann in "Photoemission and the Electronic Properties of Surfaces", Chapter 8, (Ed. B. Feuerbacher et.al.), Wiley-Interscience, 1978

[4.2] J.E. Inglesfield and B.W. Holland in "The Chemical Physics of Solid Surfaces and Heterogeneous Catalysis", Vol. 1, Chapter 3, (Ed. D.A. King and D.P. Woodruff), Elsevier, 1981

[4.3] A. Kahn, Surf. Sci. Reports, **3** (1983) 193

[4.4] W.A. Harrison, "Electronic Structure and the Properties of Solids", Chapter 10, W.H. Freeman, 1980

[4.5] M. Schmeits et. al., Phys. Rev. B, **27** (1983) 5012

[4.6] W.A. Goddard III and T.C. McGill, J. Vac. Sci. Tech., **16** (1979) 1308

[4.7] D. Post and E.J. Baerends, J. Chem. Phys., **78** (1983) 5663

[4.8]M. Simonetta and A. Gavezzotti, Advances in Quantum Chemistry, **12** (1980) 103

[4.9] A. Redondo et. al., Surf. Sci., **132** (1983) 49

[4.10] (i) J.A. Appelbaum and D.R. Hamann, Phys. Rev., **B6** (1972) 2166 (ii) J.A. Appelbaum et. al., ibid, **14** (1976) 588

[4.11] D.J. Chadi, Phys. Rev. Lett., **41** (1979) 1062

[4.12] D.J. Chadi, Phys. Rev. Lett., **52** (1984) 1911

[4.13] T.B. Grimley in "The Chemical Physics of Solid Surfaces and Heterogeneous Catalysis", Vol. 2, Chapter 5, (Ed. D.A. King and D.P. Woodruff), Elsevier, 1983

Chapter Five

[5.1] A. Khan, Surf. Sci. Reports, **3** (1983) 193

[5.2] J.H. Neave and B.A. Joyce, J. Crystal Growth, **44** (1978) 387

[5.3] W.S. Yang et. al., Phys. Rev. B, **28** (1983) 2049

[5.4] (i) P.J. Dobson et. al., Surf. Sci., **119** (1982) L339
(ii) P.K. Larsen et.al., Phys. Rev., **B26** (1982) 3222

[5.5] D.J. Chadi et. al., Surf. Sci., **120** (1982) L425

[5.6] (i) W.S. Verwoerd, Surf. Sci., **99** (1980) 581
(ii) Surf. Sci., **103** (1981) 404

[5.7] M.T. Yin and M.L. Cohen, Phys. Rev. B, **24** (1981) 2303

[5.8] R.G. Pearson, "Symmetry Rules for Chemical Reactions", Wiley-Interscience, 1976

[5.9] H.A. Jahn and E. Teller, Proc. Roy. Soc., **A161** (1937) 220

[5.10] U. Opik and M.H.L. Pryce, Proc. Roy. Soc., **A238** (1957) 425

[5.11] R.F.W. Bader, Can. J. Chem., **40** (1962) 1164

[5.12] H.C. Longuet-Higgins, Proc. Roy. Soc., **A235** (1956) 537

[5.13] W.A. Goddard and T.C. McGill, J. Vac. Sci. Tech., **16** (1979) 1308

[5.14] W.A. Harrison, "Electronic Structure and the Properties of Solids", Freeman, San Francisco, 1980

[5.15] R.B. Woodward and R. Hoffmann, "The Conservation of Orbital Symmetry", Academic Press, New York, 1970

[5.16] B.A. Joyce, Private Communication

[5.17] J.A. Appelbaum et. al., Phys. Rev. B, **11** (1975) 3822

[5.18] J.A. Appelbaum et. al., ibid., **14** (1976) 588

[5.19] P.J. Dobson, Private Communication

[5.20] T. Nakajima et. al., Bull. Chem. Soc. Jap., **45** (1972) 1022

[5.21] E. Tosatti and P.W. Anderson, Solid State Comm., **14** (1974) 773

Chapter Six

[6.1] N. Matsunaya et. al., Jpn. J. Appl. Phys., **16** (1976) 443

[6.2] R. Heckingbottom et. al., J. Electrochem. Soc., **127** (1980) 444

[6.3] T.B. Grimley in "The Chemical Physics of Solid Surfaces and Heterogeneous Catalysis", Vol. 2, chapter 5, (Ed. D.A. King and D.P. Woodruff), Elsevier, 1983

[6.4] K.H. Johnson, Int. J. of Quantum Chemistry, Quantum Chemistry Symposium 11, (1979) 39

[6.5] E. Shustarovich et. al., J. Phys. Chem., **87** (1983) 1100

[6.6] T.H. Upton, J. Am. Chem. Soc., **106** (1984) 1561

[6.7] R.G. Pearson, "Symmetry Rules for Chemical Reactions", Wiley-Interscience, 1976

[6.8] G. Laurence et. al., Surf. Sci., **68** (1977) 190

[6.9] R. Ludeke and A. Koma, J. Vac. Sci. Tech., **13** (1976) 241

[6.10] R.Z. Bachrach et. al., J. Vac. Sci. Tech., **18** (1981) 797

[6.11] J.H. Neave and B.A. Joyce, J. Crystal Growth, **44** (1978) 387

[6.12] B.A. Joyce and C.T. Foxon, Jap. J. Appl. Phys., **16** (1972) 17

[6.13] C.E.C. Wood et. al., J. Appl. Phys., **53** (1982) 4230

[6.14] R. Heckingbottom et. al., Surf. Sci., **132** (1983) 375

[6.15] R.F.C. Farrow et. al., Appl. Phys. Lett., **39** (1981) 954

[6.16] G. Klopman in "Chemical Reactivity and Reaction Paths", chapter 4, (Ed. G. Klopman), Wiley-Interscience, 1974

[6.17] W.C. Swope and H.F. Schaeffer III, J. Am. Chem. Soc., **98** (1976) 7962

[6.18] D. Post and E.J. Baerends, J. Chem. Phys., **78** (1983) 5663

[6.19] R.O. Jones, J. Chem. Phys., **72** (1980) 3197

[6.20] L.A. Curtiss and D.J. Frurip, Chem. Phys. Lett., **75** (1980) 69

[6.21] M.J.S. Dewar and H.S. Rzepa, J. Am. Chem. Soc., **100** (1978) 777

Chapter Seven

[7.1] G.M. Blom, J. Crystal Growth, **36** (1976) 125

[7.2] M. Ettenberg and H. Kressel, Appl. Phys. Lett., **26** (1975) 478

[7.3] T. Yi and K. Nishada, Jpn. J. Appl. Phys., **15** (1976) 2247

[7.4] A. Humbert and L. Hollan, J. Appl. Phys., **47** (1976) 4137

[7.5] P. Blood and J.J. Harris, J. Appl. Phys., **56** (1984) 993

[7.6] D.T.J. Hurle, J. Phys. Chem. Solids, **40** (1979) 613

[7.7] A. Munoz-Yague and Baceiredo, J. Electrochem. Soc., **129** (1982) 2108

[7.8] R.M. Logan and D.T.J. Hurle, J. Phys. Chem. Solids, **32** (1971) 1739

[7.9] J.A. Van Vechten in "Handbook on Semiconductors", Vol. 3, Chapter 1, North-Holland, 1980

[7.10] F.A. Kroger, "The Chemistry of Imperfect Crystals", (2nd Ed.), Vol. 2, North-Holland, 1974

[7.11] J.R. Arthur, J. Phys. Chem. Solids, **28** (1967) 2257

[7.12] M. Hoch and K.S. Hinge, J. Chem. Phys., **35** (1961) 451

[7.13] S.Y. Chiang and G.L. Pearson, J. Appl. Phys., **46** (1975) 2986

[7.14] R.A. Swalin, J. Phys. Chem. Solids, **18** (1961) 290

[7.15] P.J. Anthony, Solid State Elect., **25** (1982) 1171

[7.16] A. Mircea and D. Bois, Inst. Phys. Conf. Ser., **46** (1979) 82

[7.17] A.G. Milnes, Advances in Electronics and Electron Physics, **61** (1983) 63

[7.18] (i) J. Lagowski et.al., Appl. Phys. Lett., **40** (1982) 342 (ii) Walukiewicz et.al., ibid., **43** (1983) 192

[7.19] P.K. Bhattacharya et. al., Appl. Phys. Lett., **36** (1980) 304

[7.20] U. Kaufmann, et.al., Appl. Phys. Lett., **29** (1976) 312

[7.21] R. Worner et.al., Appl. Phys. Lett., **40** (1982) 141

[7.22] A. Chantre et.al., Phys. Rev., **B23** (1981) 5335

[7.23] E.R. Weber et.al., J. Appl. Phys., **53** (1982) 6140

[7.24] T. Ishida et.al., Appl. Phys., **21** (1980) 257

[7.25] T.L. Reineke, Physica **117B** and **118B**, (1983) 194

[7.26] P.J. Lin-Chung and T.L. Reineke, Phys. Rev., **27** (1983) 1101

[7.27] G.B. Bachelet et. al., Phys. Rev. B, **24** (1981) 4736

[7.28] P.W. Yu et.al., Appl. Phys. Lett., **41** (1982) 532

[7.29] D.V. Lang et. al., Phys. Rev. B, **15** (1977) 4874

[7.30] K. Hikosaka et.al., Inst. Phys. Conf. Ser., **63** (1982) 233

[7.31] E.E. Wagner et. al., J. Appl. Phys., **51** (1980) 5434

[7.32] R. Heckingbottom and G. Davies, J. Crystal Growth, **50** (1980) 644

[7.33] A. Madhukar, Surf. Sci., **132** (1983) 344

[7.34] P. Blood and J.J. Harris, J. Appl. Phys., **56** (1984) 993

[7.35] P.K. Bhattacharya et. al., J. Appl. Phys., **53** (1982) 6391

[7.36] D.S. Day et.al., J. Elect. Mat., **10** (1981) 445

[7.37] S.R. McAfee et. al., J. Appl. Phys., 52 (1981) 6165

[7.38] J.H. Neave et.al., Appl. Phys. Lett., 36 (1980) 311

[7.39] P.M. Petroff et. al., Appl. Phys. Lett., **44** (1984) 217

[7.40] T.J. Drummond et. al., Appl. Phys. Lett., **42** (1983) 615

[7.41] W.T. Masselink et. al., Appl. Phys. Lett., **44** (1984) 435

[7.42] B.A. Joyce, Private Communication

[8.1] B. Tuck, "Introduction to Diffusion in Semiconductors", IEE Monograph Series, No. 16, 1974

[8.2] F.C. Frank and D. Turnbull, Phys. Rev., **104** (1956) 617

[8.3] B. Tuck and M.A.H. Khadim, J. Mater. Sci., **7** (1972) 581

[8.4] U. Gosele and F. Muirhead, J. Appl. Phys., **52** (1981) 4617

[8.5] A.H. Van Ommen, J. Appl. Phys., **54** (1983) 5055

[8.6] R.K. Ball et. al., Phil. Mag. A, **46** (1982) 913

[8.7] H.C. Casey and G.L. Pearson in "Point Defects in Solids", (Ed. J.H. Crawford and L.M. Slifkin), Plenum, New York, 1975

[8.8] M.B. Small et. al., Appl. Phys. Lett., **41** (1982) 1068

[8.9] E.A. Poltoratskii and V.M. Stuchebnikov, Sov. Phys.-Solid State, **8** (1966) 770

[8.10] K. Masu et. al., J. Appl. Phys., **54** (1983) 1574

[8.11] E. Silberg et. al., Inst. Phys. Conf. Ser., **65** (1982) 187

[8.12] B. Tuck and A.J.N. Houghton, J. Phys. D, **14** (1981) 2147

[8.13] S.E. Blum et. al., Appl. Phys. Lett., **42** (1983) 108

[8.14] Y.R. Yuan et. al., J. Appl. Phys.,
54 (1983) 6044

[8.15] T. Ambridge and M.M. Factor, Inst. Phys. Conf. Ser.,
24 (1975) 320

[8.16] P. Blood, Private Communication

[8.17] J. Crank, "The Mathematics of Diffusion",
Oxford, London, 1956

[8.18] B. Tuck and A. Hooper, J. Phys. D,
8 (1975) 1806

[8.19] M. Yamada et. al., Appl. Phys. Lett.,
43 (1983) 594

[8.20] Y. Yamamoto and H. Kanbe, Jap. J. Appl. Phys.,
19 (1980) 121

[8.21] M. Ilegems, J. Appl. Phys., 48 (1977) 1278

[8.22] P.J. Anthony, Solid State Electronics, 25 (1982) 1171

[8.23] B.A. Joyce and C.T. Foxon, Jap. J. Appl. Phys.,
16 (1972) 17

[8.24] K.A. Arseni et. al., Phys. Stat. Sol.,
35 (1969) 1053

Chapter Nine

[9.1] W.D. Laidig et. al., Appl. Phys. Lett.,
38 (1981) 776

[9.2] J.J. Coleman et. al., Appl. Phys. Lett., **40** (1982) 904

[9.3] K. Meehan et. al., Appl. Phys. Lett., **45** (1984) 549

[9.4] M.D. Camras et. al., Appl. Phys. Lett., **42** (1983) 185

[9.5] W.D. Laidig et. al., J. Appl. Phys., **54** (Nov. 1983)

[9.6] S.M. Bedair et. al., to be published (see [9.7])

[9.7] J.W. Lee and W.D. Laidig, J. Elect. Mat., **13** (1984) 147

[9.8] G. Bastard, Phys. Rev. B, **25** (1982) 7584

[9.9] R. Dingle et. al., Phys. Rev. Lett., **33** (1974) 827

[9.10] R. Dingle in Festkorperprobleme XV, Pergamon Press, 1975

[9.11] J.A. Van Vechten, J. Appl. Phys., **53** (1982) 7082

[9.12] J.A. Van Vechten, J. Vac. Sci. Tech., (1984)

[9.13] R.K. Ball et. al., Phil. Mag. A, **46** (1982) 915

[9.14] The computer program was supplied by Dr. G. Duggan of Philips Research Laboratories.

APPENDIX A

THE METHOD OF LINEAR COMBINATION OF ATOMIC ORBITALS

Consider an atom with Atomic Orbitals (AOs) ϕ_i. When two or more atoms are brought together to form a molecule the electrons are contained in Molecular Orbitals (MOs) which may be expressed as a linear combination of the constituent AOs thus ;

$$\psi_n = \sum_i C_{ni}\ \phi_i \qquad \text{(A.1)}$$

where ψ_n is a MO and the C_{ni} are the expansion coefficients. This approach is the most generally applicable and useful representation of a MO.

Before any calculations can be carried out using this model, the functional form of the AOs must be known. In the days before large electronic computers became available, the AOs were often taken to be single Slater-Type-Functions (STFs or STOs), the general form of which is ;

$$\chi_{nlm}(r,\xi) = R_{nl}(r,\xi)Y_{lm}(\theta,\varphi) \qquad \text{(A.2)}$$

where,

$$R_{nl}(r,\xi) = r^{n-1}\ e^{-\xi r} \qquad (n > 1) \qquad \text{(A.3)}$$

i.e. a radial function, and the angular function $Y_{lm}(\theta,\varphi)$ is a normalised spherical harmonic. This function determines the spatial symmetry properties of the orbital. The above STF can then be used to determine the coulomb and exchange integrals described in chapter 3.

By the very nature of the variational method, an increase in the number of component functions in the expansion leads to greater variational flexibility and to an improvement in the solution obtained (in the present case a lower energy). Hence an improved solution would be obtained by using two STFs for each AO, rather

than one.

The use of STFs in the evaluation of the integrals leads to computational difficulties and for this reason they are rarely used nowadays. A more efficient function in this respect is the Gaussian, which has a radial factor ;

$$R_{nl}(r,\xi) = r^{n-1}\, e^{-\xi r^2} \qquad (n > 1) \tag{A.4}$$

The angular factor being identical to that for (A.2). The product of two Gaussians on different centres is equivalent to a single Gaussian on a new centre, which is not the case for STFs, and this leads to the improved computational efficiency.

The main disadvantage in using a Gaussian basis set is that about two to five as many Gaussian as Slater functions are required to produce a given accuracy. The advantages outweigh the disadvantages, however, and Gaussians are the most common basis function in general use today.

Obviously there are many alternative sets of Gaussians which can be used depending on the factors which are considered to be important in the calculation. The calculation of the coefficients and exponents of such Gaussian basis sets is a very active field of investigation, and many alternative sets are in existence.

It is important to note that there are two main types of basis set, (i) minimal and (ii) extended. A minimal basis set is one in which the coefficients and exponents are appropriate only to the occupied orbitals of an atom. However, it has been established that the use of basis functions which simulate unoccupied, and hence more diffuse, AOs normally leads to some improvement in the description of the MOs and the total energy of the molecule. This is known as an extended basis set and, in line with common practice, are denoted by a superscript in Table 6.2.

The basis sets used in the calculations in chapter 6 are obtained from two main sources, (i) the article by Dunning and Hay [A.1] and (ii) the series of articles by Huzinaga and co-workers [A.2]-[A.4], all of which are referred to below.

[A.1] T.H. Dunning, Jr. and P.J. Hay, "Gaussian Basis Sets for Molecular Calculations" in Modern Theoretical Chemistry, Vol. 3, chapter 1, (Ed. H.F. Schaefer III), Plenum, New York, 1976

[A.2] H. Tatewaki and S. Huzinaga, J. Comp. Chem., 1 (1980) 205

[A.3] Y. Sakai et. al., ibid., 2 (1981) 100

[A.4] H. Tatewaki et. al., ibid., 2 (1981) 278

ADDENDUM

Quantum Chemistry Programs

The MNDO and MINDO/3 programs are standard packages written by Dewar's group at the University of Austin, Austin, Texas (being the originators of the basic methods). The programs themselves are available from the Quantum Chemistry Program Exchange at the University of Indiana, U.S.A.

The ATMOL package was developed by the SERC and is available on many large mainframes at university computing centres throughout the country.

MBE Growth

All of the layers were grown by myself at Philips Research Laboratories on a growth system built at PRL. The system was diffusion pumped and was equipped with substrate rotation, RHEED, a flux monitor and an optical pyrometer for substrate temperature measurement. The Si-doped substrates were all chemically prepared before mounting on the sample holder. This preparation involved an initial de-greasing followed by etching in a H_2SO_4 : H_2O_2 : H_2O (15 : 2 : 2) mixture. The substrates were then rinsed in de-ionised water before being blow-dried.